MASTER COPY KEEP THIS COPY FOR REPRODUCTION PURPOSES

(2)

REPORT DOCUMENTATION PAGE

Form Approved
OMB No. 0704-0188

AD-A238 668

2. REPORT DATE	3. REPORT TYPE AND DATES COVERED
3/91	Final 1 Oct 87 - 30 Sep 90

4. TITLE AND SUBTITLE
Optics with semiconductors: Ultrafast physics for devices

5. FUNDING NUMBERS
DAAL03-87-K-0145

6. AUTHOR(S)
P. M. Fauchet

7. PERFORMING ORGANIZATION NAME(S) AND ADDRESS(ES)
Princeton University
Princeton, NJ 08544

8. PERFORMING ORGANIZATION REPORT NUMBER

9. SPONSORING/MONITORING AGENCY NAME(S) AND ADDRESS(ES)
U. S. Army Research Office
P. O. Box 12211
Research Triangle Park, NC 27709-2211

10. SPONSORING/MONITORING AGENCY REPORT NUMBER
ARO 25267.13-PH

11. SUPPLEMENTARY NOTES
The view, opinions and/or findings contained in this report are those of the author(s) and should not be construed as an official Department of the Army position, policy, or decision, unless so designated by other documentation.

12a. DISTRIBUTION/AVAILABILITY STATEMENT
Approved for public release; distribution unlimited.

12b. DISTRIBUTION CODE

13. ABSTRACT (Maximum 200 words)

Femtosecond optical pulses have been used to study ultrafast phenomena in semiconductors that may be useful for future high-bit rate optoelectronic and photonic devices. A complete characterization of femtosecond pulse formation in a dye laser has been performed. Several experiments have been performed in different semiconductors with emphasis on nonlinearities near the band edge in GaAs. We find large refractive and absorptive nonlinearities near the band edge, which are due to many-body hot-carrier effects. Other materials which we have tested, such as crystalline or amorphous silicon, appear less promising for device applications. Waveguide switches and spatial light deflectors using the AC Stark effect nonlinearity have also been analyzed.

91-05284

14. SUBJECT TERMS
Nonlinearity; femtosecond pulses; GaAs; Stark effect; many-body hot-carrier effects; optoelectronic and photonic devices

15. NUMBER OF PAGES

16. PRICE CODE

17. SECURITY CLASSIFICATION OF REPORT	18. SECURITY CLASSIFICATION OF THIS PAGE	19. SECURITY CLASSIFICATION OF ABSTRACT	20. LIMITATION OF ABSTRACT
UNCLASSIFIED	UNCLASSIFIED	UNCLASSIFIED	UL

This final report summarizes the results obtained during the 3-year funding cycle of the project Optics with Semiconductors: Ultrafast Physics for Devices, DAAL03-87-K-0145. The goals of the project were 1) to develop a reliable laser source of tunable femtosecond pulses; 2) to investigate the physical mechanisms responsible for femtosecond and picosecond nonlinearities in selected semiconductors; 3) to develop new device concepts which use ultrafast nonlinearities. During the course of this project, we have achieved the stated goals. We have performed what is probably the most definitive experimental work on the formation of solitons and soliton-like pulses in the colliding pulse modelocked dye laser. We have also built a copper vapor laser driven amplifier of these femtosecond pulses which held the record for the highest efficiency. We have performed several crucial experiments in selected semiconductors, namely silicon and especially gallium arsenide, with the goal of investigating their ultrafast response. In particular, we have demonstrated a method of obtaining directly and simultaneously the real and imaginary parts of the optical nonlinearity after excitation and with femtosecond time resolution. We have then investigated in detail the nonlinearities near the bandgap of GaAs due to injection of hot carriers. We reported what we believe is the first measurement of the nonlinearities due to the many-body effects associated with the presence of hot carriers. Finally, we have investigated the novel concept of semiconductor waveguide switches based on the control of the birefringence through nonlinearities such as the AC Stark effect. A subpicosecond light beam spatial deflector appears to be possible.

In the first part of the project, we have emphasized the development of a reliable source of femtosecond pulses that are tunable. We felt that this was our first priority because all the experiments we had planned relied on this source. We built a colliding pulse modelocked dye laser and amplified the pulses with a copper vapor laser. This is the technology now present in about 20 laboratories all over the world. Our work was unique in two respects. First, we performed a detailed study of the conditions necessary for the formation of solitons and soliton-like pulses in the CPM dye laser. We were able to measure the temporal and spectral evolution during the period of the soliton-like pulses. We also demonstrated how these pulses can become true soliton solutions of the nonlinear Schrodinger equation. In doing so, we identified an additional source of nonlinearity in the cavity, which we interpreted as stimulated Raman scattering in the saturable absorber. In many respects, our work is the most definitive experimental study of periodic pulse evolution in the CPM dye laser. It allowed us to understand and control much better our primary laser source. It also led to four publications, two conference

presentations and several seminars. When this was completed, we then took care to develop an amplifier that could produce reliable pulses over a long period of time. We definitely have achieved that goal, since several experiments have since been performed which have required the continuous use of the system for up to 40 hours, with less than 30 % pulse energy degradation! Thanks to a careful engineering of the amplifier, we achived what was then the highest efficiency for a copper vapor amplifier (1.5 %), while keeping the pulses below 100 fs. Our design was published in one paper and presented at two conferences.

In the second part of the project, we used short pulses (mostly from the CPM laser system described above) to investigate ultrafast phenomena in semiconductors. The goal was to learn about the physical mechanisms that could be useful in optoelectronic or photonic devices. Before we turn our attention to the most important part of this section, let us first mention several other contribution. A novel technique for enhancing the signal to noise ratio in time-resolved reflectivity measurements was demonstrated and analyzed in detail. It basically consists in having the probe beam be incident near Brewster's angle. This led to three publications and one conference presentation. Picosecond and femtosecond phenomena that occur in highly excited crystalline and non-crystalline silicon have also been studied and summarized in one publication. Although this work on silicon was mostly supported by other agencies, one publication (out of many publications and conference presentations and seminars) was supported in part by ARO because it reviewed some processes which might have been useful. However, the bulk of this second part is our work on GaAs. Here, a method which we developed earlier for the simultaneous measurement of the changes of absorption coefficient and index of refraction in thin films was applied to GaAs. The real and imaginary parts of the optical nonlinearities produced by the injection of hot carriers with a femtosecond pulses were measured as a function of time and wavelength, with emphasis on the near band edge response. The most significant achievement at the end of the 3-year period was the measurement of the nonlinearities associated with the presence of a large number of carriers in an a-thermal distribution. In particular, we mapped these nonlinearities below and above the original bandgap and identified the contributions of bandgap renormalization, electron-hole plasma screening and band filling. Additional new information on the thermalization of hot carriers was also obtained. This was described in two publications and one conference presentation. In the time interval between the end of the funding period and the writing of this report, a large number of significant new results have been obtained. These include the first observation of a refractive index hole burning near the initial

excited states, the direct observation of the role of plasmons in the initial carrier scattering rate, and the investigation of the gain dynamics on a femtosecond time scale. These new results are being written for publication and are in the process of being presented at several conferences. We have been helped by an active collaboration with a theoretical group at the National Research Council in Ottawa, which was started several months ago.

In the third part of the project, we investigated the design of novel optoelectronic and photonic waveguide devices made of semiconductors. Although we focussed exclusively on the quantum confined AC Stark effect as the nonlinearity, our devices should also be operational with other nonlinearities, such as those associated with the injection of carriers, although the ultimate bit rate of the device might be reduced. Our concept is novel, in that we will use the nonlinearity to alter the natural birefringence that exists in quantum well waveguides. The main idea is to have a four terminal device, with one input, two complementary outputs, and one gate. The optical gate signal produce the nonlinearity, which alters the rate of polarization rotation of the input pulse as it propagates in the device. A polarizer at the output separates the two states of polarizations, thus producing two complementary outputs. Using the AC Stark effect offers the promise of a device using the refractive part of the nonlinearity, thus the promise of low dissipation and very high bit rate. We have designed, grown, and processed several of these waveguides. In the only test performed to date, some changes of the output beam were observed upon application of a gate pulse. However, the weakness of the effect did not allow us to identify the nonlinearity at work. We also fabricated arrays of many identical waveguides, which led us to propose a phased array capable of steering an optical beam on a subpicosecond time scale. This work was presented at one conference.

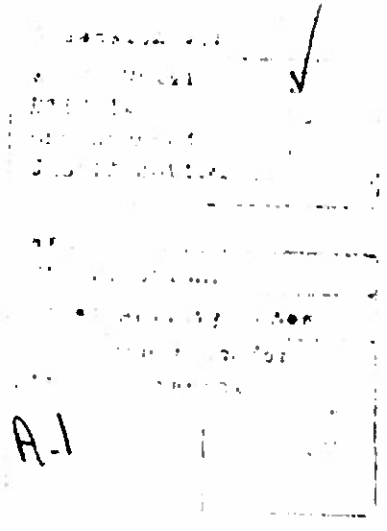

CONTROL OF SOLITONS IN A FEMTOSECOND DYE LASER

W.L. Nighan Jr., T. Gong and P.M. Fauchet

Princeton Laboratory for Ultrafast Spectroscopy
Department of Electrical Engineering
Princeton University, Princeton NJ 08544

The order, period and pulselength of soliton-like pulses present in a colliding pulse modelocked dye laser are controlled by adjusting the group velocity dispersion through the translation of one prism and the self-phase modulation by varying the thickness of the saturable absorber jet or the intracavity intensity in that jet. Spectrum, intensity autocorrelation and interferometric autocorrelation are recorded at different points in the soliton period. The remarkable stability achieved allows for accurate characterization and control.

We have built a 7 mirror/4 prism colliding pulse modelocked (CPM) dye laser [1] that delivers 35 fs pulses around 630 nm at a repetition rate of 100 MHz. The beam intensity in the saturable absorber can be so large that self phase modulation (SPM) takes place. Translation of one of the prisms allows for adjustments of the group velocity dispersion (GVD). Recently, it has been reported that the properties of the output pulse train could become modulated periodically when the cavity parameters are slightly modified from those leading to production of the shortest pulses [2-4]. This periodic pulseshaping has some similarities with the behavior of one class of modelocked color center lasers [5], which are thought to support solitons and are thus called soliton lasers. In fact, the balance of SPM and negative GVD that occurs in the normal mode of operation of the CPM laser has also been compared to the shaping mechanism of the N=1 soliton in an optical fiber [6,7]. In this paper, we demonstrate that control of complicated pulseshaping is possible and we report on the properties of the pulses we have obtained [8].

We control the order, period and duration of the soliton-like pulses by adjusting GVD and SPM inside the laser cavity. Starting from the shortest pulse configuration, higher order "solitons" are achieved by increasing the amount of SPM by translating the absorber jet closer to the intracavity focus or using a thicker jet, by increasing the amount of negative GVD by translating a prism to reduce the beam path in the glass, or in general, by optimizing the alignment of the cavity. In Figure 1, we show several intensity autocorrelation traces taken for different situations. The pulses obtained during the normal mode of operation of the laser can be as short as 35 fs. By translating the jet closer to the

focus over a 250 μm distance, N=1 to N=4 "solitons" are achieved. Starting from the N=2 situation, another N=3 "soliton" is obtained by reducing the amount of glass traversed by 150 μm. Note that the stability of the N=1 and N=2 "solitons" is exceptional (they can be kept and reproduced for days); the N=3 "soliton" is stable enough to allow characterization, while the N=4 "soliton" can hardly be maintained.

The traces of Figure 1 clearly indicate oscillations between two or more extreme pulseshapes. We have consistentiy observed that the average output power of the laser for N>1 is modulated, typically by 10 %. However, the spectrum of the pulses is modulated much more strongly and can be used to generate short trigger pulses necessary for the study of the pulse properties during a period. In Figure 2, we show the modulation of the average output power, the modulation that can be obtained by spectrally filtering all frequencies outside a narrow band, and the resulting gate pulses generated using this modulated signal. The position of the gate pulses in the period is adjustable. Three characterization techniques were used. The spectrum was recorded using an optical multichannel analyzer (OMA) from Princeton Instruments triggered by 50 ns long gate pulses. The intensity autocorrelation and interferometric autocorrelation were measured by second harmonic generation and a Stanford Research boxca averager using a 100 ns long window. Both autocorrelations were taken during a single sweep of the translation stage in the variable delay arm. To resolve the fringes in the interferometric autocorrelation, the frequency at which the shaker was driven was limited to 0.5 Hz. Finally, since the clockwise and counterclockwise beams generated by the CPM laser are asymmetric, we are reporting results for the clockwise beam only.

Consider the N=2 "soliton" characterized in Figure 3. During its 2.5 μs period, the spectrum and time structure change periodically. The spectrum has two main peaks which evolve during a period. The autocorrelation traces clearly indicate the presence of two coherent pulses whose maximum separation approaches 1 ps. The interferometric autocorrelation traces provide more information than the intensity autocorrelation traces. The two pulses are seen to remain coherent with each other, which is different from a recent report [3], and because of that coherence which leads to signal enhancement, we can observe the temporal separation of the two pulses for most of the period. Each individual pulse also appears not to be chirped.

The results of Figure 3 are related to the results of Salin et al [3], who interpreted their sampled intensity autocorrelation and spectra as evidence for an asymmetric N=2 soliton. Despite the similarities, it does not appear possible to fit our results using an asymmetric N=2 soliton. In fact, we have very recently been able to modify our laser to generate pure N=2 solitons which can be fitted with great precision by the theory of Haus et al [9]. These results will be published elsewhere. In this paper, we turn our attention to the differences and similarities between our pulses and standard solitons. In a fiber, the transition from

the N=2 to the N=3 soliton is triggered by an increase of the intensity and does not alter the period of the soliton. In the CPM laser, the period doubles and the average output power is unchanged. The second observation is not surprising, because the peak power in the medium where SPM occurs, that is, the saturable absorber jet, increases roughly as it would be expected to do in a fiber. The first observation is inconsistent with a "normal" soliton behavior. In Figure 4, we show the period doubling obtained after the transition and intensity autocorrelation traces measured during the period of the N=3 "soliton". The pulse is narrowed twice in its period, as predicted for solitons of order 3 in optical fibers.

It is already apparent that although those pulses have strong soliton-like characteristics, they are not completely identical to "normal" solitons. Figures 5 and 6 quantify some of the properties of the N=2 "soliton". The linear relationship of Figure 5 is exactly what is expected of a regular N=2 soliton. The temporal variations of Figure 6 are not expected. In their theory, Haus and Islam show that the behavior of N=2 solitons is governed by four quantities, two poles and two residus [9]. If these quantities are allowed to change periodically, the average power may vary as we have observed, and the spectrum may vary, qualitatively in agreement but quantitatively in disagreement with our observations. It has been suggested that the presence of discrete elements in the cavity or the presence of saturable gain or loss would invalidate the description of the pulse as a soliton. As already mentioned, we have been able to generate N=2 solitons by slight modifications in the cavity, so we can rule out both objections. We believe that other nonlinear effects do exist inside the cavity. Their influence will be discussed elsewhere.

In conclusion, we have demonstrated control and accurate characterization of soliton-like pulseshaping in a femtosecond dye laser. Although our pulses have many properties that are reminiscent of solitons, they are not identical to "normal" solitons. Our results will allow accurate modelization of this type of lasers. We acknowledge support from NSF (ECS-8606531 and ECS-8657263), Coherent Inc. through the NSF Presidential Young Investigator program, and ARO (DAAL03-87-K-0145). P.M. Fauchet is an Alfred P. Sloan research fellow.

REFERENCES

1 J.A. Valdmanis, R.L. Fork and J.P. Gordon, Opt. Lett.**10**, 131, 1985
2 F. Salin et al, Phys. Rev. Lett.**56**, 1132, 1986
3 F.W. Wise, I.A. Walmsley and C.L. Tang, Opt. Lett.**13**, 129, 1988
4 F. Salin et al, Phys. Rev. Lett.**60**, 659, 1988
5 L.F. Mollenauer and R.H. Stolen, Opt. Lett.**9**, 13, 1984
6 J.C. Diels et al, J. Opt. Soc. Am.**B2**, 680, 1985
7 O.E. Martinez, R.L. Fork and J.P. Gordon, J. Opt. Soc. Am.**B2**, 753, 1985
8 W.L. Nighan, T. Gong and P.M. Fauchet, in Ultrafast Phenomena VI, in press
9 H.A. Haus and M.N. Islam, IEEE J. Quantum Electron. **QE-21**, 1172, 1985

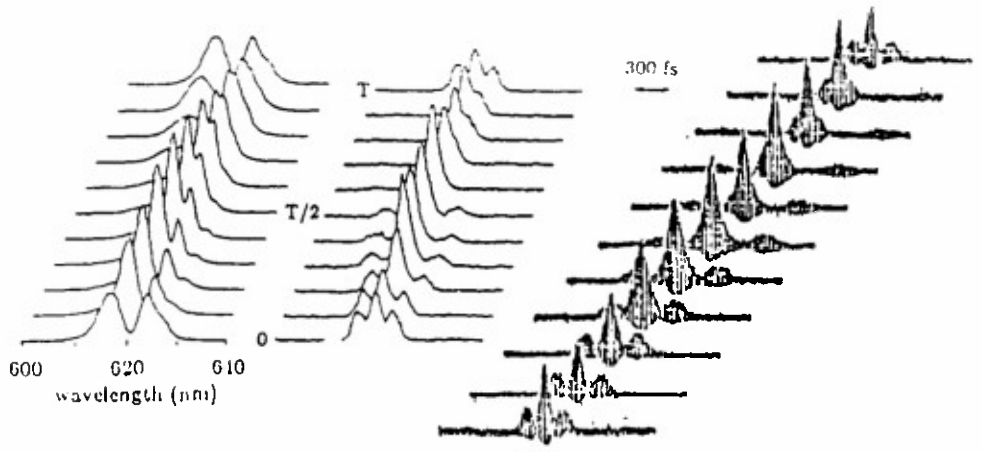

Fig. 3 Time-resolved spectra, intensity autocorrelation and interferometric autocorrelation traces during the 2.5 μs period of an N=2 "soliton".

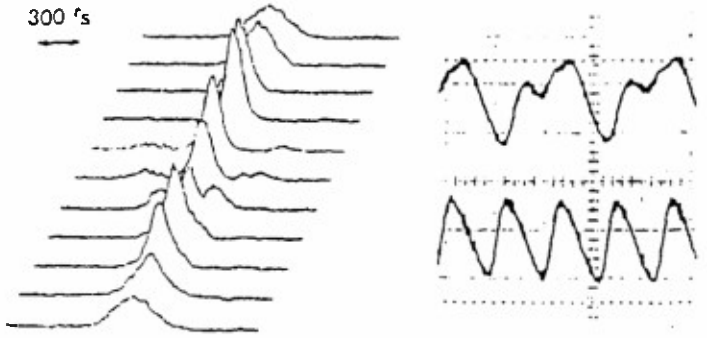

Fig.4 Time-resolved intensity autocorrelation traces during the 5 μs period of an N=3 "soliton", and period doubling between the N=2 and N=3 cases.

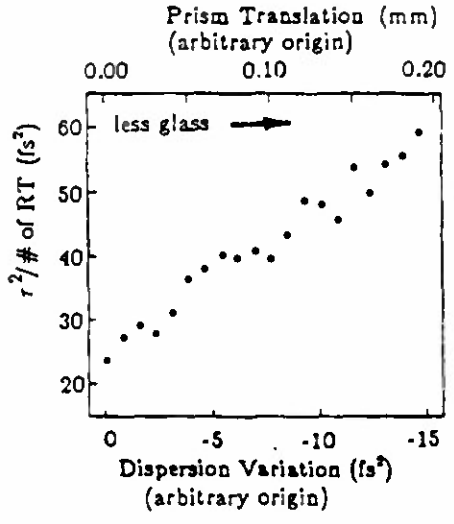

Fig. 5 Linearity of the ratio "soliton" pulsewidth squared over number of roundtrips in the period vs. cavity dispersion.

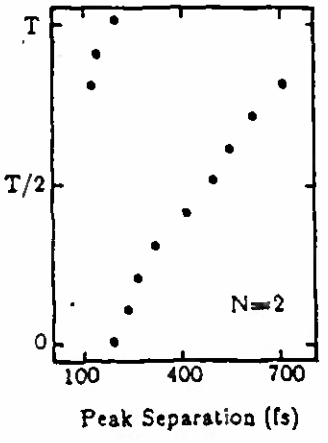

Fig. 6 Periodic evolution of the temporal peaks.

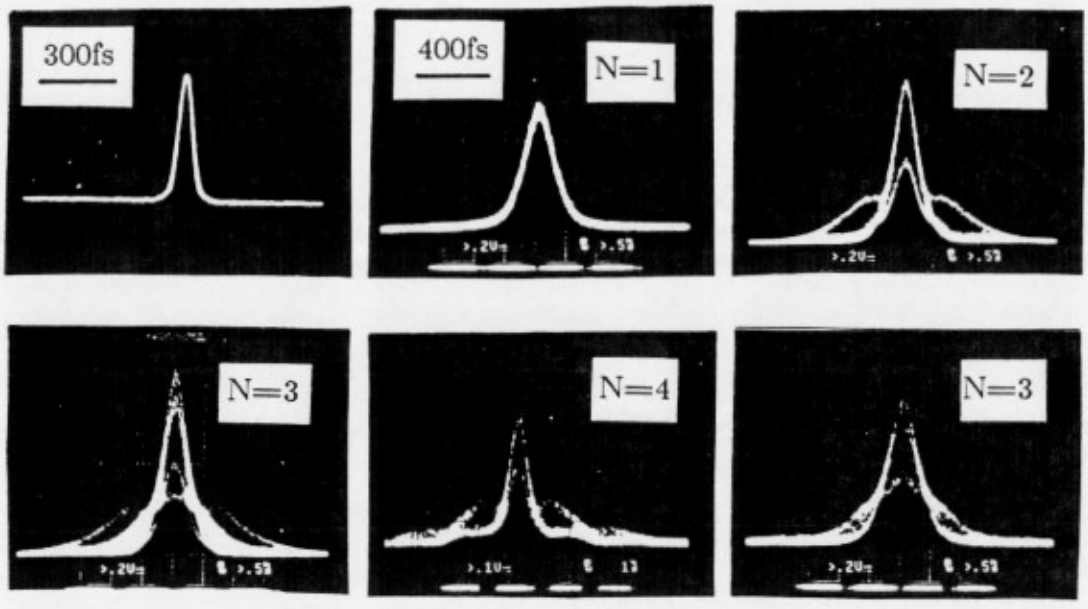

Fig. 1 Single-sweep intensity autocorrelation traces for different cavity configurations. The time scale is different in the first trace.

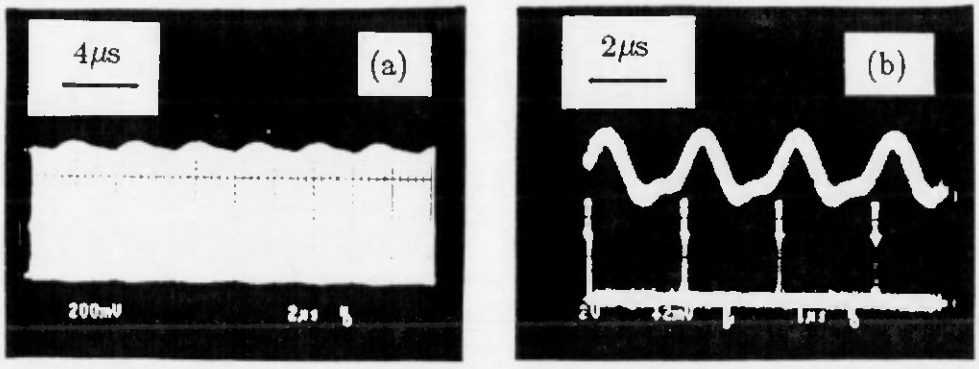

Fig. 2 (a): Average output power (b): average power in a narrow frequency range of the spectrum and gate pulses (N=2 "soliton"). The time scales are different.

TEMPORAL RESHAPING OF ULTRASHORT PULSES REFLECTED BY GaAs

I.H. Campbell, S.K. Kirby and P.M. Fauchet

Princeton Laboratory for Ultrafast Spectroscopy
Department of Electrical Engineering
Princeton University, Princeton NJ 08544

Femtosecond or picosecond pulses undergo dramatic temporal reshaping after reflection from a semiconductor surface, provided that the angle of incidence is close to Brewster's angle. For GaAs and laser frequencies in the near infrared, pulse breakup and increase in duration from 100 femtoseconds to many picoseconds is easily achieved. The sensitivity of the effect to the GaAs parameters, especially the exciton resonance in the dielectric function, suggests a novel type of experiments.

Since the introduction of the dispersion compensated, colliding pulse modelocked (CPM) dye laser [1], the field of femtosecond phenomena has experienced tremendous growth. Femtosecond pulses have a large bandwidth, which has forced the re-examination of previously well-accepted concepts. For example, after reflection from a multiple-layer dielectric coating, significant pulse distorsion has been measured [2]. On the other hand, it is still accepted that single nonlinear interfaces do not alter the pulseshape. We have introduced a method for enhancing the sensitivity of time-resolved reflectivity measurements in solids [3]. By performing experiments close to Brewster's angle, we have been able to study the lifetime of carriers [3,4] and the dynamics of picosecond laser-induced phase transitions [5-7] in silicon with approximately one order of magnitude increase in sensitivity.

Near Brewster's angle θ_B, a small change in refractive index n leads to a large change in the amplitude and phase of the reflectivity, as shown in Figure 1. When a short pulse is incident near θ_B and its wavelength is near a resonance. the various frequency components have different reflectivities, and thus the reflected pulse can be reshaped. It seems clear that the effect will be more pronounced near a strong and narrow resonance. In order to quantify the importance of the effect, we have considered GaAs in the neighborhood of the exciton resonance [8]. The dielectric function $\epsilon(\omega)$ is given by

$$\epsilon(\omega)=\epsilon_\infty+\frac{\omega_p^2}{\omega_o^2-\omega^2+j\gamma\omega} \qquad (1)$$

At low temperature for high quality GaAs, $\epsilon_\infty = 12.35$, $\omega_p = 0.2$ eV, $\omega_o = 1.51389$ eV and $\gamma = 0.266$ meV. The reflectivity $r(\omega,\theta)$, where $R=rr^*$, is given by the Fresnel reflection coefficient [9]. The reflected electric field is given by the inverse Fourier transform of $F(\omega)r(\omega,\theta)$, where F is the Fourier transform of the incident electric field. The validity of this simple model is justified in Ref. 8.

In Figure 2, we show a series of reflected pulseshapes calculated for the following default conditions: $\theta-\theta_B=-10^{-4}$ degrees, $\tau_p=100$ fs (the input pulse is a sech^2), $\omega_{laser}-\omega_o=-100$ meV, and for GaAs, the parameters mentioned above. The proximity to Brewster's angle, the pulse duration, the width of the resonance, and the detuning between the laser and the resonance all affect the reflected pulseshape. The dominant factor in the reshaping is the phase shift that occurs between the low and high frequency components of the incident pulse. When the $\sim 180°$ phase shift occurs in the wing of the spectrum or when the total phase shift across the entire spectrum is much less than 180° (i.e., when γ exceeds the input pulse bandwidth), very little reshaping is observed. When two sharp phase changes, each by 180°, exist within the pulse spectrum, the reflected pulseshape breaks up into many peaks. This is observed when the incident pulse near Brewster's angle is near resonance. A rough analogy with a bandpass filter is possible. As the filter becomes narrower, it can no longer support very short pulses and the reflected pulse is lenghtened.

The tremendous lenghtening of the reflected pulse and its oscillatory behavior are best seen in the semi-logarithmic plot of Figure 3. Here, we plot the reflected pulse up to 20 ps after the 100 fs long incident pulse has hit the surface of GaAs. As the detuning decreases from -100 meV to -0.1 meV, the shape and duration of the tail change. The oscillatory behavior is similar to the results of very recent calculations [10]. It is clear that this reshaping is observable in experiments involving either autocorrelation of the reflected pulse or cross-correlation with part of the incident pulse. To our knowledge, there has been no report yet of such measurements. If, instead of considering a short pulse, we consider a strongly focussed beam, related *spatial* reshaping takes place. Provided that $\theta\sim\theta_B$, the spread in **k**-vectors can be such that different components have different reflectivities, leading to reshaping across the wavefront. We have performed simple angle resolved reflectivity measurements using a cw HeNe and verified the good agreement with calculations [11]. The similarity between temporal and spatial reshaping is another example of the well-known space-time analogy in electromagnetism.

In conclusion, we have shown that reflection from a simple linear interface can lead to temporal distorsion. The conditions that must be met to produce measurable reshaping have been investigated. They explain why the effect has not been reported so far and has not been a factor in our time-resolved experiments [3-7]. On the other hand, the sensitivity of the reshaping on the parame-

ters of the material suggests that by measuring the time evolution of the reflected pulse, it should be possible to learn the properties of the reflector.

This research was supported by the U.S. Army Research Office (DAAL03-87-K-0145) with additional support from the National Science Foundation through the Presidential Young Investigator program (ECS-8657263). P.M. Fauchet is an Alfred P. Sloan research fellow.

REFERENCES

1 J.A. Valdmanis, R.L. Fork and J.P. Gordon, Opt. Lett.**10**, 131, 1985
2 A.M. Weiner, J.G. Fujimoto and E.P. Ippen, Opt. Lett.**10**, 71, 1985
3 P.M. Fauchet and W.L. Nighan Jr., Appl. Phys. Lett.**48**, 721, 1986
4 N.K.Bambha, W.L. Nighan Jr., I.H. Campbell, P.M. Fauchet and N.M. Johnson, J. Appl. Phys.**63**, 2316, 1988; Mat. Res. Soc. Symp. Proc.**106**, 323, 1988
5 K.D. Li and P.M. Fauchet, Solid State Commun.**61**, 207, 1987
6 K.D. Li and P.M. Fauchet, Appl. Phys. Lett.**51**, 1747, 1987
7 P.M. Fauchet and K.D. Li, J. Non-Cryst. Solids**97&98**, 1267, 1987; Mat. Res. Soc. Symp. Proc.**100**, 477, 1988
8 I.H. Campbell and P.M. Fauchet, Opt. Lett.**13**, 634, 1988
9 E. Hecht and A. Zajac, *Optics*, Addison-Wesley, Reading, 1979, Ch. 4
10 J. Aaviksoo, J. Lippmaa and J. Kuhl, J. Opt. Soc. Am.**5**, 1631, 1988
11 P.M. Fauchet, "Enhanced sensitivity of time-resolved reflectivity measurements near Brewster's angle", submitted to IEEE J. Quantum Electron.

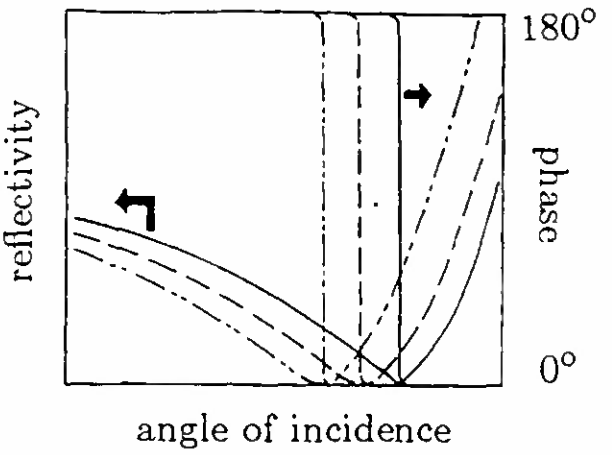

Fig. 1 Amplitude and phase of the reflectivity vs angle of incidence for large (full line) and small (dot-dashed line) index of refraction

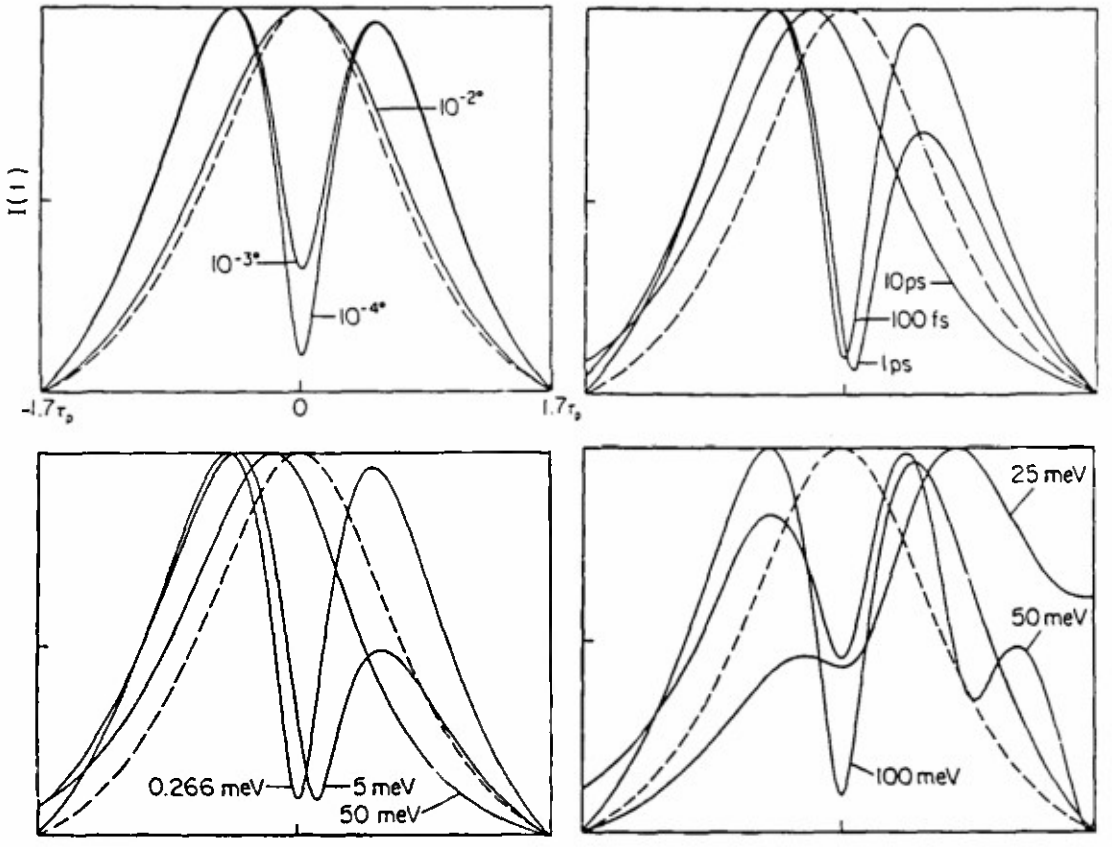

Fig. 2 Calculated pulseshapes for different values θ-θ_B, τ_p, γ, and ω_o-ω_{laser}. The dashed line shows the input pulse. All the curves are normalized. See the text for details.

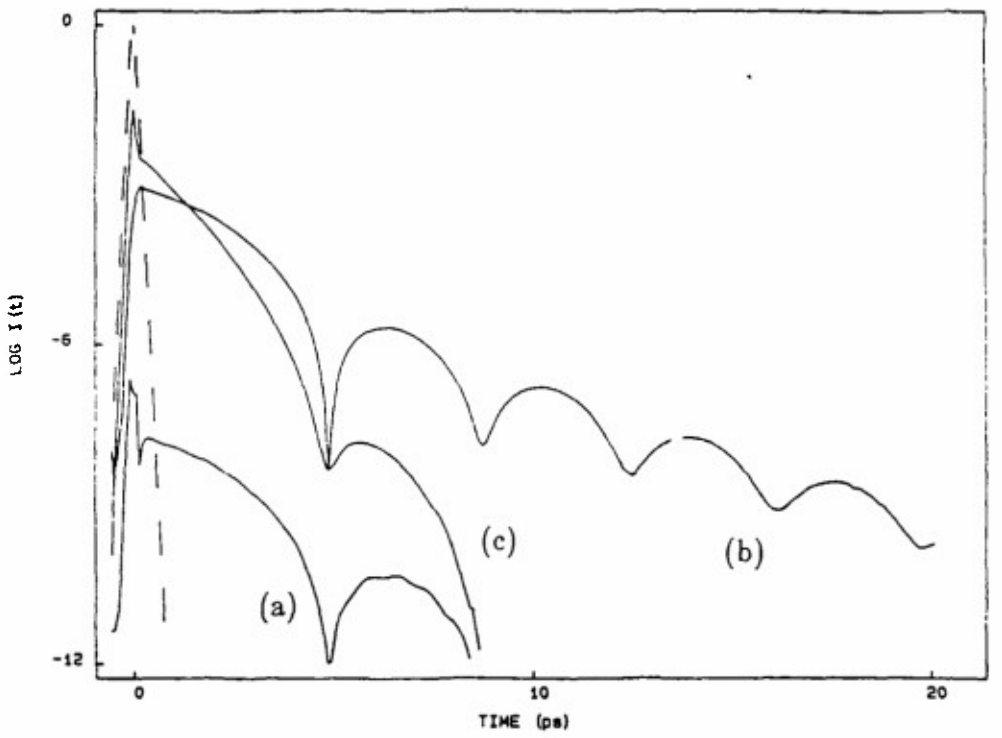

Fig. 3 Semilogarithmic plot of the reflected intensity as a function of time. The incident pulse is shown by the dashed line. The default values discussed in the text are assumed, except for the detuning which is (a) 50 meV, (b) 10 meV, and (c) 0.1 meV.

Enhanced Sensitivity of Time-Resolved Reflectivity Measurements Near Brewster's Angle

PHILIPPE M. FAUCHET

Reprinted from
IEEE JOURNAL OF QUANTUM ELECTRONICS
Vol. 25, No. 5, 1989

Enhanced Sensitivity of Time-Resolved Reflectivity Measurements Near Brewster's Angle

PHILIPPE M. FAUCHET

Abstract—A method for enhancing the sensitivity of time-resolved reflectivity measurements in semiconductors is proposed, analyzed, and demonstrated. By appropriate choice of the angle of incidence near Brewster's angle, the photoinduced reflectivity changes are easily increased by one order of magnitude. Two examples, the lifetime of a dense electron-hole plasma and the picosecond laser-induced melting transition in silicon, illustrate the method. Extension to the case of thin films is possible, as demonstrated by experiments performed on thin polycrystalline silicon films. Possible complications due to the use of very tightly focused beams and ultrashort pulses near a strong resonance are considered and, together with other considerations of a more experimental nature, lead to general guidelines for signal enhancement and easy implementation and data analysis.

I. Introduction

REFLECTIVITY (R) measures many important parameters of solids such as semiconductors. The implementation varies from the simplest (power R measured near normal incidence at a fixed wavelength) to very sophisticated (spectroscopic ellipsometry [1]). In contrast to transmission measurements, which are also usually simple to perform, the sample can be either transparent or opaque, and need not be thinned down, in which case the measurement would no longer be nondestructive.

In many situations, the time evolution of the optical properties of a sample must be monitored. Examples include studies of carrier lifetime [2], hot carrier relaxation [3], or laser-induced phase transitions [4]. In pump and probe R measurements, a short laser pulse (the pump) produces a change in the properties of the sample and another short laser pulse (the probe) that is synchronized with the pump pulse measures R as a function of the time delay between the two pulses. Experiments of this type are routinely performed with pulses (and time resolution) much shorter than 100 fs [5].

Several generic problems arise with this type of time-resolved experiments. First, the laser wavelength is usually limited to one or a few discrete values. This usually makes an unambiguous interpretation of the data difficult. Second, the experiments are usually performed with the probe beam incident at a fixed angle, typically close to normal incidence ($\theta = 0°$). Correct interpretation of the data is sometimes difficult and the magnitude of the transients is usually small. Third, small transient changes of the optical properties translate into small changes of R near $\theta = 0°$, and this limits our ability to improve the signal-to-noise (S/N) ratio, especially in low repetition rate experiments or to detect changes under lower excitation density. These considerations have led us to develop new ways to lift ambiguities and to increase the S/N ratio, while keeping the experimental arrangement as simple as possible. The solution we propose and demonstrate is to perform experiments near Brewster's angle ($\theta = \theta_B$), and, if necessary, to repeat the measurement at one or more additional angles of incidence near θ_B.

This paper is organized as follows. First, we perform a simple analysis of the technique for realistic situations. Then, we consider two concrete examples, the lifetime of a dense plasma in Si and the melting phase transition of Si. Next, we discuss the extension to thin films and various considerations which may play a role in some specific situations. Finally, we conclude by a brief comparison to other methods and a summary.

II. A Simple Analysis

Let us consider a solid with dielectric function $\tilde{\epsilon} = \epsilon_R - i\epsilon_I$ or index of refraction $\tilde{n} = n - ik$, with $\tilde{n} = (\tilde{\epsilon})^{1/2}$. R is calculated from the Fresnel coefficient r_p for any angle of incidence θ:

$$r_p = \frac{\cos\theta_1 - \tilde{n}\cos\theta}{\cos\theta_1 + \tilde{n}\cos\theta} \tag{1}$$

where $\sin\theta_1 = \sin\theta/\tilde{n}$. For p (TM) polarization, R ($= r_p \cdot r_p^*$) has a minimum at Brewster's angle $\theta_B = \arctan(n)$, as shown in Fig. 1. Several methods, based on the measurement of R at two angles, allow the determination of n and $\alpha = 4\pi k/\lambda$ [6]. Here we want to measure a *change* in $\tilde{n}$ or $\tilde{\epsilon}$ produced by a laser pulse. For example, absorption of photons across the bandgap E_g generates an electron-hole plasma of density N. For probe photon energy below E_g, the changes in optical properties can be described by a Drude model. Both real and imaginary parts of $\tilde{n}$ change and the ratio is given by $\Delta k/\Delta n = \omega\tau$ where $\hbar\omega$ is the photon energy and τ is the scattering time. In the usual limit where $\omega\tau >> 1$, $\Delta\alpha$ can be neglected. The change in the real part of the index becomes $\Delta n =$

Manuscript received August 30, 1988; revised October 18, 1988. This work was supported by the Office of Naval Research under Contract N00014-86-K-0711, the U.S. Army Research Office under Contract DAAL03-87-K-0145, and the National Science Foundation through the Presidential Young Investigator Program under Grant ECS-8657263. The author is also supported by an Alfred P. Sloan Research Fellowship.

The author is with the Princeton Laboratory for Ultrafast Spectroscopy, Department of Electrical Engineering, Princeton University, Princeton, NJ 08544.

IEEE Log Number 8926859.

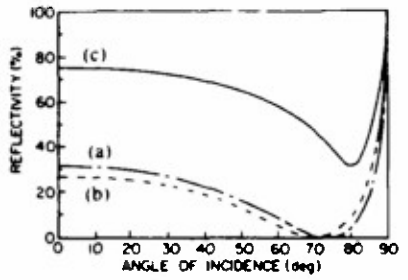

Fig. 1. Reflectivity R versus angle of incidence θ for p-polarized, 1.06 μm beam for (a) silicon, (b) silicon in the presence of a dense plasma, and (c) molten silicon.

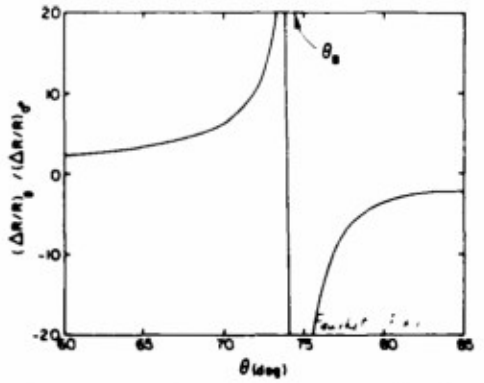

Fig. 2. Relative changes of R normalized to that for $\theta = 0°$ versus θ for silicon at 1.06 μm in the presence of 10^{20} carriers/cm^3, calculated neglecting k.

$\omega_p^2/2\omega^2 n$ (where ω_p is the plasma frequency, given by $\omega_p^2 = Ne^2/m\epsilon_0$, with e the charge of the electron, m the effective electron-hole plasma mass, and ϵ_0 the dielectric function of vacuum) and is negative. The curve R versus θ is modified as shown in Fig. 1.

Inspection of the figure indicates that for a given Δn, the magnitude of $\Delta R/R$ will increase as θ_B is approached. The sign of ΔR also changes as Brewster's angle is exceeded. In order to make the analysis more concrete, consider Si at 1.06 μm. Its index of refraction is 3.56. When 10^{20} carriers/cm^3 are injected, n decreases to 3.466. In Fig. 2, we plot $(\Delta R/R)_\theta/(\Delta R/R)_0$ as a function of θ for $N = 10^{20}$ cm^{-3} or $\Delta n/n = -2.6$ percent. The enhancement becomes very large between 70° and 80°, in the neighborhood of $\theta_B = 74.3°$. As we will discuss later, some surprising effects may arise very close to Brewster's angle, especially with tightly focused beams or very short pulses. In addition, some practical considerations suggest that a region of one to two degrees around θ_B should be avoided in routine characterization for the following reasons: 1) when R is very small, surface roughness and sources of unavoidable noise prevent R from reaching its true value; 2) when R changes rapidly, any uncertainty in the determination of θ leads to large errors; 3) as N varies during the experiment, the instantaneous Brewster's angle may swing from one side to the other side of the angle of incidence, leading to oscillations in R and potentially to confusing results; 4) the theoretical lower bound of R very close to θ_B is set by k: for Si at 1.06 μm, the free carrier absorption cross section [7] is such that even for $N = 10^{20}$ cm^{-3}, k would affect the result only for $R \ll 10^{-3}$, whereas for metals or any other solid with large k, R only has a broad minimum (that could be as large as 50 percent) at an angle called the pseudo-Brewster's angle.

III. Examples

In this section, we consider two examples. First, the generation and recombination of a dense electron-hole plasma in crystalline Si is monitored with picosecond pulses from a Nd:YAG laser. This corresponds to a small Δn and $k = 0$. Second, the solid-liquid phase transition produced in Si by an intense ps pulse is characterized. This corresponds to large Δn and large Δk.

A. Electron-Hole Plasma

After injection of electrons and holes close to the surface of a semiconductor, several phenomena can take place including radiative or nonradiative recombination, diffusion into the bulk or laterally, and trapping at the surface. In contrast to GaAs, where radiative recombination and trapping due a very large surface recombination velocity are predominant, in Si, "bulk" recombination is often responsible for a decrease in the carrier density close to the surface. In our experiments, which are performed on a many picosecond time scale and with a plamsa density in the 10^{20} cm^{-3} range, Auger recombination controls the carrier dynamics. By performing our measurements a few degrees below or above θ_B, we can easily enhance the signal by a factor of 5 or 10 compared to near-normal incidence measurements. In order to measure the Auger recombination coefficient γ with a probe beam at 1.06 μm and a laser repetition rate of 10 Hz, such an enhancement is necessary. For example, in experiments performed near-normal incidence, R dropped by only 10-20 percent for $N \sim 5 \times 10^{20}$ cm^{-3} and recovered to its initial value within the accuracy of the measurement in less than 50 ps [8].

In Fig. 3, we show some typical results [9] for injection of approximately 3×10^{20} cm^{-3} in a silicon wafer for $\theta < \theta_B$ and for $\theta > \theta_B$ (in all figures, the choice of $t = 0$ is arbitrary). Those angles were chosen for easy experimental implementation and for significant signal enhancement. As expected from the analysis of Fig. 2, the sign of ΔR is different for those two angles. Despite the moderate S/N ratio in this experiment, the signal was enhanced enough that a fit to the data allowed extraction of the Auger recombination coefficient γ in the presence of a large carrier density ($\sim 10^{20}$ cm^{-3}). We find that $\gamma = 2 \times 10^{-31}$ cm$^6 \cdot$ s^{-1}. This value is a factor of two smaller than a widely accepted value, obtained at much lower density [10]. A strong reduction of γ in the presence of high-density plasmas has been predicted [11], [12] and measured [13] in direct gap semiconductors. It is very likely that a similar effect is taking place in Si. The smaller

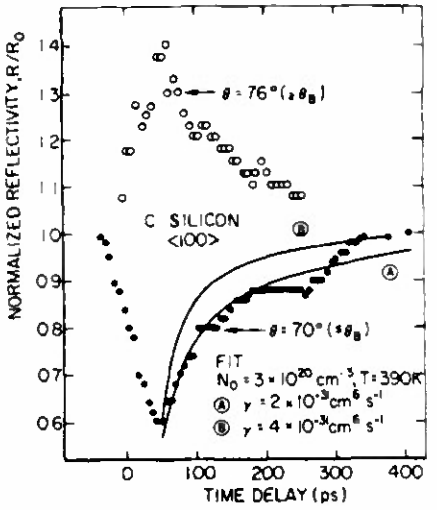

Fig. 3. Reflectivity changes at 1.06 μm above and below θ_B for silicon injected with $N \sim 3 \times 10^{20}$ cm^3. The fits are explained in the text and include the effect on n of a temperature rise to 390 K.

reduction is probably due to the combined effect of a much larger effective mass and of an indirect gap.

B. Laser-Induced Melting

Several groups have investigated ultrafast laser-induced melting of Si by monitoring R on a nanosecond to femtosecond time scale [4], [8], [14], [15]. Molten Si is a metal [16]. In the near infrared and visible parts of the spectrum, near-normal incidence R approximately doubles upon melting [8], [14]. The irreversible nature of melting and of most other destructive photoinduced effects limits data accumulation, and thus the S/N achievable in practice. As shown in Fig. 1, $\Delta R/R$ becomes very large as $\theta \sim \theta_B$. The very large k of molten Si prevents R from decreasing much as θ approaches the pseudo-Brewster's angle. Since k and thus Δk are large, it is necessary to measure R at a minimum of two angles to determine both n and k [17].

In Fig. 4, we show picosecond R measurements at several angles, showing clearly the dramatic enhancement of the S/N ratio close to θ_B. From such results, we have obtained the complex dielectric function of molten Si and monitored some interesting aspects of the nonequilibrium phase transition. Approximately 100 ps after excitation, the molten layer is optically thick and close to the melting temperature T_m, provided that the pump energy does not exceed the melting threshold by more than 50 percent. The plateau observed at longer times is thus a good measure of $\tilde{\epsilon}$. From data taken at 1064, 532, and 355 nm, we find that molten Si is a Drude metal with $\omega_p = 2.5 \times 10^{16}$ rad/s and $\tau = 212 \times 10^{-18}$ s [18]. Our values agree very well with other measurements, performed using CW spectroscopic ellipsometry on a pool of molten silicon [19] or using monochromatic nanosecond time-resolved ellipsometry during melting produced by an ns-long pulse [20]. Other measurements, using spectroscopic nanosecond time-resolved ellipsometry, have given different values

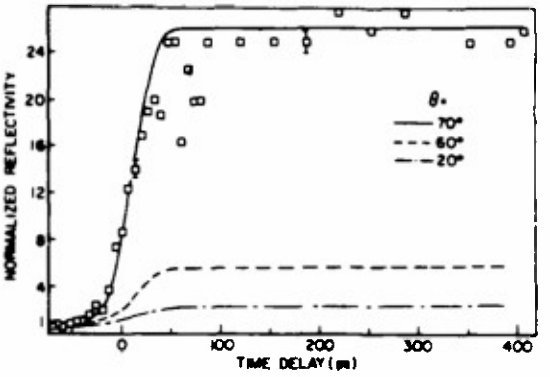

Fig. 4. Reflectivity jump due to melting of silicon, measured at 1.06 μm for three angles of incidence. The lines are the fits to the data.

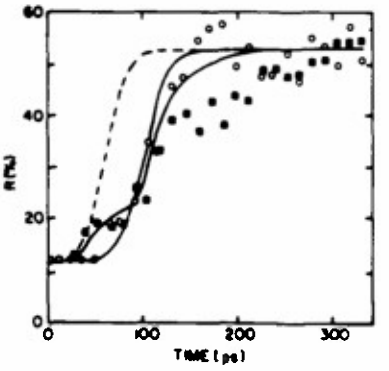

Fig. 5. Reflectivity jump at 532 nm due to melting of silicon, measured at 60° and for two pump energies just above threshold E_T (□) and $\sim 4 \times E_T$ (■). The full lines are obtained from a computer simulation which includes heating of the liquid, while the dashed line assumes that the temperature never exceeds T_m for the higher pump energy.

[21]. Possible reasons for this discrepancy are discussed elsewhere [18]. Note that our values are consistent with four electrons per Si atom and a mass equal to the free electron mass, which is generally expected of Si.

If the pump energy is increased well above threshold, part of the additional energy heats up the liquid layer to temperatures well beyond T_m. The optical properties of metals change as a function of temperature because τ decreases. Again, especially close to θ_B, R should be strongly affected. We have indeed been able to observe unambiguously heating of the liquid Si layer as a function of excitation energy [23], [24]. Typical results are shown in Fig. 5. A kink is observed during the R rise. It is the signature of a hot liquid which, however, cools rapidly towards T_m because of heat diffusion into the much cooler bulk. Our model predicts that the instantaneous R reaches the value for molten Si at T_m, then decreases as more pump energy is deposited into the liquid layer, and finally recovers to that same value. The time resolution of this experiment (30–50 ps) was not enough to observe the dip. After convolution with the finite probe pulse duration, this dip becomes a kink. Using a one-dimensional code, we have been able to show that at $\sim$ four times threshold, the boiling temperature is exceeded for ~ 10 ps in a thin (~ 20 nm) surface layer and yet no ablation is observed

[24]. Superheating of the liquid phase without bubble nucleation and material ejection has recently been confirmed using a streak camera [25]. Our measurements open new possibilities for the study of nonequilibrium phase transitions [26].

IV. Discussion

In the previous sections, we have demonstrated that a large signal enhancement is obtained by performing measurements close to θ_B and that a simple analysis could be used to fit the data. In this section, we investigate the important situations where such a simple analysis breaks down. These are experiments on thin films, with strongly focused beams and near a strong resonance in $\tilde{\epsilon}$.

A. Thin Films

Thin films are an integral part of modern technology. Because the optical constants of the film(s) and of the substrate differ, multiple reflections alter the reflectivity. Pump and probe R experiments can no longer be analyzed using the analysis of Section II. It has long been recognized that interference effects can be used advantageously to enhance R changes [27]. We have used a straightforward extension of our method developed for semi-infinite samples to the study of thin films of Si on SiO_2 (SOI) deposited on a Si substrate. Consider the measured R versus θ curves shown in Fig. 6 for a Si wafer and for an SOI sample having a ~ 1 μm thick polycrystalline Si film on top. There is an angle at which R is minimum for the SOI sample. This angle will replace Brewster's angle for experiments with thin films. In the analysis of the data, the Fresnel coefficient of (1) is replaced by the appropriate thin film equations [28].

Fig. 7 demonstrates the validity of the concept for thin films. The three curves are taken for θ smaller than, approximately equal to, and greater than the angle of minimum R, θ_{min}. The sign and magnitude of ΔR change as expected for the choice of angles. Note the oscillatory behavior of R for $\theta \sim \theta_{min}$, which is related to that noted in Section II for semi-infinite samples. We have carried out experiments on a series of SOI samples, which had been treated in various ways, and we have analyzed our results using the thin-film equations, and accounting for carrier trapping at grain boundaries and for heating by emission of phonons [29], [30]. Thanks to the enhanced sensitivity of the technique, we have been able to extract the trapping time in as-grown samples, in ion-implanted samples following different annealing schedules, and in H-diffused samples. Annealing increases the trapping time if the grain size is increased, heavy doping with phosphorous does not affect the trapping time if the grain size is unaffected, and the presence of hydrogen increases the trapping time through passivation of the traps at the grain boundaries. In addition, we have established that, on average, the traps are rather shallow and that recombination of the trapped carriers does not occur immediately following trapping (the delay is at least several hundred ps). If we accept that

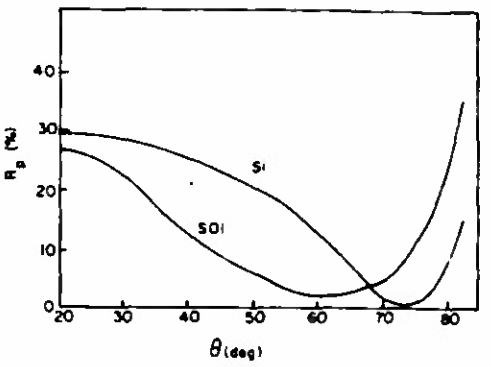

Fig. 6. Measured reflectivity at 1.06 μm for a silicon wafer and an SOI sample having a ~ 1 μm thick polycrystalline layer on top.

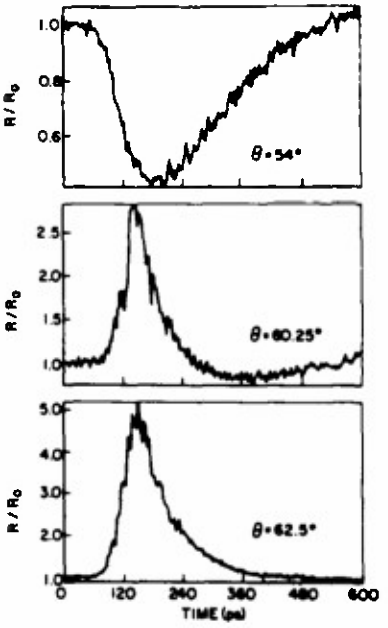

Fig. 7. Reflectivity changes measured at 1.06 μm in a processed SOI sample injected with $N \sim 10^{20}$ cm^{-3}, measured at 1.06 μm and three different angles of incidence.

the density of states at the grain boundaries is similar to that of amorphous silicon [31], this new result is consistent with recent femtosecond experiments performed on a-Si:H [2], [32], [33].

B. Strongly Focused Beams

The analysis so far has been carried out for plane waves. In practice, however, the beams have a Gaussian transverse profile. The probe beam, which must be smaller than the pump beam to insure uniform excitation, can be very tightly focused. The k vectors of the incident probe beam have then a distribution around the beam axis related to the spot size of the beam through $A(k_x) \sim \exp[-(k_x w_0/2)^2]$ where the incident beam is decomposed into plane wave components with amplitude A and wavenumbers k_x and k_z ($k_x = 0$ for the on-axis component), and w_0 is the spot size at the waist, which is located on the surface [34]. Each plane wave component sees a dif-

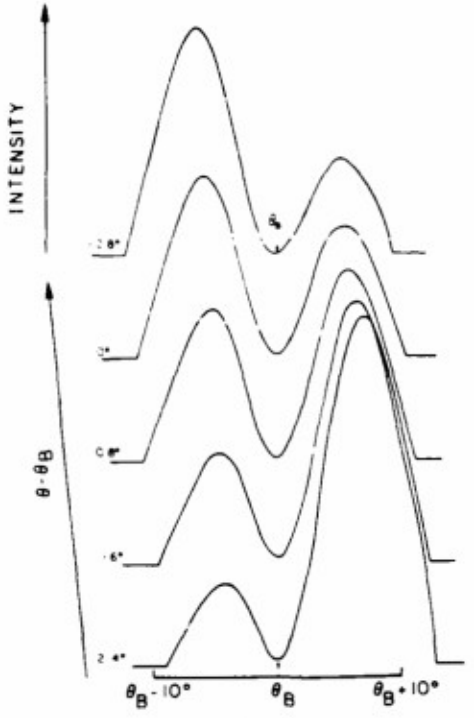

Fig. 8. Angular dependence of the reflectivity of an HeNe laser beam focused to ~ 1 μm on silicon as a function of the relative angle between the beam axis and Brewster's angle.

ferent Fresnel coefficient and the reflected signal is thus given by the Fourier transform of the product $r_p(\theta) \cdot A(k_x)$. It is clear that the magnitude and the transverse profile of the reflected beam will be more strongly affected for more tightly focused beams.

To illustrate the limitations, we performed a very simple experiment which consisted of focusing a CW HeNe laser beam to a 1 μm spot on a Si wafer and measuring the angular distribution of the reflected beam with a photomultiplier [35]. In Fig. 8, we show some results obtained with the beam axis close to Brewster's angle. The transverse reshaping of the reflected beam is quite dramatic and can be fitted very well using the beam parameters, the optical constants of Si, and the Fresnel coefficient. Several implications are clear. First, special care must be taken in the collection and detection of the reflected beam. In fact, there is an angular shift of the reflected beam [34]. Second, the interpretation of time-resolved R measurements becomes almost impossible when different parts of the incident beam effectively sample completely different signals, both in magnitude and in sign. Clearly, this situation is to be avoided. In practice, if $w_0 = \gtrsim 20\lambda$ and $|\theta - \theta_B| > 1°$, the simple analysis of Section II holds. If tighter focusing is required, the experiment must be performed farther from Brewster's angle.

C. Strong Resonance

It is very frequently desirable to follow the carrier dynamics of a picosecond or femtosecond time scale. If the probe pulse is sufficiently short, temporal reshaping can take place. The analysis is analogous to that outlined above. The incident pulse is decomposed in its plane wave Fourier components $F(\omega)$, each component sees a differ-

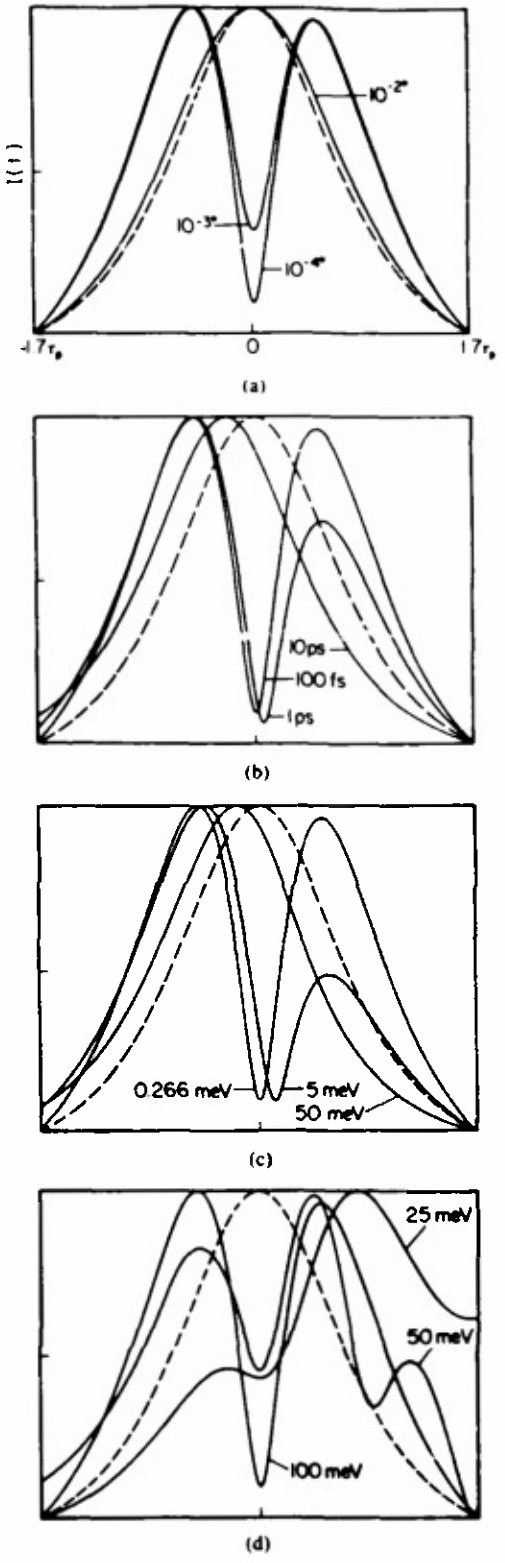

Fig. 9. Normalized reflected pulses from GaAs near its exciton resonance. The default conditions are $\Delta\theta = 10^{-4}$°, $\tau_p = 100$ fs, $\gamma = 2.66 \times 10^{-4}$ eV, and $\Delta\omega = 0.1$ eV. The dashed line shows the incident pulse.

ent Fresnel coefficient, provided that $\tilde{n}$ is frequency dependent in that spectral region, and the reflected signal is given by the Fourier transform of the product $F(\omega) \cdot r_p(\omega)$. Temporal reshaping will be stronger close to θ_B because both the phase and the amplitude of the Fresnel coefficient vary rapidly with $\tilde{n}$.

To illustrate this reshaping, we have carried out numerical simulations of the reflectivity of ultrashort pulses with frequencies close to the GaAs exciton absorption region [36]. Fig. 9 shows some typical results. In general, reshaping becomes noticeable if θ is very close to θ_B, the pulse is very short ($\tau_p <<$), the resonance is very strong and narrow ($\gamma <<$), or the detuning between the laser frequency and the resonance is small ($\Delta\omega <<$). When the amplitude and phase of the Fresnel coefficient change significantly in a frequency region defined by the pulse spectrum, strong reshaping takes place [36]. The magnitude of the reshaping and its sensitivity to the properties of the sample suggest that careful experiments involving, for example, cross correlation of the reshaped, reflected pulse with part of the incident probe pulse would yield interesting information. However, if the total reflected energy is measured, as it is in nearly all experiments, interpretation of time-resolved R measurements becomes very complicated and reshaping is to be avoided in routine laser diagnostics. If $|\theta - \theta_B| > 1°$, and the pulse spectrum does not overlap with the resonance, temporal reshaping can be avoided. In silicon, where there is no excitonic resonance, temporal reshaping is never observed in practice.

V. Conclusions

We have proposed, analyzed, and demonstrated a method for enhancing the sensitivity of time-resolved reflectivity measurements, which was suggested by earlier experiments [37]. By remaining $-1°$ away from Brewster's angle, away from sharp resonances, and by not focusing the probe beam too tightly, the experiments are very easily implemented and analyzed. Time-resolved ellipsometry [20], [21], [38], [39] is also a very useful method, but its implementation is more complicated and the analysis more involved. The simplicity of our method suggests that it can be applied to routine laser diagnostics of semiconductors in an industrial environment. In fact, an apparatus which uses the same principles but without time resolution so far has been developed and is being used for high-spatial-resolution nondestructive testing of wafers [40].

Acknowledgment

I thank B. Nighan, I. Campbell, K. Li, and N. Bambha who all contributed to this research.

References

[1] D. E. Aspnes, "The accurate determination of optical properties by ellipsometry," in *Handbook of Optical Constants of Solids*, E. D. Palik, Ed. Orlando: Academic, 1985, ch. 5.

[2] P. M. Fauchet, D. Hulin, A. Migus, A. Antonetti, J. Kolodzey, and S. Wagner, "Initial stages of trapping in a-Si:H observed by femtosecond spectroscopy," *Phys. Rev. Lett.*, vol. 57, pp. 2438-2441, 1986.

[3] J. L. Oudar, D. Hulin, A. Migus, A. Antonetti, and F. Alexandre, "Subpicosecond spectral hole burning due to nonthermalized photoexcited carriers in GaAs," *Phys. Rev. Lett.*, vol. 55, pp. 2074-2077, 1985.

[4] M. C. Downer, R. L. Fork, and C. V. Shank, "Femtosecond imaging of melting and evaporation at a photoexcited silicon surface," *J. Opt. Soc. Amer.*, vol. B2, pp. 595-599, 1985.

[5] P. C. Becker, R. L. Fork, C. H. Brito Cruz, J. P. Gordon, and C. V. Shank, "Optical Stark effect in organic dyes probed with optical pulses of 6-fs duration," *Phys. Rev. Lett.*, vol. 60, pp. 2462-2464, 1988.

[6] W. R. Hunter, "Measurement of optical constants in the vacuum ultraviolet spectral region," in *Handbook of Optical Constants of Solids*, E. D. Palik, Ed. Orlando: Academic, 1985, ch. 4.

[7] K. G. Svantesson and N. G. Nilson, "Determination of the temperature dependence of free carrier and interband absorption in silicon at 1.06 μm," *J. Phys. C: Solid State Phys.*, vol. 12, pp. 3837-3842, 1979.

[8] D. von der Linde and N. Fabricius, "Observation of an electronic plasma in picosecond laser annealing of silicon," *Appl. Phys. Lett.*, vol. 41, pp. 991-993, 1982.

[9] P. M. Fauchet and W. L. Nighan, Jr., "Recombination mechanisms in Si and Si thin films determined by picosecond reflectivity near Brewster's angle," *Appl. Phys. Lett.*, vol. 48, pp. 721-723, 1986.

[10] J. Dziewior and W. Schmid, "Auger coefficients for highly doped and highly excited silicon," *Appl. Phys. Lett.*, vol. 31, pp. 346-348, 1977.

[11] A. Haug, "Carrier density dependence of Auger recombination," *Solid State Electron.*, vol. 21, pp. 1281-1284, 1978.

[12] C. Tanguy and M. Combescot, "Direct Auger recombination in degenerate direct gap semiconductors," *Solid State Commun.*, vol. 57, pp. 539-541, 1986.

[13] P. M. Fauchet, "The Auger rate in highly excited indium antimonide," *Phys. Status Solidi (b)*, vol. 110, pp. K11-K15, 1982.

[14] D. H. Auston, C. M. Surko, T. N. C. Venkatesan, R. E. Slusher, and J. A. Golovchenko, "Time-resolved reflectivity of ion-implanted silicon during laser annealing," *Appl. Phys. Lett.*, vol. 33, pp. 437-440, 1978.

[15] J. M. Liu, H. Kurz, and N. Bloembergen, "Picosecond time-resolved plasma and temperature-induced changes of reflectivity and transmission in silicon," *Appl. Phys. Lett.*, vol. 41, pp. 643-646, 1982.

[16] V. M. Glazov, S. N. Chizhevskaya, and N. N. Glagoleva, *Liquid Semiconductors*. New York: Plenum, 1969.

[17] K. D. Li and P. M. Fauchet, "Picosecond determination of the dielectric function of liquid silicon," *Solid State Commun.*, vol. 61, pp. 207-209, 1987.

[18] ——, "Drude parameters of liquid silicon at the melting temperature," *Appl. Phys. Lett.*, vol. 51, pp. 1747-1749, 1987.

[19] K. M. Shvarev, B. A. Baum, and P. V. Gel'd, "Optical properties of liquid silicon," *Sov. Phys. Solid State*, vol. 16, pp. 2111-2112, 1975.

[20] G. M. Gusakov, A. A. Komarnitskii, and S. S. Sarkisyan, "Measurement of the complex refractive index of silicon during pulsed laser annealing," *Sov. Tech. Phys. Lett.*, vol. 12, pp. 74-75, 1986.

[21] G. E. Jellison, Jr. and D. H. Lowndes, "Time-resolved ellipsometry measurements of the optical properties of silicon during pulsed excimer laser irradiation," *Appl. Phys. Lett.*, vol. 47, pp. 718-721, 1985; "Measurements of the optical properties of liquid silicon and germanium using nanosecond time-resolved ellipsometry," *Appl. Phys. Lett.*, vol. 51, pp. 352-354, 1987.

[22] K. Ujihara, "Reflectivity of metals at high temperatures," *J. Appl. Phys.*, vol. 43, pp. 2376-2383, 1972.

[23] P. M. Fauchet and K. D. Li, "The dielectric function of laser-produced molten Si," *J. Non-Cryst. Solids*, vol. 97 & 98, pp. 1267-1270, 1987.

[24] ——, "Picosecond laser induced melting: The dielectric function of molten silicon and superheating in the liquid phase," in *Mater. Res. Soc. Symp. Proc.*, vol. 100, 1988, pp. 477-481.

[25] J.-K. Wang, P. Saeta, M. Buijs, M. Malvezzi, and E. Mazur, "Single-shot reflectivity study of the picosecond melting of silicon using a streak camera," in *Ultrafast Phenomena VI*, T. Yajima, K. Yoshihara, C. B. Harris, and S. Shionoya, Eds. Berlin: Springer-Verlag, 1988, pp. 236-239.

[26] F. Spaepan, "Thermodynamics and kinetics of melting, evaporation and crystallization, induced by picosecond pulsed laser irradiation,"

in *Ultrafast Phenomena V*, G. R. Fleming and A. E. Siegman, Eds. Berlin: Springer-Verlag, 1986, pp. 174-178.
[27] K. Murakami, K. Takita, and K. Masuda, "Measurements of lattice temperature during pulsed-laser annealing by time-dependent optical reflectivity," *Japan. J. Appl. Phys.*, vol. 20, pp. L867-L870, 1981.
[28] O. S. Heavens, *Optical Properties of Thin Solid Films*. New York: Academic, 1955.
[29] N. K. Bambha, W. L. Nighan, Jr., I. H. Campbell, P. M. Fauchet, and N. M. Johnson, "Picosecond optical determination of carrier lifetime in polysilicon film," in *Mater. Res. Soc. Symp. Proc.*, vol. 106, 1988, pp. 323-327.
[30] ——, "Trapping time in processed polycrystalline silicon measured by picosecond time-resolved reflectivity," *J. Appl. Phys.*, vol. 63, pp. 2316-2321, 1988.
[31] W. B. Jackson, N. M. Johnson, and D. K. Biegelsen, "Density of gap states of silicon grain boundaries determined by optical absorption," *Appl. Phys. Lett.*, vol. 43, pp. 195-197, 1983.
[32] P. M. Fauchet, D. Hulin, A. Migus, A. Antonetti, J. P. Conde, and S. Wagner, "Femtosecond spectroscopy in amorphous silicon and silicon-germanium alloys," *J. Non-Cryst. Solids*, vol. 97 & 98, pp. 145-148, 1987.
[33] C. Tanguy, D. Hulin, A. Mourchid, P. M. Fauchet, and S. Wagner, "Free carrier and temperature effects in amorphous silicon thin films," *Appl. Phys. Lett.*, vol. 53, pp. 880-882, 1988.
[34] C. C. Chan and T. Tamir, "Angular shift of a Gaussian beam reflected near the Brewster's angle," Opt. Lett., vol. 10, pp. 378-380, 1985.
[35] P. M. Fauchet, N. K. Bambha, and I. H. Campbell, "Temporal and spatial beam reshaping on reflection near the Brewster's angle," *J. Opt. Soc. Amer.*, vol. A4, p. P101, 1987 (Abstract only).
[36] I. H. Campbell and P. M. Fauchet, "Temporal reshaping of ultrashort laser pulses after reflection from GaAs at Brewster's angle," *Opt. Lett.*, vol. 13, pp. 634-636, 1988.
[37] S. A. Jamison, A. V. Nurmikko, and H. J. Gerritsen, "Fast transient spectroscopy of the free-carrier plasma edge in Ge," *Appl. Phys. Lett.*, vol. 29, pp. 640-643, 1976.
[38] D. H. Auston and C. V. Shank, "Picosecond ellipsometry of transient electron-hole plasmas in germanium," *Phys. Rev. Lett.*, vol. 32, pp. 1120-1123, 1974.
[39] G. E. Jellison, Jr. and D. H. Lowndes, "Time-resolved ellipsometry," *Appl. Opt.*, vol. 24, pp. 2948-2955, 1985.
[40] G. E. Carver and J. D. Michalski, "Defect detection in silicon by optical beam induced reflectance (OBIR)," in *Modern Optical Characterization Techniques for Semiconductors and Semiconductor Devices*, O. J. Glembocki, F. H. Pollak, and J. J. Sung, Eds., *Proc. SPIE*, vol. 794, 1987, pp. 152-158.

Philippe M. Fauchet, for a photograph and biography, see this issue, p. 963.

Generation and control of solitons and solitonlike pulses in a femtosecond ring dye laser

W. L. Nighan, Jr., T. Gong, and P. M. Fauchet

Princeton Laboratory for Ultrafast Spectroscopy, Department of Electrical Engineering, Princeton University, Princeton, New Jersey 08544

Received November 7, 1988; accepted February 17, 1989

We control the generation of solitons and solitonlike pulses in a passively mode-locked dye laser by adjustment of group-velocity dispersion, self-phase modulation, and spectral filtering. Without spectral filtering, periodic pulse shaping reminiscent of higher-order solitons is observed. The pulses differ from the classic solitons because of additional shaping mechanisms. With spectral filtering, pulses are generated that can be described analytically as asymmetric $N = 2$ solitons. The results indicate an effect analogous to the soliton self-frequency shift observed in optical fibers. The remarkable stability achieved allows for accurate characterization and control.

Pulse shaping in the dispersion-compensated colliding-pulse mode-locked (CPM) laser has been compared to the propagation of $N = 1$ solitons in optical fibers.[1-3] The nonlinear index of the dye-jet solvent contributes to a positive self-phase modulation (SPM), while the prism sequence provides a tunable group-velocity dispersion[1,3] (GVD). Theoretical treatments of passive mode locking indicate that ultrashort-pulse formation is enhanced when these mechanisms are properly balanced.[2] The performance of the CPM laser is consistent with the predicted presence of these solitonlike shaping mechanisms.[1,3] Recent experimental observations suggest that the laser may support higher-order solitons as well.[4-6] In this Letter we demonstrate control of solitonlike pulse shaping in the CPM laser and report the properties of the pulses that we have obtained. We find that adjustments of intracavity SPM and GVD lead to pulse evolutions that share certain similarities with higher-order solitons.[7] Despite the similarities, it does not appear possible to describe the pulses in the unmodified laser as classic solitons. A simple intracavity filter leads to the generation of true $N = 2$ asymmetric solitons that are fitted with great precision by established soliton theory.[5,8] This modification inhibits an effect analogous to the soliton self-frequency shift (SSFS) observed in fibers.[9]

We have built a seven-mirror–four-prism CPM laser[1,3] that produces pulses as short as 35 fsec peaked near 633 nm. Starting from this optimized $N = 1$ solitonlike condition, we can adjust the SPM and the GVD to achieve periodic solitonlike pulse shaping, exhibiting similarities to and differences from both solitons in optical fibers and the periodic actions observed by others in CPM lasers.[4-6,10] The adjustments are as follows: (1) The SPM is increased by using a thicker region of the absorber jet (50 instead of 40 μm) and by translating the jet to within 100 μm of the intracavity focus, increasing both the interaction length and the intensity in the nonlinear medium.[11] (2) A more negative GVD is then introduced with a minute prism translation, reducing the amount of intracavity glass by ~150 μm. (3) Finally, on the slight realignment of an end mirror, a periodic pulsing condition is achieved. The normally smooth real-time autocorrelation trace (as displayed on an oscilloscope) now exhibits a rapid oscillation between extreme pulse shapes (see Ref. 7). This differs from what has been reported by others.[4-6,10]

The characteristic period of these evolutions is typically 2–5 μsec, which corresponds to 200–500 round trips of the resonator. The output pulse energy is modulated at the same frequency as the autocorrelations, with a depth of ~10%. Certain spectral components are modulated by nearly 100%, facilitating the generation of a sampling pulse train that was used to trigger the boxcar averager that sampled the raw autocorrelations. Also triggered was a high-voltage pulser that gated an optical multichannel analyzer, both from Princeton Instruments. We adjusted the phase of the sampling train relative to the spectral modulation with a digital delay and resolved the intensity autocorrelations, interferometric autocorrelations, and spectra as they evolved during the solitonlike period.

Figure 1 depicts one full 2.5-μsec period of the sampled autocorrelations and spectra of an evolution typical to this regime. Particularly notable are the interferometric autocorrelations of Fig. 1(c), which indicate two *coherent* peaks, with one peak rising as the other decays and moves away. The coherence between peaks is maintained even for separations approaching nearly 1 psec. This is unlike what was reported by Wise *et al.*, who observed no fringes in the wings of an interferometric autocorrelation attributed to a simultaneous $N = 3$ soliton and dispersive wave.[6] However, their measurement was different in that it was not time resolved with respect to the soliton period. The spectra of Fig. 1(b) are primarily single peaked early in the period, but a secondary, shorter-wavelength, feature arises and gains equal weight as the pulse evolves. The robustness, stability, and reproducibility of the condition characterized in Fig. 1 permitted an additional measurement. Salin *et al.* extended the results

0146-9592/89/090447-03$2.00/0

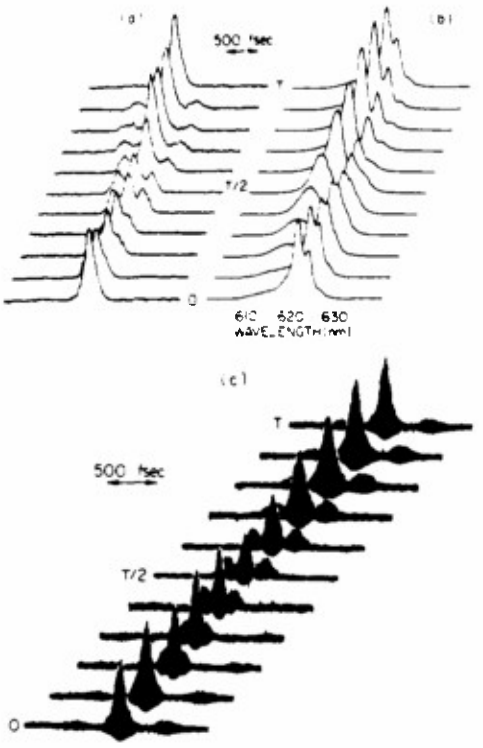

Fig. 1. Periodic pulsing condition resolved over one T = 2.5-μsec period: (a) intensity autocorrelations, (b) spectra, (c) interferometric autocorrelations.

of the nonlinear Schrödinger equation to formulate an expression for the period of a soliton in CPM laser.[4] It can be rearranged with the following result:

$$\tau^2/N_0 = 2\phi''/(0.322\pi) = 1.98\phi''. \qquad (1)$$

Implicit in Eq. (1) is the assumption that the change in pulse shape per round trip is small and that the laser may therefore be approximated as a distributed medium. We measured τ^2/N_0 versus ϕ'', as plotted in Fig. 2. The cavity dispersion ϕ'' was varied with a prism translation. N_0 was the number of round trips in the cavity corresponding to one period of the mode, and τ was taken as the FWHM of the tallest intensity autocorrelation normalized by 1.543. The plot in Fig. 2 is indeed linear, with a slope of ~2.3, compared with the predicted 1.98.

There are qualitative similarities between the evolution of Fig. 1 and that of an asymmetric N = 2 soliton.[5] Among the similarities with solitons we note (1) the relation of Fig. 2, (2) the coherence between the multiple peaks of the pulse, (3) the spectral evolution, and (4) a transition from lower- to higher-order modes accomplished by increasing the intensity in the nonlinear medium, which in this case is the absorber jet. Translating the jet 50 μm closer to the focus results in a condition reminiscent of an N = 3 soliton, featuring broad, narrow, and triple-peaked autocorrelations in its evolution.[12] These results were published elsewhere.[7] Despite these similarities, it does not appear possible to fit the results of Fig. 1 as a pure N = 2 soliton. The discrepancies include (1) the increasing temporal separation between the two peaks during the N = 2-like period and (2) the transition from N = 2-like to N = 3-like pulsing accompanied by doubling of the period from 2.5 to 5.0 μsec. It may be possible to describe these pulses as solitons perturbed by shaping effects such as saturable gain and saturable loss.[4,5,8] Avramopoulos *et al.* have included such mechanisms in numerical simulations of a ring dye laser.[10] Their results predict periodic evolutions that have certain qualitative similarities to those that we have observed. The simulated evolutions can closely resemble those of higher-order solitons when the relative magnitudes of shaping mechanisms other than a simple positive SPM and a negative GVD are reduced. An experimentally analogous simplification of the intracavity shaping mechanisms has enabled us to generate true asymmetric N = 2 solitons.

In fibers, solitons can be significantly reshaped by nonlinearities additional to the simple SPM. Specifically, for pulses of duration less than 1 psec, a stimulated Raman effect in fused silica gives rise to the SSFS, which manifests itself as a continuous downshift in carrier frequency as a soliton propagates.[9] We believe that an analog to the SSFS is observable in the CPM laser. The evidence is the long-wavelength tail that appears in the spectra of CPM pulses shorter than ~60 fsec, which often features a peak between 640 and 650 nm.[3,13] This feature may be due to an SSFS-like stimulated Raman shift in the DODCI absorber. A shift of ~620 cm^{-1} has been identified for DODCI in ethylene glycol,[14] which closely matches the energy separation between the spectral wings observed for the shortest pulses.[3,13] Schehrer *et al.* found that intracavity filtering of the long-wavelength feature did not increase the pulse length but in fact enhanced the stability of the laser.[13] The long-wavelength feature is therefore not a Fourier component of the short pulse. We interpret it as a shifted feature indicative of an effect analogous to the SSFS, which is apparently related to the onset of instability in the vicinity of the shortest pulses.

We observe similar effects in our CPM laser when we use a translatable straight edge in the prism se-

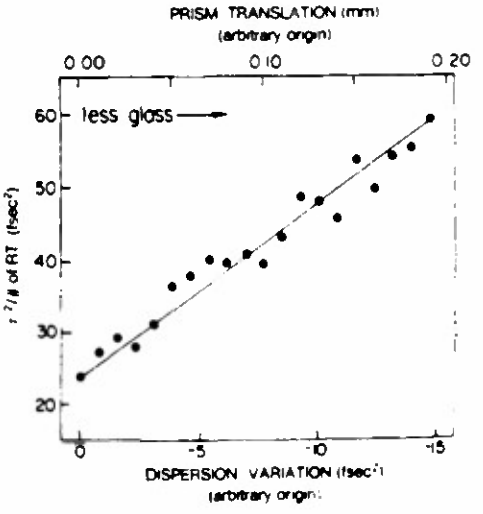

Fig. 2. Plot of the pulse duration squared over the number of round trips per period versus cavity dispersion.

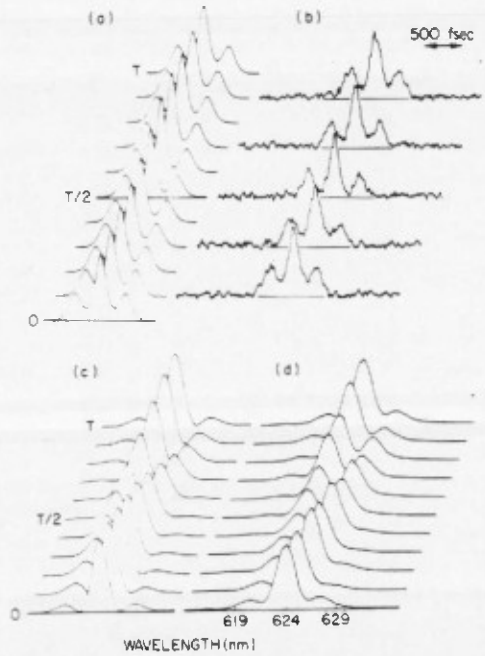

Fig. 3. Asymmetrical $N = 2$ soliton generated by using an intracavity filter. The period is 5 μsec. The soliton is described by poles $\eta_1 = 0.75$, $\eta_2 = 1.25$ and residues $c_1 = 0.3$, $c_2 = 1.1$. A sinusoidal motion has been imposed on the poles that reduces their values by 10% at midperiod and restores them at the end of one soliton period. (a) Theoretical intensity autocorrelations. (b) Experimentally observed autocorrelations. (c) Theoretical spectra. (d) Experimentally observed spectra.

quence as a long-wavelength filter.[13] Additionally, we find that the insertion of this edge filter allows the laser to operate stably for values of intracavity GVD at which it was previously unstable, namely, values closer to zero. Further, we observe pulses in this configuration that are *quantitatively* described as asymmetric $N = 2$ solitons. The procedure is as follows: (1) optimize the laser for the shortest $N = 1$-like pulses, (2) insert an edge to remove the spectral tail, and (3) add more glass by translating a prism. On the final step, the autocorrelation trace broadens, until on the addition of ~145 μm of glass it splits into three peaks, as in Fig. 3(b). A smooth, sinusoidal modulation in energy is observed in the raw pulse train, with a period of 5 μsec and a depth of ~15%. The intensity autocorrelations sampled from the period show only the subtle modulation of the "bridge" between the central peak and the adjacent peaks, but the accompanying spectral evolution of Fig. 3(d) is striking.

The experimentally observed spectra from our CPM laser with a filter are in particularly good agreement with those expected for an asymmetric $N = 2$ soliton, reproducing all the features shown in the fit of Fig. 3(c). The evolutions of Figs. 3(a) and 3(c) are those of the asymmetric $N = 2$ soliton characterized by $\eta_1 = 0.75$, $\eta_2 = 1.25$, $c_1 = 0.3$, and $c_2 = 1.1$, where these two poles and two residues characterize the soliton shape and propagation.[5,8] The energy of the soliton pulse is proportional to $(\eta_1 + \eta_2)^2$. To fit the observed energy modulation, a sinusoidal motion has been imposed on the poles, including a 10% reduction in η_1 and η_2 at midperiod, but with the net motion returning to zero after one soliton period.[5,8] This motion of the poles is not strictly solitonlike, since the unmodified nonlinear Schrödinger equation predicts a constant energy for solitons.[8] The precise cause of this slight motion is not clear. Similar pulses were observed in an unmodified CPM laser by Salin *et al.*, who fitted their results as an asymmetric $N = 2$ soliton.[5] Certain spectral features predicted by theory, notably the spectral wings expected early in the period, were not recovered in their data.

Appropriate removal or prevention of shaping mechanisms other than balanced SPM and GVD will result in a condition for the CPM that more closely approximates the soliton pulse shaping predicted by the nonlinear Schrödinger equation. We have demonstrated that asymmetric $N = 2$ solitons can be generated when an SSFS-like effect is prevented by intracavity filtering. Without the filter, periodic pulsing reminiscent of higher-order solitons is observed and controlled, but it appears that these pulses in the unmodified laser cannot be described as classic solitons. Nevertheless, a simple modification to the laser can allow soliton-shaping mechanisms to dominate, as illustrated by the generation of asymmetric $N = 2$ solitons in the research reported here.

We acknowledge support from the National Science Foundation (NSF; contracts ECS-8606531 and ECS-8657263), Coherent Inc. and the Newport Corporation through the NSF Presidential Young Investigator program, and the U.S. Army Research Office (contract DAAL03-87-K-0145). P. M. Fauchet is an Alfred P. Sloan Research Fellow.

References

1. J. A. Valdmanis, R. L. Fork, and J. P. Gordon, Opt. Lett. **10**, 131 (1985).
2. O. E. Martinez, R. L. Fork, and J. P. Gordon, Opt. Lett. **9**, 156 (1984).
3. J. A. Valdmanis and R. L. Fork, IEEE J. Quantum Electron. **QE-22**, 112 (1986).
4. F. Salin, P. Grangier, G. Roger, and A. Brun, Phys. Rev. Lett. **56**, 1132 (1986).
5. F. Salin, P. Grangier, G. Roger, and A. Brun, Phys. Rev. Lett. **60**, 569 (1988).
6. F. W. Wise, I. A. Walmsley, and C. L. Tang, Opt. Lett. **13**, 129 (1988).
7. W. L. Nighan, T. Gong, and P. M. Fauchet, in *Ultrafast Phenomena VI*, T. Yajima, K. Yoshihara, C. B. Harris, and S. Shionoya, eds. (Springer-Verlag, Berlin, 1988), p. 109.
8. H. A. Haus and M. N. Islam, IEEE J. Quantum Electron. **QE-21**, 1171 (1985).
9. F. M. Mitschke and L. F. Mollenauer, Opt. Lett. **11**, 659 (1986).
10. H. Avramopoulos, P. M. W. French, J. A. R. Williams, G. H. C. New, and J. R. Taylor, IEEE J. Quantum Electron. **QE-24**, 1884 (1988).
11. We find that the jet thickness must also be tuned to achieve the shortest $N = 1$-like pulses.
12. See, for example, R. H. Stolen, L. F. Mollenauer, and W. J. Tomlinson, Opt. Lett. **8**, 186 (1983).
13. K. L. Schehrer, E. S. Fry, and G. T. Bennett, Appl. Opt. **27**, 1910 (1988).
14. Y. G. Fuh, R. F. Code, and R. P. Wolf, J. Lumin. **26**, 329 (1982).

Reprinted from Optics Letters, Vol. 13, page 634, August 1988.

Temporal reshaping of ultrashort laser pulses after reflection from GaAs at Brewster's angle

I. H. Campbell and P. M. Fauchet

Department of Electrical Engineering, Princeton Laboratory for Ultrafast Spectroscopy, Princeton University, Princeton, New Jersey 08544

Received February 17, 1988; accepted May 26, 1988

A femtosecond or even a picosecond laser pulse may undergo dramatic temporal reshaping or distortion after reflection from a simple linear interface, provided that the angle of incidence is close to Brewster's angle. The dependence of the reshaping on the properties of the reflector and of the incident pulse is investigated numerically for a material having a dielectric function exhibiting a resonance that could be that of the GaAs exciton. The practical implications of these results are also discussed.

The discovery of a reliable source of femtosecond laser pulses[1] has opened many new avenues of research. To generate pulses well below 100 fsec and to avoid extracavity pulse broadening or distortion, a reexamination of the properties of common optical components such as mirrors was undertaken. In particular, significant femtosecond pulse disortion was predicted[2] and measured[3] on reflection from multiple-layer dielectric mirror coatings. The use of such coatings, either inside or outside the laser cavity, would thus produce unreliable femtosecond pulses. The following rule of thumb was thus adopted by the femtosecond laser community: metallic or single-stack dielectric coating components should be used exclusively. A widely held assumption is that such components do not alter the temporal profile of femtosecond pulses.

In this Letter we show that, contrary to the commonly accepted opinion, short laser pulses can undergo dramatic temporal reshaping on reflection at an interface exhibiting linear optical properties. Near Brewster's angle, the phase and magnitude of the Fresnel coefficients change rapidly with the angle.[4] For a fixed angle, a relatively small modification in the complex dielectric function (or the index of refraction) can also lead to large modifications of the Fresnel coefficients. If a short laser pulse is incident close to Brewster's angle, the various frequency components of the pulse will be reflected differently, yielding reflected pulses that are reshaped. We investigate this reshaping as a function of the angle of incidence, of the material's properties, and of the incident pulse's characteristics. The dielectric function of GaAs at low temperature in the exciton region is used as the starting point of our numerical calculations.

The reflected pulse $g(t)$ is given by

$$g(t) = \frac{1}{2\pi}\int_{-\infty}^{\infty} F(\omega) r(\omega, \theta) \exp(j\omega t)\,\mathrm{d}\omega, \tag{1}$$

where $F(\omega)$ is the Fourier transform of the incident electric field and $r(\omega, \theta)$ is the frequency-dependent Fresnel reflection coefficient. The Fresnel reflection coefficient[4] for a TM wave incident from a vacuum onto a medium of index of refraction $\tilde{n}(\omega) = \sqrt{\epsilon(\omega)} = n(\omega) - jk(\omega)$ is

$$r(\omega, \theta) = \frac{\cos\theta_1 - \tilde{n}(\omega)\cos\theta}{\cos\theta_1 + \tilde{n}(\omega)\cos\theta}, \tag{2}$$

where θ is the incident angle and $\sin\theta_1 = \sin\theta/\tilde{n}(\omega)$. If $k(\omega)$ is small enough, the reflectivity is near zero at Brewster's angle $\theta_B = \arctan[n(\omega)]$. The reflector under consideration has a frequency-dependent dielectric function, which we write as

$$\epsilon(\omega) = \epsilon_\infty + \frac{\omega_p^2}{\omega_0^2 - \omega^2 + j\gamma\omega}. \tag{3}$$

Here ϵ_∞ represents the constant background dielectric function and the second term is a Lorentz resonance, where ω_0 is the resonance frequency, γ is the damping factor, and ω_p is the plasma frequency. This dielectric function was chosen to model that of GaAs in the neighborhood of the band gap. In doing so, we make several approximations that will not modify our results much for GaAs: (i) only the ground state 1s exciton is considered; this is acceptable because the other states have a weaker contribution to $\epsilon(\omega)$ and such small binding energy that, except for experiments done at liquid-helium temperature with the purest samples, they merge with the continuum states[5]; (ii) the frequency dependence and the imaginary part of ϵ_∞ are neglected; for $\omega \sim \omega_0$, the Lorentz contribution completely overshadows that of ϵ_∞ (Ref. 6); for $\omega > \omega_0$, the imaginary part of ϵ_∞ increases slowly, which will not affect the pulse shape (see our results for a 50-meV resonance); and (iii) the nonlocality or **k** dependence of $\epsilon(\omega)$ is neglected; by not including it, we lose no insight, make a small approximation, and avoid the difficult problem of the proper choice of additional boundary conditions.[5] Note that the reflector's properties are linear; it has been shown that at nonlinear interfaces, interesting beam phenomena may occur.[7] Here we show that one needs to invoke only linear properties to obtain especially interesting temporal reshaping.

We now consider the results of numerical simula-

0146-9592/88/080634-03$2.00/0

tions by using parameters typical of GaAs at low temperature: $\epsilon_\infty = 12.35$, $\omega_p = 0.2$ eV, $\omega_0 = 1.51389$ eV, and $\gamma = 0.266$ meV.[8] The input-pulse profile is sech^2, which is characteristic of well-mode-locked femtosecond lasers generating transform-limited pulses. For a pulse, we define Brewster's angle to be $\theta_B \equiv \arctan[n(\omega_c)]$, where ω_c is the central frequency of the pulse. In the first column of Fig. 1 we show the dependence of the reflected pulse shape on $\Delta\theta \equiv \theta - \theta_B$, input pulse duration τ_p, resonance width γ_1, and detuning $\Delta\omega \equiv \omega_c - \omega_0$. The amplitude of the reflected pulse has been normalized because it is usually small and is sensitive to the above parameters. The dependence on pulse duration, detuning, and resonance width suggests that it is easy to obtain a dramatic reshaping of picosecond or femtosecond pulses; however, the critical dependence of the effect on $\Delta\theta$ shows that this reshaping is observable only under strict experimental conditions ($|\Delta\theta| \lesssim 10^{-2}$ deg for GaAs). We have verified that our conclusions remain valid for linearly chirped pulses. This dramatic temporal reshaping can be understood if we examine the magnitude, ρ, and phase, ϕ_r, of the reflectivity $r \equiv \rho \exp(j\phi_r)$ as a function of frequency. In the second and third columns of Fig. 1 we plot $\log_{10} \rho(\hbar\omega)$ and $\phi_r(\hbar\omega)$, respectively, corresponding to the various temporal shapes plotted in the first column.

The effects of varying $\Delta\theta$ are seen by plotting $\log_{10} \rho(\hbar\omega)$ and $\phi_r(\hbar\omega)$ for the three different angles of incidence along with the frequency spectrum of the incident pulse. For $\Delta\theta = -10^{-4}$ deg, where there is strong reshaping, the magnitude of the reflectivity has a sharp minimum, and the phase changes sharply from 0 to π near the central frequency of the incident pulse. As $|\Delta\theta|$ increases, the position of the reflectivity minimum and phase change moves to a lower frequency. For $\Delta\theta = -10^{-2}$ deg, neither the magnitude nor the phase changes dramatically near the central frequency of the incident pulse, and the pulse is not reshaped. The dominant factor in the pulse reshaping is the large phase shift that occurs between the lower- and higher-frequency components of the incident pulse. The

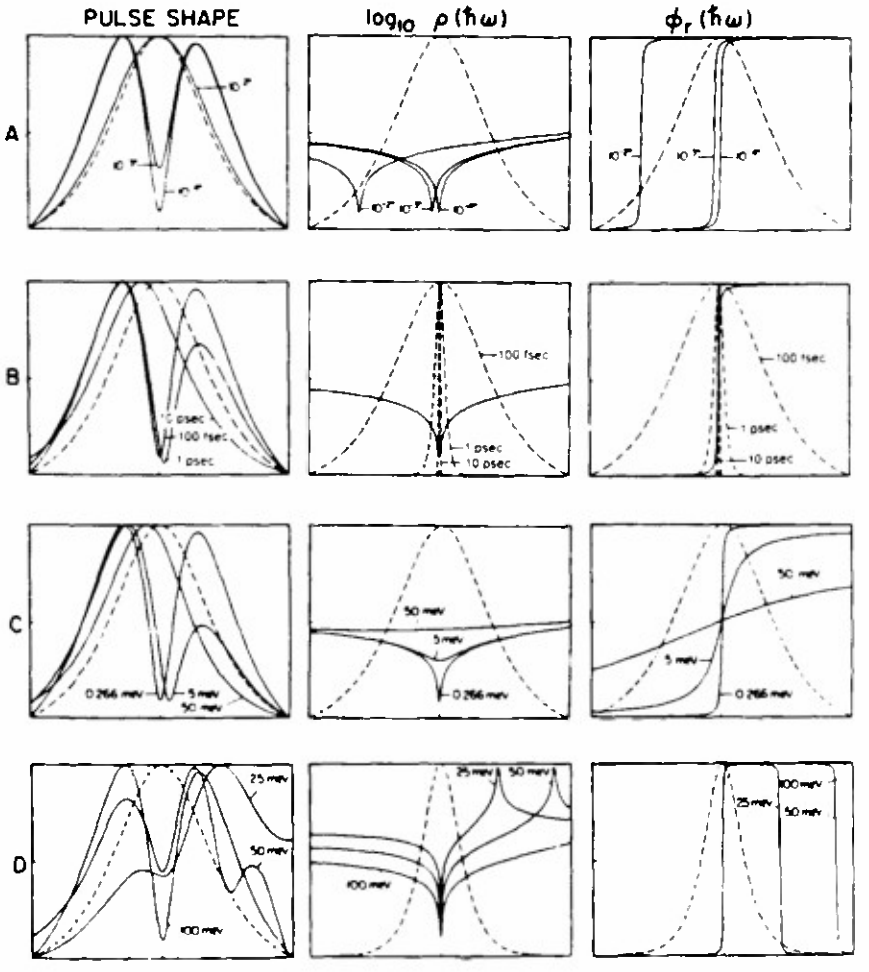

Fig. 1. Pulse shape, magnitude, and phase of the reflectivity for various angles of incidence, pulse durations, resonance widths, and detunings. The pulse shapes are normalized, the magnitude $\log_{10} \rho(\hbar\omega)$ of the reflectivity is plotted from -6 to 0, and the phase $\phi_r(\hbar\omega)$ of the reflectivity is plotted from 0 to π. Except where noted, the time scale for the pulse shapes is ± 170 fsec and the energy scale for the reflectivity is $\hbar\omega_c \pm 25$ meV. The default conditions are $\Delta\theta = -10^{-4}$°, $\tau_p = 100$ fsec, $\gamma = 0.266$ meV, and $\Delta\omega = -0.1$ eV. The temporal profile and the spectrum of the incident pulse are indicated by the dashed lines. A: $\Delta\theta = -10^{-4}$°, -10^{-3}°, and -10^{-2}°. B: $\tau_p = 100$ fsec, 1 psec, and 10 psec. The time scale of the first figure is $\pm 1.7\tau_p$ for each pulse. C: $\gamma = 0.266$, 5, and 50 meV. D: $\Delta\omega = -0.1$, -0.05, and -0.025 eV. The energy scale for the magnitude and phase of the reflectivity is $\hbar\omega_c \pm 50$ meV.

~180° phase shift leads to destructive interference and a minimum in the pulse envelope.

To examine the dependence of the reshaping on the duration of the incident pulse, note that the magnitude and the phase of the reflectivity are constant, but the input-pulse bandwidth decreases as the length of the pulse increases. In this case we plot the frequency spectrum of each incident pulse superimposed on the constant reflectivity. The 100-fsec pulse has a bandwidth of ~20 meV; the phase changes by 180° within the pulse spectrum, and the pulse is strongly reshaped. For a 10-psec pulse the bandwidth is ~0.2 meV; there is little phase change across the pulse spectrum, and the pulse is largely unaffected. The pulse is reshaped only if there is sufficient bandwidth to undergo a large phase change.

The reshaping depends on the resonance width, because as the material resonance becomes broader the magnitude of the phase change decreases and the frequency range over which the phase changes increases. For $\gamma = 0.266$ meV the frequency range over which the phase changes significantly is ~0.5 meV, and the phase changes by 180°, leading to substantial reshaping. For $\gamma = 50$ meV the frequency range over which the phase changes is ~100 meV, and the phase changes by only 70°, yielding a smooth pulse. The pulse is no longer dramatically reshaped when there is no large, sudden phase change across the pulse spectrum.

As the central frequency of the incident pulse approaches the resonance frequency, the effect of the imaginary part of the dielectric function becomes important. For $\Delta\omega = -0.1$ eV, the reflectivity has a single minimum and one sharp phase change that leads to a reflected pulse with a single minimum. Nearer the resonance, at $\Delta\omega = -50$ meV, the reflectivity has two sharp phase changes, one due to Brewster's angle and one due to the resonance. The magnitude of the reflectivity, in addition to a minimum at Brewster's angle, now has a maximum at the resonance frequency. These two changes result in the formation of a second minimum in the reflected pulse. Closer to resonance, at $\Delta\omega = -25$ meV, the pulse is reshaped and is also lengthened. The pulse is now many picoseconds (off scale): 1 order of magnitude longer than the incident pulse of 100 fsec. This effect can be attributed to the magnitude of the reflectivity. A narrow spectral range around the material resonance frequency is strongly reflected, dominating the reflected pulse spectrum. This effectively reduces the bandwidth available to the reflected pulse and causes the temporal broadening. Near the resonance, the restrictions on $\Delta\theta$ are somewhat relaxed to ~0.1°, although the pulse reshaping is accompanied by significant pulse lengthening. In addition, it is possible to have pulse reshaping arbitrarily far from resonance. Unfortunately, for large detuning the angle of incidence must be prohibitively close to Brewster's angle in order to reshape the pulse.

These observations explain why, to our knowledge, there has been no report of such unexpected reshaping: $\theta - \theta_B$ must remain extremely small. We have already exploited the sensitivity of the reflectivity near Brewster's angle to enhance the effect of a given laser-induced index-of-refraction change in picosecond time-resolved measurements of carrier lifetime[9,10] and phase transitions[11,12] in semiconductors. The effects considered in this Letter can safely be excluded as a source of unwanted pulse distortion in those experiments. Although such dramatic reshaping may be useful in some situations, it is not easy to conceive of a practical arrangement in which reshaping close to Brewster's angle is used in a device: by definition, for $\theta \simeq \theta_B$, the reflectivity is small and thus the throughput of any such device could be too small (note that all the curves shown in this Letter are normalized). On the other hand, our results support a new type of scientific experiment designed to uncover some properties of the reflector, such as γ, to which reshaping is sensitive. In this new type of experiment, the reflected pulse would be correlated with part of the incident pulse in a nonlinear crystal. A fit to the second-harmonic signal would yield γ.

In conclusion, we have shown that contrary to commonly held opinion, dramatic reshaping of femtosecond and even picosecond pulses can take place after reflection from a simple linear interface. We have investigated the dependence of the reshaping on the reflector's properties, on the pulse's properties, and on the geometry of the experiment. By far the most restricting condition is on the angle of incidence, which must remain close to Brewster's angle for the optical carrier frequency. The reshaping in most cases will not be a source of unwanted pulse distortion but could be used in experiments to obtain some properties of the reflector.

This research was supported by the National Science Foundation through the Presidential Young Investigator award program and by the U.S. Army Research Office.

References

1. R. L. Fork, B. I. Greene, and C. V. Shank, Appl. Phys. Lett. 38, 671 (1981).
2. S. D. Silvestre, P. Laporta, and O. Svelto, IEEE J. Quantum Electron. **QE-20**, 533 (1984).
3. A. M. Weiner, J. G. Fujimoto, and E. P. Ippen, Opt. Lett. 10, 71 (1985).
4. O. S. Heavens, *Optical Properties of Thin Solid Films* (Academic, New York, 1955), Chap. 4.
5. J. L. Birman, in *Excitons*, E. I. Roshba and M. D. Sturge, eds. (North-Holland, New York, 1982), Chap. 2.
6. D. D. Sell, H. C. Casey, and K. W. Wecht, J. Appl. Phys. 45, 2650 (1974).
7. A. E. Kaplan, Opt. Lett. 6, 360 (1981).
8. J. P. Lowenau, S. Schmitt-Rink, and H. Haug, Phys. Rev. Lett. 49, 1511 (1982).
9. P. M. Fauchet and W. L. Nighan, Jr., Appl. Phys. Lett. 48, 721 (1986).
10. N. K. Bambha, W. L. Nighan, Jr., I. H. Campbell, P. M. Fauchet, and N. M. Johnson, J. Appl. Phys. 63, 2316 (1988).
11. K. D. Li and P. M. Fauchet, Solid State Commun. 61, 207 (1987).
12. K. D. Li and P. M. Fauchet, Appl. Phys. Lett. 51, 1747 (1987).

Control and Characterization of Soliton-like Pulses in a Femtosecond Dye Laser

W.L. Nighan, Jr., T. Gong, and P.M. Fauchet

Princeton Laboratory for Ultrafast Spectroscopy,
Department of Electrical Engineering, Princeton University,
Princeton, NJ 08514, USA

The balance of positive self-phase modulation (SPM) and negative group velocity dispersion (GVD) that enhances ultrashort pulse formation in a dispersion compensated, colliding pulse modelocked (CPM) dye laser [1,2] has been compared to the shaping mechanism for the N=1 soliton in an optical fiber [3,4]. Periodic pulseshaping reminiscent of higher order solitons has also been observed [5-7]. It is however unclear how far the analogy with solitons in an optical fiber can be extended. We report here results of our investigation of periodic pulseshaping in a 7 mirror/4 prism CPM laser that delivers pulses as short as 35fs at 100 MHz. The stability achieved allows for reproducibility and full time-resolved characterization.

We control the order, period and duration of the soliton-like pulses (henceforth abbreviated as solitons) by adjusting the group velocity dispersion (GVD) and self-phase modulation (SPM) within the laser cavity. Starting from the shortest pulse (N=1) configuration, higher order solitons are achieved by (1) increasing the amount of SPM by translating the absorber jet much closer to the intracavity focus or using a thicker (+ 10 μm) region of the jet, (2) increasing the magnitude of the negative GVD by translating a prism to reduce the amount (- 150 μm) of glass traversed, (3) optimizing the alignment of the laser cavity. The clockwise and counterclockwise beams are typically asymmetrized by step (3), indicating that a precise balance of gain and loss is required to support the higher order solitons.

The single sweep real-time intensity autocorrelations of Fig. 1 are an illustration of this control. Solitons of order 3, 2 and 1 are seen as the absorber jet is translated away from the focus. Modulation at the soliton frequency is clearly evident in these single sweeps. Full and accurate characterization of the solitons is possible by sampling intensity autocorrelations, interferometric autocorrelations and spectra during the soliton period. This is achieved by using the deep ($\sim$ 50%) modulation in a narrow spectral bandwidth near the central wavelength to generate a short gate pulse train for a boxcar sampler and for an optical multichannel analyzer (OMA). Both intensity and interferometric autocorrelations taken at points in the 2.5 μsec period of the N=2 soliton of Fig. 1(b) are shown in Fig. 2(b) and Fig. 2(c). Figure 2(a) shows spectra sampled from the period of a similar N=2 soliton. The autocorrelation traces show that the pulse is always composed of two coherent peaks with a separation that increases up to nearly one picosecond. The signal enhancement achieved by interferometric autocorrelation allows observation of the weaker peak even where it is no longer seen with intensity autocorrelation. The spectra indicate the presence of two major components whose peak positions and relative amplitude vary periodically.

The evolution characterized in Fig. 2 is reminiscent of the results of SALIN et al. [6], who interpreted their sampled intensity autocorrelations and spectra as evi-

Springer Series in Chemical Physics, Vol. 48: Ultrafast Phenomena VI
Editors: T. Yajima · K. Yoshihara · C.B. Harris · S. Shionoya

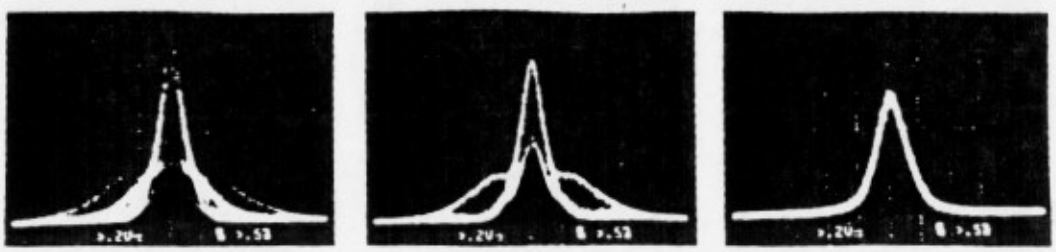

Fig.1. Single sweep real-time autocorrelation traces for different jet positions.
(a) N=3: Jet at focus (b) N=2: Jet 50 μm from focus (c) N=1: Jet 250 μm from focus

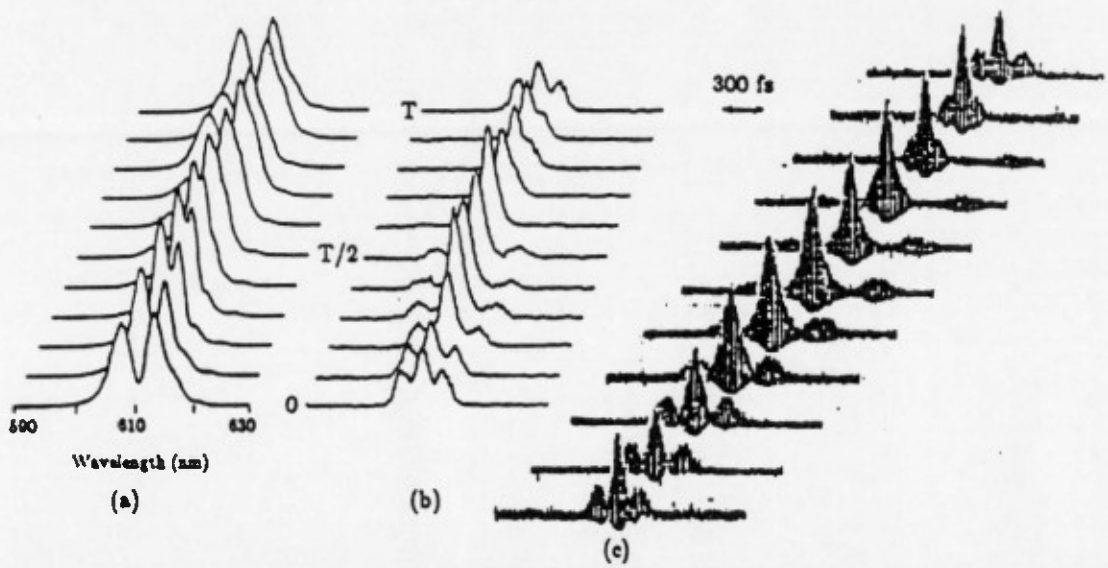

Fig.2. Time-resolved evolution of the N=2 soliton of Fig.1(b).
(a) Spectra (b) Intensity autocorrelations (c) Interferometric autocorrelations

dence for an asymmetric N=2 soliton. Our output pulse energy is modulated by $\sim 10\%$ with a period of 2.5 μsec, which corresponds to the soliton period. The two peaks of this soliton vary in separation (Fig. 3) but are coherent with one another (unlike the results of Ref. 7 which, however, were obtained under different conditions) and never merge into a single peak. These characteristics may correspond to a periodic motion of the poles and residues used to describe the N=2 soliton [5,8]. Fig. 4 shows the linearity of the soliton dispersion relation as defined in [5]. The transition from N=2 to N=3 as described in Fig. 1 is analogous to increasing the input intensity in a fiber. However, the period of the evolution abruptly doubles upon this transition, unlike what happens in a fiber. The spectral components do, however, exhibit N-1 frequencies of modulation. The sampled autocorrelations for the N=3 case show that the pulse is narrowed twice in its period, as predicted for asymmetric solitons of this order in optical fibers. The abrupt change in period upon the N=2 to N=3 transition may result from the alteration in saturation effects that accompanies the translation of the jet to a point of higher intracavity intensity. The average output pulse energies remain nearly constant through the transition.

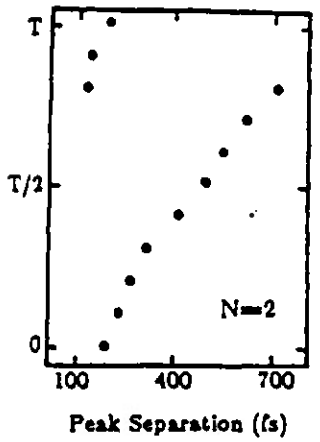

Fig.3. Peak separation during N=2 soliton period.

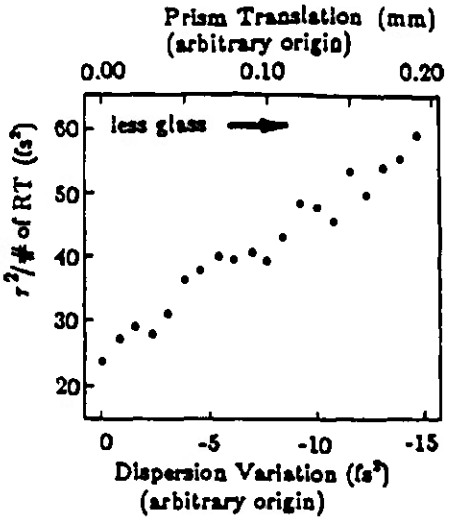

Fig.4. N=2 soliton dispersion relation. τ = pulsewidth of soliton at single-peaked point of period. # of RT= number of cavity roundtrips corresponding to a single soliton period.

We have demonstrated control of soliton pulseshaping in a femtosecond CPM laser. Accurate characterization is possible since the pulseshapes are stable and reproducible. Similarities and differences with solitons in an optical fiber have been pointed out. The principles are general and could be applied to other short pulse lasers in different wavelength regimes.

This work is supported by NSF (ECS-8606531), the NSF Presidential Young Investigator Program (ECS-8657263) and ARO (DAAL03-87-K-0145).

References

1. R.L. Fork, B.I. Greene and C.V. Shank, Appl. Phys. Lett. 41, 671 (1981).
2. J.A. Valdmanis, R.L. Fork and J.P. Gordon, Opt. Lett. 10, 131 (1985).
3. J.C. Diels, W. Dietel, J.J. Fontaine, W. Rudolph and B. Wilhelmi, J. Opt. Soc. Am. B2, 680 (1985).
4. O.E. Martinez, R.L. Fork and J.P. Gordon, J. Opt. Soc. Am. B2, 753 (1985).
5. F. Salin, P. Grangier, G. Roger and A. Brun, Phys. Rev. Lett. 56, 1132 (1986).
6. F. Salin, P. Grangier, G. Roger and A. Brun, Phys. Rev. Lett. 60, 569 (1988).
7. F.W. Wise, I.A. Walmsley and C.L. Tang, Opt. Lett. 13, 129 (1988).
8. H.A. Haus and M.N. Islam, IEEE J. Quantum Electron. QE-21, 1172 (1985).

Solitons and Related Periodic Pulse Evolutions in a Femtosecond Ring Dye Laser

William L. Nighan Jr.
Ting Gong
Philippe M. Fauchet

Reprinted from
IEEE JOURNAL OF QUANTUM ELECTRONICS
Vol. 25, No. 12, December 1989

Solitons and Related Periodic Pulse Evolutions in a Femtosecond Ring Dye Laser

WILLIAM L. NIGHAN JR., TING GONG, AND PHILIPPE M. FAUCHET

Abstract—We control the generation of solitons and other related periodic pulse evolutions in a passively mode-locked dye laser by adjustment of group velocity dispersion, self-phase modulation, and spectral filtering. Without spectral filtering, periodic pulse evolutions reminiscent of higher order solitons are observed. The pulses differ from the classic solitons because of additional shaping mechanisms. With spectral filtering, pulses are generated that can be described analytically as *true* asymmetric $N = 2$ solitons. The introduction of the filter appears to simplify the intracavity shaping mechanisms in such a way that the nonlinear Schrodinger equation becomes a good approximation for pulse generation in the laser. The remarkable stability achieved allows for accurate characterization and control.

I. Introduction

THE generation of pulses by the dispersion-compensated colliding-pulse mode-locked (CPM) dye laser has been compared to the propagation of $N = 1$ solitons in optical fibers [1], [2]. It has been shown that the laser may support more complex evolutions as well, reminiscent of higher order solitons [3]–[8]. The comparison to the higher order soliton solutions of the nonlinear Schrodinger equation (NLSE) is attractive since the positive self-phase modulation (SPM) in the absorber jet solvent and the negative group velocity dispersion (GVD) provided by the prism sequence replicate the balanced chirping mechanisms that allow solitons to arise [9]. While the lowest order (nonperiodic) pulse generation in the laser has been analytically described by models that include these soliton effects [2], [10], [11], to date no analytic model exists for the higher order periodic evolutions that have been experimentally observed [3]–[8]. A fundamental difficulty lies in the fact that the typical analytic boundary condition of pulse shape restoration after a single round-trip of the laser [2] must be relaxed in order to allow for periodic evolution over hundreds of roundtrips, requiring many hundreds of pulse shaping operations before the restoration of the initial pulse shape. The recent numerical model of Avramopoulos *et al.* has demonstrated some success [6]. However, on the basis of this model, it has been argued that despite several striking similarities with solitons in fibers, these pulses are not true solitons because of the presence of saturable gain, saturable loss, and complex phase modulations, which can also act as strong shaping mechanisms [6]. In addition, the discrete nature of the elements in the laser cavity differs from the distributed medium of the optical fiber [6].

In this paper, we present the phenomenology of higher order pulse evolution that we have observed and controlled in our CPM laser. We demonstrate precise control of soliton-like pulse shaping in the CPM laser and fully characterize the higher order pulses during their periodic evolution. The spectra, intensity autocorrelations, and interferometric autocorrelations are resolved throughout the period. We have identified two regimes of operation. For the otherwise unmodified laser, adjustments to intracavity SPM and GVD lead to pulses similar to higher order solitons which, however, cannot be described as true solitons. The removal or limitation of mechanisms other than a balanced SPM and GVD will result in a pulse shaping condition that more closely approximates the soliton shaping supported by the NLSE. Indeed, it is a simple modification to the laser cavity that leads to the second regime of higher order pulses, which can be described as *true* $N = 2$ asymmetric solitons [4]. The pulses generated are fit with great precision by established analytic soliton theory [4], [12]. The intracavity filter [13] that gives rise to this regime also allows stable pulsing at values of GVD much closer to zero. We attribute this generation of true higher order soliton pulses in the laser to the inhibition of an effect analogous to the soliton self-frequency shift (SSFS) observed in fibers [14]. Our findings indicate that while the NLSE may not be the most general basis for an analytic model of pulse generation in the laser, there are certain conditions under which the pulses are very well described by soliton solutions to the NLSE. We present and interpret the detailed experimental results of our periodic pulse evolution experiments in the classic CPM laser in order to contribute to the development of suitable analytic and numerical models for ultrashort pulse generation.

This paper is organized as follows. Section II is a description of the experimental procedures used to achieve, stabilize, and characterize the periodic pulse evolutions in the CPM laser. In Section III, the results obtained with the unmodified laser are presented. Section IV presents

Manuscript received April 13, 1989; revised July 13, 1989. This work was supported by the National Science Foundation under Grants ECS-8606531 and ECS-8657263, Coherent, Inc., and the Newport Corporation through the Presidential Young Investigator Program, and the Army Research Office under Contract DAAL03-87 K 0145. The work of P. M. Fauchet was also supported by an Alfred P. Sloan Research Grant.

The authors are with the Princeton Laboratory for Ultrafast Spectroscopy, Department of Electrical Engineering, Princeton University, Princeton, NJ 08544.

IEEE Log Number 8931068.

the results for the modified laser corresponding to a true $N = 2$ asymmetric soliton. Section V is an interpretation of the behavior we have observed, and Section VI presents our conclusions.

II. Experimental

We have built the now classic seven mirror/four prism CPM laser [1], [15], [18]. Pulses as short as 35 fs are delivered at 100 MHz, peaked near 633 nm. All mirrors are single stack dielectric coatings, optimized for maximum reflectivity at their respective angles of incidence with a 100 nm bandwidth peaked at 630 nm [1], [15], [18]. A 1.3 percent output coupler was used for this work, resulting in output powers of ~10 mW per beam for ~4 W of pump power. The use of the standard Rh6G/DODCI as the gain/absorber dye pair can be considered an advantage in these pulse shaping experiments since a wide body of information is available regarding the behavior of these dyes [16], [17]. All of the work presented here was performed with relatively fresh dye mixtures (it was always possible to generate pulses of length less than 50 fs). The DODCI pump station is refrigerated and purged with dry nitrogen [18], which noticeably lengthens the performance lifetime of the dye (typically up to ~2 months of daily use). Also, the argon ion laser (Coherent Innova 200) used to pump the CPM features an active stabilization mechanism which clearly enhances the long-term beam pointing stability of the pump laser and obviates the need to adjust the alignment of the pump beam during experiments.

Both of the first two stable transverse modes (characterized by a TEM_{∞} profile and encountered by increasing the distance between the focusing mirrors around the absorber jet) allowed $N = 1$ soliton-like (normal) pulsing and higher order pulsing. The next stable modes (reached by increasing the separation still further) did not allow for the shortest pulses or higher order pulses, presumably because the enlarged beam sizes in the absorber jet result in a lower intensity in the jet and thus less SPM.

In order to achieve higher order pulsing, we first optimize the unmodified laser in its shortest pulse configuration as described in [1], successively tuning the absorber position and the amount of intracavity glass by a prism translation until a pulse length of less than 50 fs is achieved. We refer to the shortest pulses as $N = 1$ soliton-like since it is generally accepted that generation of pulses shorter than ~60 fs by this laser is only possible upon proper addition of soliton shaping mechanisms [1], [2]. Using this optimized $N = 1$ soliton-like condition as a starting point, the SPM and GVD can be adjusted in a way analogous to that which allows higher order solitons to propagate in optical fibers. The adjustments are as follows. 1) The SPM is increased by using a thicker region of the absorber jet (~50 μm instead of ~40 μm, the thickness varying as a function of distance from the nozzle), and by translating the jet to within 100 μm of the intracavity focus. In this way, both the interaction length and intensity in the nonlinear medium are increased [19]. 2) A more negative GVD is then introduced with a minute prism translation, reducing the amount of intracavity glass by ~150 μm. 3) Finally, a slight, primarily vertical alignment of an end mirror results in a periodic evolution of the laser output, with a period corresponding to between 200 and 500 round-trips of the laser cavity. The periodic, higher order evolutions we achieve exhibit similarities and differences with both solitons in optical fibers and the periodic actions observed by others in CPM lasers [3]–[6]. The real-time autocorrelations, displayed on an oscilloscope, provide the most dramatic indication of this higher order condition as the laser is tuned through steps 1)–3). As depicted in Fig. 1(a) and (b), the single sweep intensity autocorrelations are clearly modulated. The output pulse energy is modulated at the same frequency as the autocorrelations, as depicted in Fig. 2, with typical frequencies between 200 and 500 kHz. The counterpropagating beams in the laser are typically rendered significantly different from one another upon step 3). This is addressed in detail in Section III.

As described above, we start with the normal $N = 1$ soliton-like mode and tune SPM and GVD to obtain higher order periodic modes. Adjusted for the higher order pulses, the prism sequence provides ~200 μm less intracavity quartz (a more negative GVD) than does the configuration for the shortest pulses. This differs from the procedure used by Salin *et al.* [3] who started with the unstable mode that corresponds to the presence of too much intracavity quartz [2], [3]. They achieved an evolution attributed to an $N = 3$ soliton by reducing the pump power, which restabilized the CPM laser output [3]. Wise *et al.* [5] identified a regime where a normal pulse and a higher order soliton coexist. The prism and absorber jet positions were qualitatively similar to our own as described in this section, although we have not observed a simultaneous nonperiodic pulse. In Section IV, we present a simple modification to the laser which allows periodic evolutions for a negative GVD of smaller magnitude, and thus may be closer to the operating points described by Salin [3], [4] and Avramopoulos [6].

The real-time oscillation between extreme pulse shapes indicated by the single sweep autocorrelations of Fig. 1 differs from what has been reported by others [3]–[6]. A description of the measurement is in order. Each of these sweeps takes ~5 ms; in other words, the moveable arm of the autocorrelator introduces ~1500 fs of optical delay in 5 ms. A single sweep therefore traces ~1000 periods of the 200–500 kHz evolution. It should be stressed that an autocorrelation taken in this way is *not* an average of the varying autocorrelations in the period of the soliton-like evolution, but actually resolves them all if the detector used has sufficient bandwidth. If sampled appropriately (as described below), these single sweep autocorrelations give access to the pulse autocorrelations at any point in the period. A description of the techniques used to sample the autocorrelations and spectral evolutions corresponding to Fig. 1(a) and (b) follows.

The output power is modulated at the same frequency

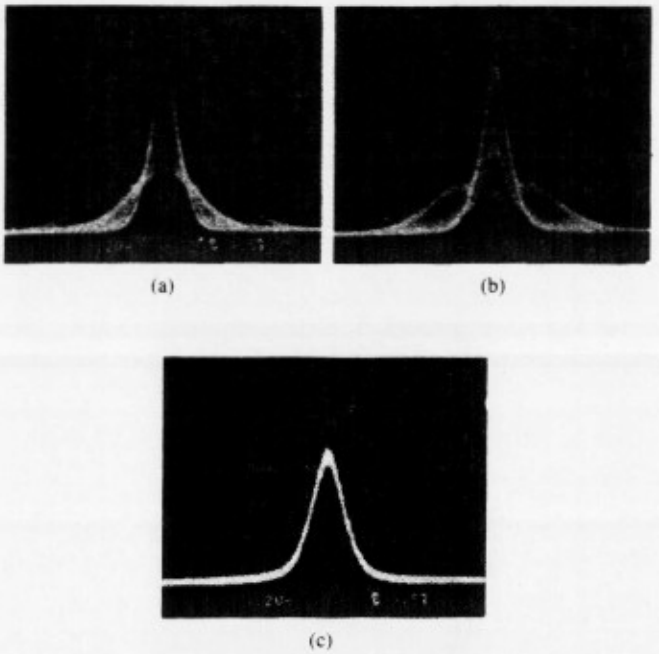

Fig. 1. Single-sweep intensity autocorrelations. 1 division = 160 fs. (a) Absorber jet at focus. (b) Jet 50 μm away from focus. (c) Jet 250 μm away from focus.

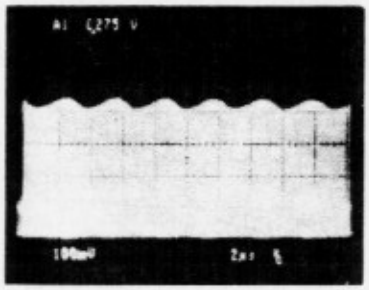

Fig. 2. Energy modulation of output pulse train for conditions similar to those of Fig. 1(b). (1 division = 2 μs.)

as the autocorrelations, with a depth of about 10 percent, as seen in Fig. 2. Certain spectral components are modulated by nearly 100 percent, which facilitated the generation of a sampling pulse train that was in phase with the modulation. The experimental arrangement appears schematically in Fig. 3. A leakage beam from an end mirror was spectrally filtered and sent into a photodiode. A constant fraction discriminator (EG&G 934) generated a sampling pulse train from the amplified diode signal. A digital delay (BNC 7050) was used to adjust the phase of the sampling with respect to the spectral modulation. The pulse train was used to trigger the boxcar averager (Stanford Research SR 250) used to sample the raw single sweep autocorrelations at a subharmonic of the triggering frequency, with approximately 100 ns real-time resolution. The sampled *single sweep* autocorrelations were stored on a digital oscilloscope (LeCroy 9400A). The sampling pulse train also triggered a high-voltage pulser (Princeton Instruments FG-100) that gated an optical multichannel analyzer (Princeton Instruments DIDA-512), allowing the display of spectra on a personal computer, with

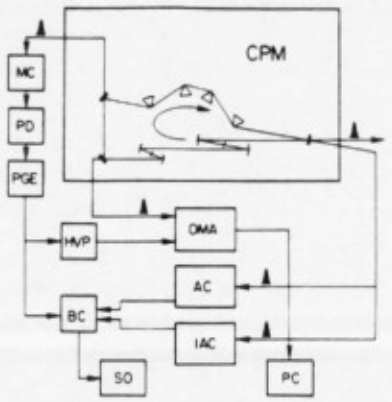

Fig. 3. Experimental arrangement. CPM = colliding pulse modelocked laser, MC = monochromator, PD = photodiode, PGE = pulse generating electronics, HVP = high-voltage pulser, OMA = optical multichannel analyzer, BC = boxcar, SO = storage oscilloscope, AC = intensity autocorrelator, IAC = interferometric autocorrelator, PC = personal computer.

approximately 50 ns real-time resolution. Adjusting the digital delay was equivalent to adjusting the phase of the sampling, and allowed us to resolve the intensity autocorrelations, interferometric autocorrelations [20], and spectra as they evolved during the soliton-like period. Unless otherwise specified, all traces are for the clockwise propagating pulses.

III. Results with the Unmodified Laser

The autocorrelations of Fig. 1 are typical of the regime of periodic pulse evolution that we observe in our unmodified CPM laser. Fig. 1 depicts the tuning of order of the soliton-like evolution. With all other parameters fixed, a simple translation of the absorber jet away from the intracavity focus sweeps through the traces of Fig. 1(a)–(c). The average output power did not change more than a few percent upon the jet translation; the autocorrelations have not been renormalized. With the jet at the focus, the autocorrelation trace of Fig. 1(a) is reminiscent of that expected of an $N = 3$ soliton, featuring broad, narrow, and triple-peaked autocorrelations in its evolution [9]. The period is ~ 5 μs, or 500 round-trips of the laser cavity. Translating the jet by 50 μm lowers the intensity in the jet, resulting in a decrease in the order of the evolution as seen in Fig. 1(b). An oscillation between single-peaked and triple-peaked autocorrelations is evident, which shares some similarities with an $N = 2$ asymmetric soliton [4]. The period is abruptly halved to ~ 2.5 μs upon this adjustment, as depicted in Fig. 4 where the modulation at 616 nm is compared for the conditions corresponding to Fig. 1(a) and (b). An additional 200 μm translation of the jet results in a conventional $N = 1$ soliton-like trace of Fig. 1(c), without modulation.

The results of Figs. 1 and 2 are reproducible and controllable, which allowed us to fully characterize the laser behavior. We have also observed autocorrelations and pulse train modulations which, although they could not be maintained for long periods of time, seem to corre-

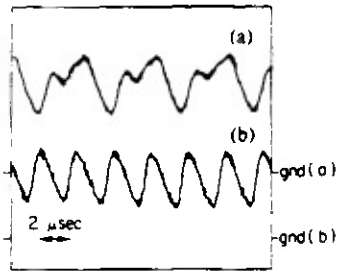

Fig. 4. Period doubling that accompanies the transition from Fig. 1(b) to (a). The modulation at 616 nm is detected by a slow diode. The upper curve (a) corresponds to Fig. 1(a). The lower curve (b) corresponds to Fig. 1(b).

Fig. 5. Single sweep intensity autocorrelation, possibly corresponding to an $N = 4$ soliton. (1 division = 290 fs.)

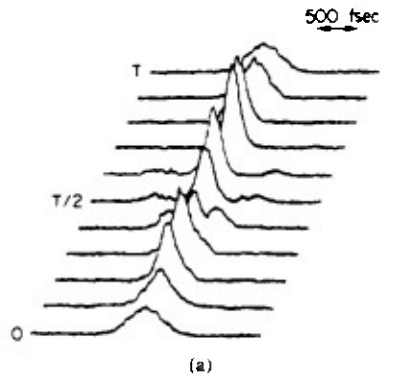

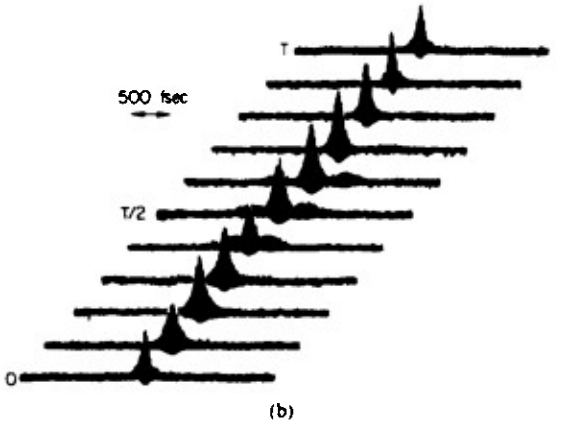

Fig. 6. (a) Intensity autocorrelations and (b) interferometric autocorrelations resolved over one 5 μs period of the condition corresponding to Fig. 1(a), which has similarities with an $N = 3$ soliton.

spond to an even higher order pulsing. An autocorrelation that may correspond to an $N = 4$ soliton-like pulse is displayed in Fig. 5. This trace was achieved with the absorber at or very near the intracavity focus, corresponding to a maximum intensity in the jet, but the condition could not be maintained long enough to allow complete characterization. Another distinct periodic regime with a significantly longer period has also been observed. A very tall spike arises in the train at a rate of 10–20 kHz, which corresponds to a much longer period than the other evolutions that we have characterized. This spike consists of series of pulses of twice the energy of the background pulses and twice the duration. This mode could not be maintained for very long and was particularly sensitive to environmental perturbations such as dust and air currents.

We return to the full characterization of the evolutions corresponding to Fig. 1(a) and (b). Fig. 6(a) shows one full period of the evolution of the intensity autocorrelation corresponding to the real-time trace of Fig. 1(a). As mentioned above, there are similarities with an $N = 3$ soliton. However, it is interesting to note that the pulse is chirped early in the period of Fig. 6, as indicated by the interferometric autocorrelations of Fig. 6(b); the pulse that has the widest intensity autocorrelation has one of the narrowest interferometric traces. This differs from what is expected for $N = 3$ solitons in fibers. Fig. 7 depicts the sampled autocorrelations corresponding to the lower order case of Fig. 1(b). Particularly notable are the interferometric autocorrelations of Fig. 7(c) which indicate a pulse composed primarily of two *coherent* peaks, with one peak rising in amplitude as the other decays and moves away. At midperiod, the autocorrelations indicate two peaks of equal magnitude, spaced ~200 fs apart, each of duration ~120 fs, apparently unchirped, and completely coherent with one another. The ~5 nm FWHM of each spectral peak at midperiod is indeed sufficient to support 100 fs pulses at these wavelengths. It should also be noted that the spectral evolution shares similarities with that of certain $N = 2$ asymmetric solitons (see Fig. 11, as introduced below in Section IV). The coherence is unlike what was reported by Wise *et al.* who observed no fringes in the wings of an interferometric autocorrelation attributed to a simultaneous $N = 3$ soliton and dispersive wave [5]. However, their measurement was different in that it was not time resolved with respect to the soliton period. The lack of any substantial chirp on the pulses characterized in Fig. 7 is quite remarkable and indicates that the intracavity chirping mechanisms are balanced. Finally, it should be noted that the evolution of the $N = 3$ soliton-like intensity autocorrelation from $T/4$ to $3T/4$ is very similar to that of the $N = 2$ soliton-like pulse over a full period. The longer period of the $N = 3$-like pulse includes the additional broad, chirped pulse. The corresponding spectral features are also similar over this range, but the $N = 3$-like spectra are shifted by ~3–5 nm to shorter wavelengths.

It was mentioned above that these periodic conditions typically featured an asymmetry between clockwise and counterclockwise traveling beams in the ring laser. The

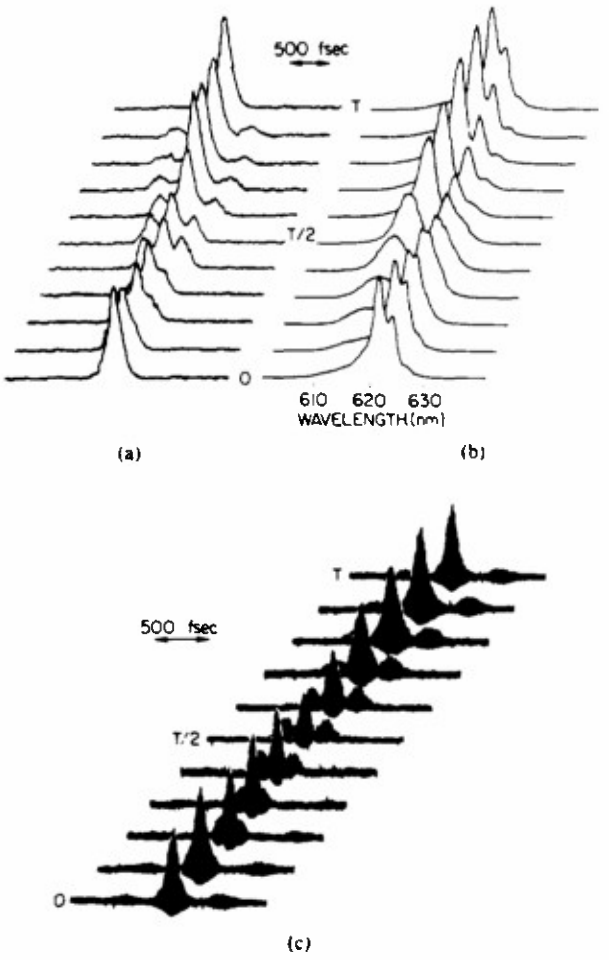

Fig. 7. (a) Intensity autocorrelations, (b) spectra, and (c) interferometric autocorrelations of the evolution corresponding to Fig. 1(b), which has similarities with an $N = 2$ asymmetric soliton.

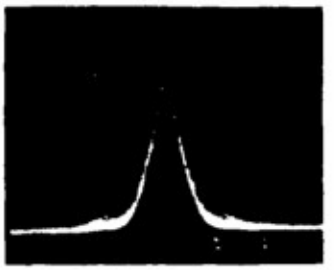

Fig. 8. Single sweep, unsampled intensity autocorrelation of the counterclockwise traveling beam. This beam counterpropagates with respect to the clockwise beam of Fig. 1 and Fig. 7.

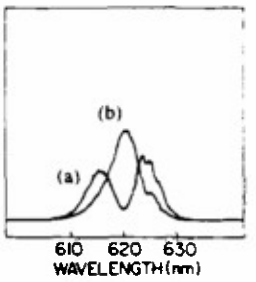

Fig. 9. Coincident spectra of the counterpropagating beams. (a) Clockwise beam, (b) counterclockwise beam. The conditions were the same as Figs. 1(b) and 7; the clockwise spectrum here corresponds to the midperiod of Fig. 7(b).

oscilloscope photograph of Fig. 1(b) and the characterizations of Fig. 7 are of the clockwise beam, for which the output power was ~12 mW. The coexisting counterclockwise beam was significantly lower in power at ~8 mW. A single sweep autocorrelation for the counterpropagating beam corresponding to Fig. 1(b) is shown in Fig. 8. The sampled autocorrelations indicate an oscillation between a broader and narrower pulse shape, with the same period as the clockwise beam, their relative phases being locked to one another. A very interesting finding is that the spectra of the counterpropagating pulses are complementary; the sampled spectra for the counterclockwise beam consistently "fill the hole" that is left in the spectra for the clockwise beam, as shown in Fig. 9. A spectrum corresponding to the midperiod of an evolution similar to Fig. 7(b) is shown. The clockwise spectrum splits into two peaks, while the counterclockwise spectrum fills this gap. It is also remarkable that a slight adjustment of alignment can cause the beams to interchange roles.

The robustness, stability, and reproducibility of the $N = 2$ soliton-like condition characterized in Fig. 1(b) and Fig. 7 allowed an additional measurement. The reduction of intracavity glass (by prism translation) lengthens the features in the autocorrelations and lengthens the period, while an increase in glass compresses the autocorrelation features (to as short as 50 fs) and shortens the period. It should be noted that the addition of too much glass (> 150 μm) results in an unstable pulsing condition similar to that observed for the lowest order pulses; the duration of the higher order pulses is therefore an asymmetric function of cavity dispersion, analogous to that which has been identified and explained for the lowest order pulses [1], [2]. The removal of too much glass causes a change in the order of the evolution similar to that depicted in Fig. 1. There is a minimum amount of glass required to allow pulsing of the order displayed in Fig. 7. Below that minimum, a period doubling occurs and the evolution becomes similar to that of Fig. 1(a) and Fig. 6, with similarities to an $N = 3$ soliton. The asymmetric relation between pulse duration and cavity dispersion for the $N = 2$ soliton-like condition appears in the upper part of Fig. 10.

The length of a soliton pulse in a fiber is related to the dispersion and nonlinear index of the fiber, as expressed explicitly in [9]. In the laser, the dispersion can be tuned, and the corresponding period and pulselength can be measured accordingly. Salin *et al.* extended the results of the NLSE to formulate an expression for the period of a soliton in a CPM laser [3]:

$$N_0 = 0.322\pi\tau^2/2\phi'' \qquad (1)$$

where N_0 is the number of round-trips in the cavity corresponding to one soliton period, τ is the typical pulse length (fs), and ϕ'' is the cavity dispersion (fs^2), which

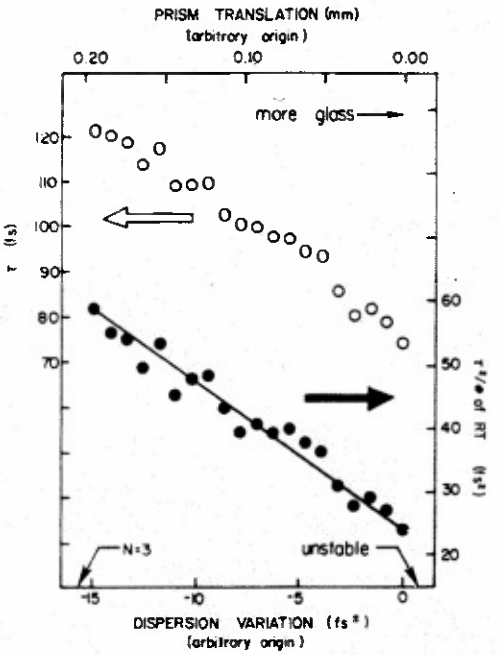

Fig. 10. Pulse duration and pulse duration squared over the number of roundtrips versus cavity dispersion for periodic pulsing with similarities to an $N = 2$ soliton as in Fig. 7.

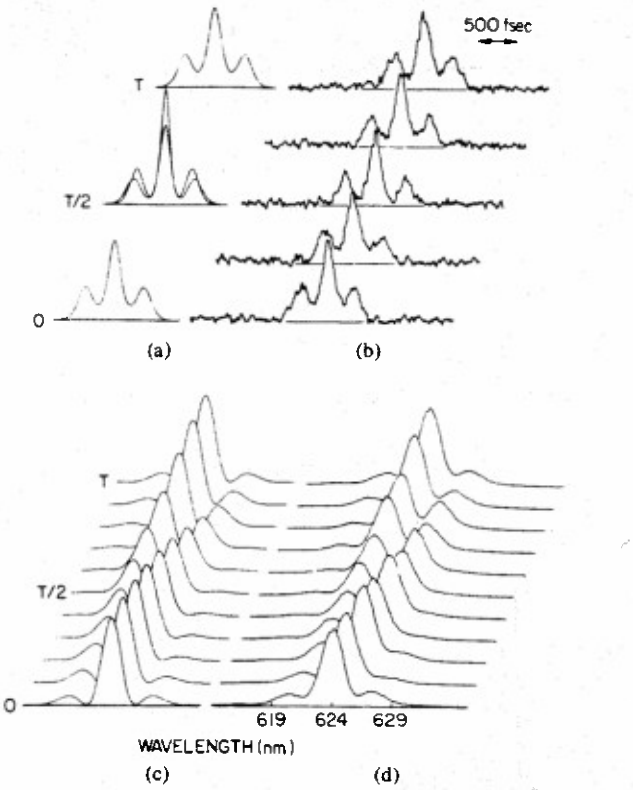

Fig. 11. Asymmetrical $N = 2$ soliton generated using intracavity filter. Period is 5 μs. The soliton is described by poles $\eta_1 = 0.75$, $\eta_2 = 1.25$, and residues $c_1 = 0.3$, $c_2 = 1.1$. A sinusoidal motion of the poles has been imposed that reduces their values by 10 percent at midperiod and restores them at the end of one soliton period. (a) Theoretical intensity autocorrelations. At midperiod, the autocorrelation with taller peak and taller wings is for the soliton with no energy modulation (constant poles). (b) Experimentally observed autocorrelations. (c) Theoretical spectra. (d) Experimentally observed spectra.

can be tuned by the prism sequence. Equation (1) can be rearranged to find

$$\tau^2/N_0 = 2\phi''/(0.322\pi) = 1.98\phi''. \qquad (2)$$

Implicit in (1) is the assumption that the change in pulse shape per round-trip is small and that the laser may therefore be approximated as a distributed medium. We measured τ^2/N_0 versus ϕ'', which is plotted in the lower part of Fig. 10. The cavity dispersion was varied with a prism translation, and τ was taken as the full width at half maximum (FWHM) of the tallest autocorrelation, normalized by 1.543 (assuming a sech^2 pulse at the beginning of the period of Fig. 7). The relation as plotted is indeed linear, with a slope of magnitude ~ 2.3, compared to the predicted magnitude of 1.98 for true solitons. Further interpretation of this and other findings presented in this section follows in Section V.

IV. The Modified Laser: True Solitons with an Intracavity Filter

A long wavelength "tail" appears in the spectra of $N = 1$ CPM pulses shorter than ~ 60 fs [1], [13]. While the spectrum peaks at ~ 630 nm, a subpeak between 640 and 650 nm can also arise [1], [13]. Schehrer *et al.* found that intracavity filtering of the long wavelength feature did not increase the pulse length, but in fact enhanced the stability of the laser [13], preventing it from degenerating into the unstable, random pulsing condition that is only a minute prism translation away from the shortest pulse configuration [1], [13]. Note that it was for similar prism positions (negative GVD of small magnitude) that higher order soliton evolutions have been reported [3]–[5].

We observe similar effects in our CPM laser, using a translatable straight edge in the prism sequence as a long wavelength filter [13]. Additionally, we find the insertion of this edge filter allows the laser to operate stably for values of intracavity GVD at which it was previously unstable, namely, values closer to zero. Further, we observe pulses in this configuration that are *quantitatively* described as asymmetric $N = 2$ solitons [4], [12]. The procedure is as follows: 1) optimize laser for shortest $N = 1$ soliton-like pulses; it should be noted that the absorber jet is displaced from the focus as in [1]; 2) insert edge filter to remove spectral "tail"; 3) add more glass by translating a prism. Upon the final step, the autocorrelation trace broadens, until upon the addition of ~ 145 μm of glass, it splits into three peaks, as in Fig. 11(b), The average output power drops from ~ 10 to ~ 4 mW per beam and a nearly sinusoidal energy modulation is observed in the raw pulse train, with a period of ~ 5 μs and a depth of ~ 15 percent. The sampled intensity autocorrelations [Fig. 11(b)] from the period show only the subtle modulation of the "bridge" between the central peak and adjacent peaks, but the accompanying spectral evolution [Fig. 11(d)] is striking. This evolution is particularly well described as a certain asymmetric $N = 2$

soliton, which belongs to a class of soliton solutions to the NLSE with pulse shapes typically consisting of two peaks of unequal amplitude [4], with the ratio of these amplitudes varying through the soliton period. The fits depicted in Fig. 11(a) and (c) will be described in the following section.

V. Interpretation of the Pulse Shaping in the Laser

A. Unmodified Laser

The similarities between the evolutions in the unmodified laser, as depicted in Fig. 6 and Fig. 7 in particular, and those of the soliton solutions of the NLSE makes the comparison to the NLSE solutions attractive since the laser replicates its key pulse shaping mechanisms. In spite of additional pulse shaping mechanisms in the laser, it seems to be possible to force the generation of *true* solitons with only a simple modification to the cavity, as described above in Section IV. The soliton solutions of the NLSE have been well studied and the analytic functional forms can provide insight for an appropriate description of the pulses produced by this laser [4], [9], [12]. Salin *et al.* proposed that a model for pulse generation in the CPM laser might be developed by starting from the NLSE and considering other pulse shaping mechanisms as perturbations [4].

We first consider the evolutions observed and controlled in the unmodified laser, concentrating specifically upon the well-characterized condition corresponding to the single sweep autocorrelation of Fig. 1(b), the sampled autocorrelations and spectra of Fig. 7, and the relationship plotted in Fig. 10. First, the perfect coherence between the subpeaks of the pulse and the absence of significant chirp on the peaks throughout the evolution of the autocorrelations of Fig. 7(a) and (c) indicate the lack of any complex phase modulation. Second, the duration of these higher order pulses is an asymmetric function of cavity dispersion, similar to that for the lowest order $N = 1$ soliton-like pulses; starting from a condition of excess negative GVD, an increase in the amount of intracavity glass results in a reduction in the pulse durations until a minimum is reached. The addition of still more glass renders the pulsing unstable, just as it does for the shortest lowest order pulses [1], [13].

These two points indicate the presence of a primarily positive SPM balanced by the negative GVD of the prism sequence. A strong asymmetry of pulse duration as a function of intracavity dispersion has been identified as evidence for the action of SPM and GVD of opposite sign [1], [2], [6]. Since the prism sequence is tuned into the negative GVD regime for these pulses, a positive SPM must be present to balance the negative linear chirp that the prisms impart upon the pulses. The lack of significant chirp or more complex phase modulation indicates that the contribution to SPM from time-dependent or off-resonance saturation of the DODCI or its photoisomer must be small [1]. The remaining potential source of simple, positive SPM is the fast Kerr effect in the ethylene glycol solvent of the absorber jet, which is at the point of highest intracavity intensity [1]. A similar interpretation of the action of the solvent and dye of absorber jet was invoked by Valdmanis *et al.* who observed enhanced pulse shortening in CPM lasers for properly balanced SPM and GVD [1]. The theoretical model of Martinez *et al.* compared this enhanced ultrashort pulse shaping to the propagation of the lowest order soliton [2].

Indeed, the evolutions we have observed have certain similarities with those expected for higher order solitons. Among the similarities, we note: 1) the coherence between the multiple peaks of the pulse, indicating a self-shaping effect as opposed to the "satellite" formation indicative of poor mode locking seen in other dye lasers; 2) the spectral evolution of Fig. 7(b) is similar to that of an asymmetric $N = 2$ soliton, as in Fig. 11(c); 3) the plot of Fig. 10 relates pulse length, period, and cavity dispersion in a way consistent with soliton propagation; and 4) the transition from lower to higher order modes is accomplished by increasing the intensity in the nonlinear medium. Despite these similarities, it does not appear possible to fit these evolutions as pure solitons. The discrepancies include: 1) the successive decreases in intensity required to sweep from the $N = 3$ mode to the next two modes, as in Fig. 1, are not in the exact expected ratio of 9 : 4 : 1 that is seen in fibers, but at most approximately 5 : 3 : 1, as determined by estimating the intensity in the absorber jet for its different positions; 2) while the higher order solitons launched in a fiber of a given dispersion have the same period, the transition from the periodic condition of Fig. 1(b) to that of Fig. 1(a) is accompanied by an abrupt doubling of the period, as seen in Fig. 7; 3) the increasing temporal separation between the subpeaks of the pulse during the period of Fig. 6 and lack of a symmetry point in the temporal evolution at $T/2$ is not expected for a pure $N = 2$ asymmetric soliton; and 4) for the evolution that was compared to an $N = 3$ soliton (jet at the focus, Fig. 1(a), Fig. 6), the large chirp on the pulses early in the period may indicate the action of a complex phase modulation mechanism.

It may be possible to describe these pulses as solitons perturbed by the important shaping effects of saturable gain and saturable loss, as suggested by Salin *et al.* [4]. Avramopoulos *et al.* have included such mechanisms in numerical simulations of a ring dye laser [6]. Their results predict periodic evolutions that have certain qualitative similarities with those that we have observed. The simulated evolutions can closely resemble those of higher order solitons only when the relative magnitudes of shaping mechanisms other than a simple positive SPM and negative GVD are reduced. This amounts to reducing the strength of the conventional mode-locking process [6]. Accordingly, the numerically predicted solitons are of noticeably longer duration than the shortest pulses. The evolutions we have observed in the unmodified laser can display autocorrelation features as short as 50 fs in duration, indicating that they would not fall under the soliton re-

gime of Avrampoulos' model, but rather in the regime of the model where the effects of saturable gain and saturable loss are significant.

An additional shaping mechanism that appears to have a strong effect on the periodic evolutions we have observed is the collision of the pulses, which is not explicitly addressed in either the model of Martinez *et al.* [2] or that of Avramopoulous [6]. Even when the evolutions of the counterpropagating pulses are strongly asymmetric, we have found them to be locked in phase and to have complementary spectra; when the spectrum of one beam features a "hole," the spectrum of the counterpropagating beam typically features a peak at the same wavelength as the hole (Fig. 9). The precise reason for this behavior is not known, but it is clear that the counterpropagating pulse evolutions are strongly coupled. It may be that *cross* phase modulation of the colliding pulses must be considered, as well as the precise nature of their interaction in the saturation of the absorber.

B. *Laser with Intracavity Filter*

In spite of the potentially complicating effects presented in the previous section, it appears that our simple modification to the CPM laser via intracavity filtering results in a condition for pulse shaping that is very well approximated by the NLSE. We have found that the addition of the intracavity filter [7] allows the generation of pulses that are particularly well described as $N = 2$ asymmetric solitons [4]. This modification simplifies the intracavity shaping mechanisms, and allows stable pulsing for values of negative GVD closer to zero.

The prevention of a shift to longer wavelengths with a simple edge filter between the prisms [7] allows stable operation for amounts of intracavity glass that otherwise result in instability, namely, amounts that bring the negative GVD closer to zero. It is in this region that *true* asymmetric $N = 2$ solitons are generated. The effect of the filter as described in Section IV can be interpreted as prevention of a shift to longer wavelengths analogous to the soliton self-frequency shift (SSFS) seen in fibers [14]. When the pulse duration is less than 1 ps, a stimulated Raman effect in fused silica gives rise to a continuous downshift in carrier frequency as a soliton propagates [9]. We believe that an analog to the SSFS is observable in the CPM laser. The evidence is the long wavelength "tail" that appears between 640 and 650 nm in the spectra of CPM pulses shorter than approximately 60 fs [1], [13]. This feature may be due to an SSFS-like stimulated Raman shift in the DODCI absorber. A shift of approximately 620 cm^{-1} has been identified for DODCI in ethylene glycol [21], which closely matches the energy separation between spectral wings observed for the shortest pulses [1], [13]. Only the shortest pulses contain Fourier components spaced apart by 620 cm^{-1}, so only the shortest pulses have the potential to undergo a stimulated Stokes shift of energy from shorter to longer wavelength components upon repeated passage through the DODCI. Note that Avrampopoulos *et al.* have identified another possible shifting mechanism which results from the combination of chirping by SPM and pulse envelope reshaping by the passive mode-locking process, possibly forcing the carrier frequency out of the gain bandpass of the laser [6].

The first report of $N = 2$ asymmetric solitons was by Salin *et al.* in an unmodified CPM laser [4]. This class of soliton is typically described as a two-peaked pulse, with one peak larger in amplitude, and the ratio of the peaks' amplitudes varying periodically as the soliton propagates. Certain spectral features predicted by theory were not recovered in Salin's data, most notably the spectral wings expected early in the period, and the deeply cut spectral hole at midperiod. The experimentally observed spectra from our CPM laser with filter are in particularly good agreement with those expected for a certain asymmetric $N = 2$ soliton, reproducing all of the features shown in the fit of Fig. 11(c). Two poles η_1 and η_2 and two residues c_1 and c_2 parameterize the soliton shape and propagation. For *true* $N = 2$ solitons, $\eta_1 + \eta_2 = 2$ is chosen [4], [12]. The energy of the true soliton is constant as it propagates, and is proportional to the square of the sum of the poles. For the evolution we have seen, the periodic energy modulation may be due to a slight motion of the poles [4], [12]. The evolutions of Fig. 11(a) and (c) are those of the asymmetric $N = 2$ soliton characterized by $\eta_1 = 0.75$, $\eta_2 = 1.25$, $c_1 = 0.3$, $c_2 = 1.1$ at the beginning and end of the period, with a sinusoidal motion imposed upon the poles η_1 and η_2 that reduces their values by 10 percent at midperiod (the pulse energy therefore drops by 19 percent), but restores them after one soliton period. This not only describes the observed energy modulation, but also provides a better fit for the autocorrelations. The taller trace shown at midperiod of Fig. 11(a) corresponds to the autocorrelation calculated for the soliton with unmodulated poles (constant energy). The taller peak and wings of this trace provide a poor fit for our data. A similar mismatch was reported by Salin *et al.* [4]. The spectral features are not altered significantly by this motion of the poles, and are in particularly good agreement with the experimental spectra of Fig. 11(d), reproducing all of the features shown in the fit of Fig. 11(c).

It is interesting to note that this regime occurs at values of negative GVD closer to zero than possible without the intracavity filter, which is where the model of Avramopoulos predicts the strongest periodic pulse shaping [6]. However, we also observe strongly periodic evolutions in the unmodified laser tuned well into a regime of negative GVD. The features of our asymmetric $N = 2$ soliton are of duration as short as ~ 150 fs, which is from three to four times the duration of the shortest pulse possible. This agrees with the interpretation that *true* solitons can arise when the passive mode-locking mechanisms are relatively weak compared to the mechanisms of balanced SPM and GVD [6]. However, the presence of weak mode locking may cause the motion of the poles. A saturable gain can preferentially amplify the leading edge of a pulse, while a slow saturable absorber can reduce it. Indeed, the pri-

mary effect of the motion we have observed is to reduce the amplitude of the leading, taller peak of the double-peaked pulse. While the saturable shaping effects should be weak in order for the soliton to propagate [6], a slight imbalance between the two may be responsible for the pole motion.

VI. Conclusions

Appropriate reduction or removal of shaping mechanisms other than a balanced self-phase modulation (SPM) and group velocity dispersion (GVD) will result in a condition for the colliding pulse mode-locked laser (CPM) that more closely approximates the soliton pulse shaping predicted by the nonlinear Schrodinger equation (NLSE). We have forced the generation of *true* $N = 2$ asymmetric solitons with an intracavity filter. The filter seems to prevent an effect similar to the soliton self-frequency shift (SSFS) and allows stable pulse generation for values of negative GVD that are closer to zero than otherwise possible. Without the intracavity filter, stable periodic pulse evolutions are observed and controlled by increasing the intracavity SPM and adjusting the GVD. We have determined that a primarily positive, simple SPM and a balancing negative GVD are important shaping mechanisms in these evolutions. In spite of this and other qualitative similarities to classic higher order solitons, it does not appear possible to fit the pulses in the unmodified laser as solitons. The differences can be traced to other shaping mechanisms, such as saturable gain and saturable loss. The numerical model of Avramopoulos *et al.* shows promise in the simulation of the evolutions like those we have seen. However, the collision of the pulses in the absorber may also require consideration since we have found the counterpropagating pulse evolutions to be strongly coupled.

References

[1] J. A. Valdmanis and R. L. Fork, "Design considerations for a femtosecond pulse laser balancing self phase modulation, group velocity dispersion, saturable absorption and saturable gain," *IEEE J. Quantum Electron.*, vol. QE-22, pp. 112-118, Jan. 1986.

[2] O. E. Martinez, R. L. Fork, and J. P. Gordon, "Theory of passively mode locked lasers including self-phase modulation and group velocity dispersion," *Opt. Lett.*, vol. 9, pp. 156-158, May 1984.

[3] F. Salin, P. Grangier, G. Roger, and A. Brun, "Observation of high-order solitons directly produced by a femtosecond ring laser," *Phys. Rev. Lett.*, vol. 56, pp. 1132-1135, Mar. 1986.

[4] —, "Experimental observation of nonsymmetrical $N = 2$ solitons in a femtosecond laser," *Phys. Rev. Lett.*, vol. 60, pp. 569-572, Feb. 1988.

[5] F. W. Wise, I. A. Walmsley, and C. L. Tang, "Simultaneous formation of solitons and dispersive waves in a femtosecond ring dye laser," *Opt. Lett.*, vol. 13, pp. 129-131, Feb. 1988.

[6] H. Avramopoulos, P. M. W. French, J. A. R. Williams, G. H. C. New, and J. R. Taylor, "Experimental and theoretical studies of complex pulse evolutions in a passively mode-locked ring dye laser," *IEEE J. Quantum Electron.*, vol. 24, pp. 1884-1892, Sept. 1988.

[7] W. L. Nighan, T. Gong, and P. M. Fauchet, "Control and characterization of soliton-like pulses in a femtosecond dye laser," in *Ultrafast Phenomena VI, Springer-Verlag Series in Chemical Physics*, T. Yajima, K. Yoshihara, C. B. Harris, and S. Shionoya, Eds., vol. 48. Berlin: Springer-Verlag, 1988, pp. 109-111.

[8] —, "Generation and control of solitons and soliton-like pulses in a femtosecond ring dye laser," *Opt. Lett.*, vol. 14, pp. 447-449, May 1989.

[9] See, for example, R. H. Stolen, L. F. Mollenauer, and W. J. Tomlinson, "Observation of pulse restoration at the soliton period in optical fibers," *Opt. Lett.*, vol. 8, pp. 186-188, Mar. 1983.

[10] J. C. Diels, W. Dietel, J. J. Fontaine, W. W. Rudolph, and B. Wilhemi, "Analysis of a mode locked ring laser: Chirped-solitary-pulse solutions," *J. Opt. Soc. Amer. B*, vol. 2, pp. 680-686, Apr. 1985.

[11] H. A. Haus and Y. Silberberg, "Laser mode locking with addition of nonlinear index," *IEEE J. Quantum Electron.*, vol. QE-22, pp. 325-331, Feb. 1986.

[12] H. A. Haus and M. N. Islam, "Theory of the soliton laser," *IEEE J. Quantum Electron.*, vol. QE-21, pp. 1172-1188, Aug. 1985.

[13] K. L. Schehrer, E. S. Fry, and G. T. Bennet, "Colliding pulse mode-locked dye laser stabilization using an intracavity spectral filter," *Appl. Opt.*, vol. 27, pp. 1908-1910, May 1988.

[14] F. M. Mitschke and L. F. Mollenauer, "Discovery of the soliton self frequency shift," *Opt. Lett.*, vol. 11, pp. 659-661, Oct. 1986.

[15] J. A. Valdmanis, R. L. Fork, and J. P. Gordon, "Generation of optical pulses as short as 27 femtoseconds directly from a laser balancing self-phase modulation, group-velocity dispersion, saturable absorption, and saturable gain," *Opt. Lett.*, vol. 10, pp. 131-133, Mar. 1985.

[16] E. P. Ippen, C. V. Shank, and A. Dienes, "Passive mode locking of the cw dye laser," *Appl. Phys. Lett.*, vol. 21, pp. 348-350, Oct. 1972.

[17] D. N. Dempster, T. Morrow, R. Ranken, and G. F. Thompson, "Photochemical characteristics of cyanine dyes," *J. Chem. Soc. Faraday II*, vol. 68, pp. 1479-1496, Sept. 1972.

[18] F. Beisser, private communication.

[19] We find that jet thickness must also be tuned to achieve the shortest $N = 1$ soliton-like pulses.

[20] In order to resolve the fringes for each sampled interferometric autocorrelation, the shaker was driven at only 0.5 Hz.

[21] Y. G. Fuh, R. F. Code, and R. P. Wolf, "Anti-Stokes Raman scattering from DODCI solutions," *J. Luminescence*, vol. 26, pp. 329-336, Jan.-Mar. 1982.

William L. Nighan, Jr. was born in Evanston, IL, in 1962. He received the Sc.B. degree in electrical engineering from Brown University, Providence, RI, in 1984.

He is presently working towards the Ph.D. degree in electrical engineering at Princeton University, Princeton, NJ. His research interests include the development of ultrashort-pulsed lasers and amplifiers and ultrafast spectroscopy of semiconductors.

Ting Gong was born in Shanghai, China, in 1964. He received the B.S. degree in applied physics from Jiao Tong University, Shanghai, China, in 1984 and the M.S. degree in electrical engineering from the State University of New York, Buffalo, in 1986.

He is currently pursuing the Ph.D. degree in electrical engineering at Princeton University, Princeton, NJ. His research interests are focused on femtosecond laser systems and their use for studying transient phenomena in semiconductors.

Philippe M. Fauchet, for a photograph and biography, see p. 963 of the May 1989 issue of this JOURNAL.

Ultrafast electronic and structural processes in highly excited crystalline and noncrystalline silicon

P. M. Fauchet, MEMBER SPIE
Princeton University
Department of Electrical Engineering
Laboratory for Ultrafast Spectroscopy
Princeton, New Jersey 08544

Abstract. The carrier dynamics of highly excited ($N \geq 10^{20}$ cm^{-3}) crystalline and amorphous silicon have been studied by picosecond and femtosecond pump and probe measurements. The Auger coefficient, trapping time, and other parameters relevant for transport have been obtained. At still higher excitation, melting occurs. The optical constants of liquid Si have been measured, and evidence for superheating of the liquid phase above the boiling temperature is presented.

Subject terms: laser-induced material modification; crystalline silicon; microcrystalline silicon; amorphous silicon; liquid silicon; Auger coefficient; picosecond time-resolved reflectivity.

Optical Engineering 28(10), 1096-1100 (October 1989).

CONTENTS

1. INTRODUCTION

The past 10 years have witnessed considerable progress in our understanding of ultrafast phenomena in solids in general and in semiconductors in particular. New avenues of research have been opened thanks to high power, short pulse lasers capable of producing very dense electron-hole plasmas and even phase transitions. High excitation of this type can be achieved only with picosecond or femtosecond lasers capable of delivering intensities in excess of 1 GW/cm^2. The nonequilibrium conditions thus achieved are unique to ultrafast laser pulse excitation and, because of the highly transient nature of the processes, are best studied with ultrafast laser spectroscopy.

In this paper, we review our recent work on ultrafast electronic and structural processes in highly excited silicon. In the first part, we compare the carrier lifetime in single crystals, thin microcrystalline films, and thin amorphous films. The Auger coefficient is obtained in c-Si, the time for trapping at grain boundaries of μc-Si is measured as a function of the film's properties, and the lifetime of carriers in extended states of a-Si:H is characterized. In the second part, the optical properties of molten silicon are measured and evidence for superheating of the liquid phase is presented. Throughout the paper, simple classical concepts, such as the Drude model, are used to explain the data and measure various parameters.

2. CARRIER LIFETIME

2.1. Crystalline silicon

Crystalline silicon is an indirect-gap semiconductor with, at low densities, a long carrier lifetime that is controlled by surface recombination for excitation of a thin layer and by recombination at bulk defects otherwise.[1] For a carrier density $N > 10^{18}$ cm^{-3}, Auger recombination becomes prevalent and the effective lifetime diminishes.[2] It is unclear whether the Auger coefficient γ remains constant in the presence of a dense ($N \sim 10^{20}$ cm^{-3}) electron-hole plasma. In fact, theory[3,4] and experiments[5] suggest that γ decreases in the presence of a degenerate plasma in direct-gap semiconductors.

Pump and probe measurements were performed near Brewster's angle (θ_B) with a picosecond Nd:YAG laser. The pump beam at 532 nm injects carriers with a total excess kinetic energy of ~ 1.2 eV. The carriers thermalize within ~ 1 ps.[6] Since the pulse direction is ~ 30 ps, thermalization is taken to be instantaneous. The reflectivity R of the p-polarized probe beam at 1064 nm is measured as a function of time delay near θ_a. Because $R(\theta \simeq \theta_B)$ is nearly zero and $\theta_B = \arctan n$, where n is the refractive index, a small Δn leads to a larger $\Delta R/R$ than at near-normal incidence.[7] We have exploited this to easily obtain an order-of-magnitude

Invited Paper LI-107 received Feb. 14, 1989; accepted for publication March 14, 1989.

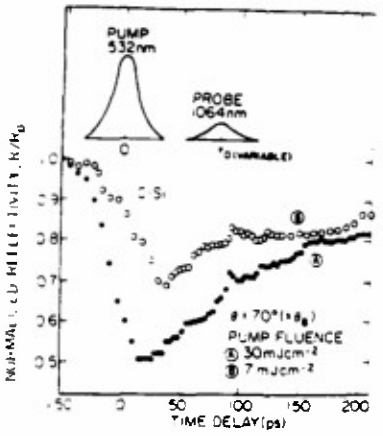

Fig. 1. Reflectivity R of Si normalized to the initial reflectivity R_0 measured at 1064 nm and $\theta = 70°$ for two pump fluences, corresponding to injection of $N > 10^{20}$ cm^{-3}.

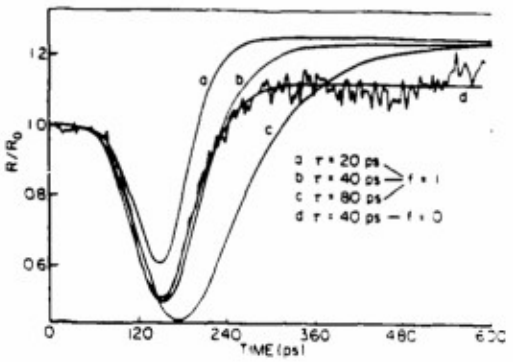

Fig. 2. Normalized reflectivity of the as-grown sample measured at 1064 nm and fits for three trapping times τ and two extrema values of f ($N_{injected} = 2 \times 10^{20}$ cm^{-3}).

improvement of the signal-to-noise ratio in pump and probe measurements.[7-10]

Figure 1 shows typical results obtained for two fluences. The increased sensitivity of probing near θ_B is demonstrated by noting that in similar experiments performed near normal incidence, $\Delta R/R_0 \sim 25\%$ a for a fluence of 110 mJ/cm^2.[11] Note that if $\theta > \theta_a$, the reflectivity increases upon carrier injection.[10] To obtain γ, the procedure is as follows[7]: the injected carrier density is calculated and recombination is assumed to occur at a rate given by γN^3; the real part of the index of refraction at 1064 nm is calculated using a simple Drude model and taking into account the increase of lattice temperature due to the thermalization of hot carriers $[n = [(n_0 + \beta T)^2 - \omega_p^2/\omega^2]^{1/2}$, where $\omega_p^2 = N(t)e^2/m^*\epsilon_0]$; R is then calculated using the Fresnel reflection coefficients in which the imaginary part of the index of refraction is neglected. Using this procedure we have found that for $N \sim 10^{20}$ cm^{-3}, $\gamma \cong 2 \times 10^{31}$ cm^6·s^{-1},[7] a value that is a factor of two smaller than the accepted coefficient at low density.[2] This reduction at large density is smaller than in direct-gap semiconductors. The difference can be traced to the larger effective mass of Si and to its indirect gap.

2.2. Microcrystalline silicon

In polycrystalline films, the grain boundaries control the electronic properties through the presence of defects, which may act as trapping centers.[12] The effective decrease of the carrier lifetime is usually detrimental although it occasionally serves a purpose, as in photoconductive Auston switches.[13] Doping, heat treatment, and other processing steps may modify the trapping time at the grain boundaries. We have investigated changes in the carrier lifetime in small grain (< 500Å) microcrystalline silicon films grown on a thermal oxide. The film and the oxide grown on a Si wafer were ~0.5 μm thick. Samples were either as-grown by low pressure chemical vapor deposition or implanted with phosphorous and annealed; in some samples, hydrogen was diffused.[14]

The experimental procedure is similar to that used in Sec. 2.1. An additional complexity arises from the thin film multilayer structure of the samples. The angle at which the films exhibited a minimum in R played the role of θ_B and in the analysis, the Fresnel reflection coefficients used to calculate R were replaced by a multilayer matrix formalism derived from Ref. 15. The equations governing the carrier dynamics and the evolution of the lattice temperature were also modified to account for trapping at the grain boundaries. In addition to the generation rate and to Auger recombination, a term describing the trapping of carriers was included to obtain N(t). The simplest description was chosen, namely, that the trapping rate is given by N/τ, where τ is the trapping time. The lattice temperature increased not only because of thermalization of the injected pairs and of the hot carriers produced by Auger recombination but also because trapping is a nonradiative event. Since the average trap's position within the bandgap is unknown, only an unknown fraction f of the bandgap energy is lost to heat. The best fit to the data will yield τ and f.

TABLE I. Summary of the findings for the five types of polySi studied here. The uncertainty on the trapping time on τ is approximately ±15%. For the implanted nonannealed sample, we can place only an upper bound on τ.

Sample	τ (ps)
as-grown	40
P+, $T_{anneal} = 1150$ °C	150
P+, $T_{anneal} = 900$ °C	50
P+, no anneal	< 10
H diffused	150

Figure 2 shows typical results. In all cases, it was found that choosing $f = 0$ yields, within the experimental accuracy, the best agreement between the model and the experiments. Table I summarizes our findings for the different types of samples investigated. Phosphorous doping by itself does not affect τ for $N \sim 10^{20}$ cm^{-3}. Annealing increases τ, provided that the average grain size increases, that is, that the density of trap states decreases. Adding hydrogen increases τ, presumable by passivation of the dangling bonds at the grain boundaries.[16] Finally, amorphization shortens τ. The fact that for all samples $f = 0$ indicates that the average trap energy is close to the band edge. It is also important to note that we have found no evidence for saturation of the traps despite the large injected carrier density. This results from

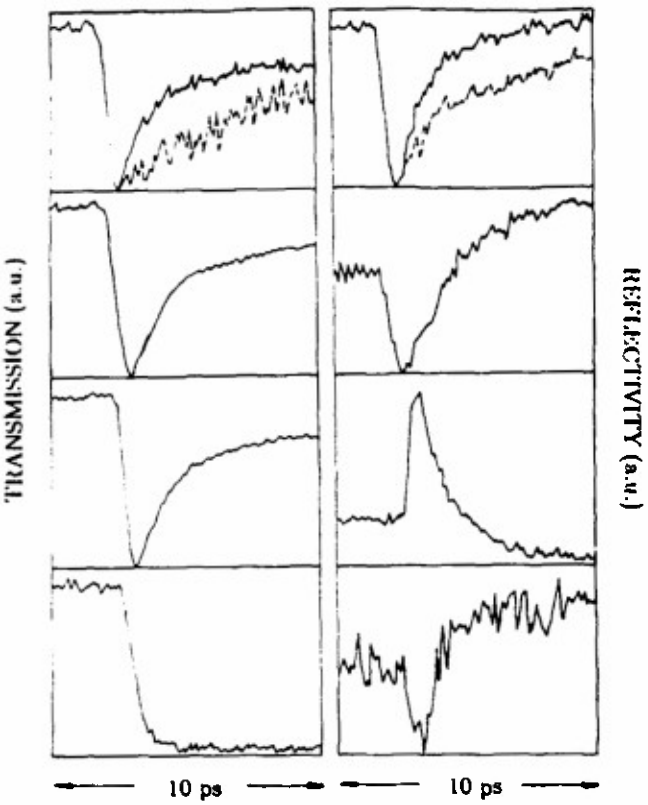

Fig. 3. Transmission and reflectivity (in arbitrary units) after injection of $N \sim 5 \times 10^{20}$ cm^{-3} with 2 eV photons, measured, from top to bottom, at 1000, 827, 722, and 525 nm. The two dashed lines correspond to lower injection ($N \sim 5 \times 10^{19}$ cm^{-3}).

the large number of trap sites at the grain boundaries and the large number of grain boundaries.

2.3. Amorphous silicon (a-Si:H)

Amorphous silicon is a material with no long range order and a very large number of trap states. By adding hydrogen, we saw in Sec. 2.2 that the total number of trap sites at grain boundaries can be decreased. Similarly, by alloying a-Si with H, it is possible to reduce the number of trap states located inside the bandgap to $\sim 10^{16}$ cm^{-3}.[17] However, close to the band edges, there exists a continuum of weakly localized states that form exponential bandtails. The total density of these states is $\sim 5 \times 10^{19}$ cm^{-3}.[18] Carriers in bandtail states are not very mobile, whereas carriers in the extended states have a mobility ($\mu \simeq 10$ cm$^2 \cdot$V$^{-1} \cdot$s^{-1}) close to that of c-Si. The energy level marking the transition between localized and extended states is called the mobility edge, and the energy difference between the valence band and conduction band mobility edges is called the mobility gap (E_{mob}). The optical bandgap E_G that is somewhat arbitrarily defined by a Tauc plot and E_{mob} are thought to be within a fraction of 1 eV of each other.

In Sec. 2.2, we observed that the carrier lifetime in amorphized Si is < 10 ps. We thus used a femtosecond dye laser system (CPM dye laser and frequency-doubled Nd:YAG laser amplification at 10 Hz) to perform time-resolved reflectivity R and transmission T experiments in a-Si:H.[19-22]

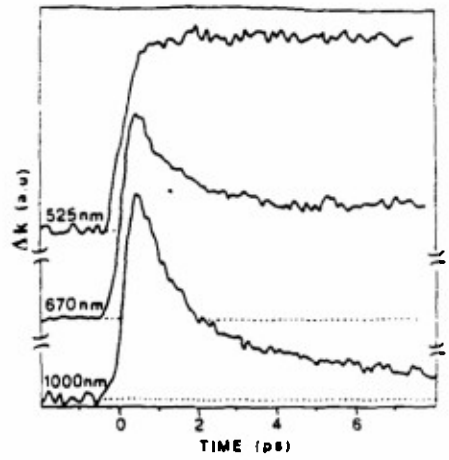

Fig. 4. Time-resolved changes of the imaginary part of the index of refraction for probe wavelengths from the transparent to the opaque spectral regions. The excitation conditions are the same for the three curves ($N \sim 2.5 \times 10^{20}$ cm^{-3}). The plateaus at 670 and 525 nm are the result of an increased interband absorption produced by the bandgap shrinkage induced by temperature.

Probe wavelengths from the blue to the infrared parts of the spectrum were conveniently available by generation of a white light continuum.[23] The pump photon energy (2 eV) was above E_G (~ 1.7 eV). The experiments were performed near normal incidence. From R and T, we obtain the real (n) and imaginary (k) parts of the refractive index by inversion of the Fabry-Perot formulae. Figure 3 shows several R and T curves taken with probe beams in the transparent region, slightly above E_G, and well above E_G. Dramatic changes already occur within 1 ps of injection. Significant recovery of the transmission is seen at all wavelengths, except for $\hbar\omega >> E_G$.

Analysis of the data yields curves such as those of Fig. 4. Here, we show the variations of the induced absorption at three photon energies. For $\hbar\omega < E_G$ and $N \sim 5 \times 10^{20}$ cm^{-3}, $\Delta\alpha(t = 0^+) \sim 10^4$ cm^{-1}. The recovery of $\Delta\alpha$ can be described by the sum of two exponentials, having time constants of ~ 1 ps and ~ 10 ps. The refractive index dips sharply at $t = 0^+ (\Delta n/n \simeq -2\%)$, then recovers and exceeds the initial value within ≥ 1 ps, and finally reaches a plateau after ~ 10 ps ($\Delta n/n \simeq 0.7\%$). For shorter probe wavelengths, $\Delta\alpha$ also increases sharply but settles down to a positive plateau whose final value increases as the wavelength decreases. The interpretation is not very different from that proposed in Sec. 2.2. At $t = 0^+$, the complex refractive index is modified by a Drude contribution, in which the phenomenological relaxation rate Γ is found to be equal to 2×10^{15} s^{-1} (Ref. 21). Within picoseconds, carriers then thermalize in the extended states, are trapped into the bandtail states, and recombine with carriers of the opposite sign. In doing so, electronic energy is transformed into phonons and the temperature of the sample increases. As E_G decreases when the temperature rises,[24] n and the interband absorption increase, leading to the positive plateau for n and to a wavelength-dependent plateau for k, when most of the electronic processes are over. A more detailed but still preliminary interpretation of the time constants for decay can be found in Ref. 22. Note however, the qualitative

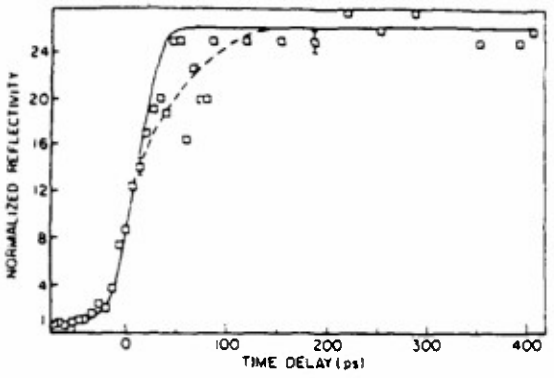

Fig. 5. Normalized reflectivity measured at 1064 nm and $\theta = 70°$ after melting with a 532 nm pulse slightly above threshold. The solid line was calculated using the data of Ref. 29.

agreement with the result of Sec. 2.2 for the amorphized sample.

3. STRUCTURAL TRANSITIONS

3.1. Melting

When the intensity of the laser is increased beyond that considered in Sec. 2, structural changes may be produced. At levels below the melting threshold of semiconductors, damage eventually occurs as a result of repetitive illumination.[25] In this section, we consider modifications produced by single pulses. It is well known that above a well-defined threshold, laser beams melt semiconductors.[26] This can be done with cw lasers[27] as well as with femtosecond laser pulses.[28] What was not well known are the optical properties of molten silicon. Ellipsometric measurements performed on Si molten in an oven suggested that it is a metal that can be described by a Drude model, with $\omega_p = 2.56 \times 10^{16}$ rad/s and $\tau = 0.217$ fs.[29] Recent nanosecond time-resolved ellipsometrie measurements during laser-induced melting of Si were, however, in disagreement with those values.[30]

We have measured the optical properties of molten Si in a pump and probe arrangement similar to that described in Sec. 2.1.[7,31,32] The probe wavelengths were the fundamental, frequency-doubled or frequency-tripled output of the Nd:YAG laser system. To obtain both the real part and the imaginary part of the dielectric function, we measured R at several angles of ineidenee (especially near θ_B). Figure 5 shows typical results obtained with a 1064 nm probe beam. The average R of the plateau that is observed ~ 100 ps after melting is the reflectivity of molten Si close to the melting temperature T_m. In Fig. 6, we have plotted the values of that plateau for different angles and probe wavelengths.

The solid line was calculated using the data of Ref. 29. It is clear that the agreement is quite good. We used our data to obtain ω_p and τ and found $\omega_p = 2.50 \times 10^{16}$ rad/s and $\tau = 0.212$ fs ($\pm 5\%$), in agreement with Ref. 29. If the mass of the electrons equals the free-electron mass, then the density N corresponds to four electrons per atom. The validity of the Drude model from the infrared to the ultraviolet indicates the absence of gaps or other features in the band structure of liquid Si in that energy range.[31] As diseussed in Ref. 31, the origin of the discrepaney with the results of Ref. 30 is not established. Note that another nanosecond time-

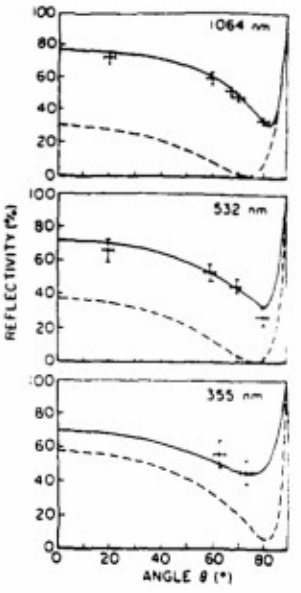

Fig. 6. Calculated (after Ref. 29) and measured reflectivity of molten Si at three wavelengths.

resolved ellipsometric study performed at 633 nm yields value of ω_p and τ within ~ 10% of our values.[33]

3.2. Superheating of the liquid

As the intensity of the laser is further increased, a visible plasma is produced in front of the sample. This requires laser pulses approximately four times above melting threshold. Visible plasma formation is accompanied by signifieant boiling at the surface, which appears strongly damaged when subsequently observed by optical microscopy. However, there is a relatively wide range of pump intensities at which significant energy is deposited in the liquid layer and yet there is no evidence for boiling or plasma formation. This excess energy heats the liquid layer beyond T_m (1683 K) and possibly beyond the boiling temperature T_b (2750 K). We are interested in the properties of this nonequilibrium liquid phase.[10,32]

The experimental arrangement is the same as before. Figure 7 compares measured and calculated reflectivity curves for two pump intensities, at melting threshold and well above melting threshold. Clearly, at high intensity, the data reach the same final plateau much later. The solid line fit is obtained by a one-dimensional computer code that solves the heat diffusion equations with the assumption that even if T_b is exceeded, the material remains in the liquid phase.[32] This assumption is valid as long as we observe no evidence for boiling or plasma formation. Under this and other assumptions discussed in Ref. 32, we find that $T > T_b$ for ~ 10 ps without measurable boiling. Note that the lower refleetivlty for $T > T_m$ results from a change in optical constants due to a decrease of τ similar to that described in Ref. 34. The faster cooling of the liquid to T_m predicted by the computer code results from the use of the thermal conductivity of molten Si at T_m, which is clearly an overestimate when $T >> T_m$. Since our experiments, superheating of the liquid layer has been confirmed by several groups.[35,36]

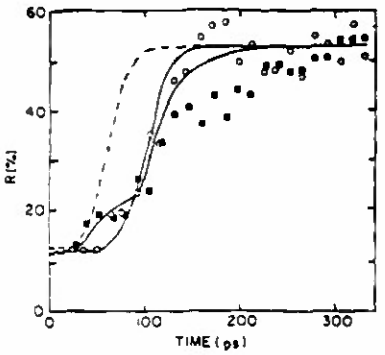

Fig. 7. Reflectivity jump measured at 532 nm and $\theta = 60°$ for two pump energies, just above threshold E_T (circles) and $-4 \times E_T$ (squares). The solid lines were obtained from a computer simulation that includes a heating of the liquid, while the dashed line assumes that the temperature never exceeds T_m for the higher pump energy.

4. CONCLUSIONS

High intensity excitation of crystalline, microcrystalline, or amorphous silicon with picosecond or femtosecond pulses has revealed a wealth of phenomena. Below melting threshold, various mechanisms for recombination of a dense electron-hole plasma ($N > 10^{20}$ cm^{-3}) have been characterized. Auger recombination, which is predominant in c-Si, is overshadowed by trapping involving localized states in μc-Si and a-Si:H. Above melting threshold, a liquid layer is produced. We have measured its optical constants and have demonstrated that heating of the liquid above the boiling temperature is possible for a very short period of time.

5. ACKNOWLEDGMENTS

I wish to acknowledge the contributions of my collaborators, N. K. Bambha, I. H. Campbell, T. Gong, K. Gzara, D. Hulin, N. Johnson, K. D. Li, A. Mourchid, W. L. Nighan, Jr., C. Tanguy, and S. Wagner. This work was supported in part by the National Science Foundation, the Army Research Office, and the Office of Naval Research. The author is supported in part by an NSF Presidential Young Investigator Award and by an Alfred P. Sloan Research Fellowship.

6. REFERENCES

1. E. Yablonovitch and T. Gmitter, Appl. Phys. Lett. 49, 586 (1986).
2. J. Dzievior and W. Schmid, Appl. Phys. Lett. 31, 346 (1977).
3. A. Haug, Solid-State Electron. 21, 1281 (1978).
4. C. Tanguy and M. Combescot, Solid State Commun. 57, 539 (1986).
5. P. M. Fauchet, Phys. Status Solidi b:110, K11 (1982).
6. L. A. Lompré, J. M. Liu, H. Kurz, and N. Bloembergen, Appl. Phys. Lett. 43, 168 (1983); Appl. Phys. Lett. 44, 3 (1984).
7. P. M. Fauchet and W. L. Nighan, Jr., Appl. Phys. Lett. 48, 721 (1986).
8. K. D. Li and P. M. Fauchet, Solid State Commun. 61, 207 (1987).
9. I. H. Campbell and P. M. Fauchet, Opt. Lett. 13, 634 (1988).
10. P. M. Fauchet, IEEE J. Quantum Electron. QE-25, 1072 (1989).
11. D. von der Linde and N. Fabricius, Appl. Phys. Lett. 41, 991 (1982).
12. J. Y. Seto, J. Appl. Phys. 46, 5247 (1975).
13. D. H. Auston, in *Picosecond Optoelectronic Devices*, p. 73, C. H. Lee, ed., Academic Press, Orlando, Fla. (1984).
14. N. K. Bambha, W. L. Nighan, Jr., I. H. Campbell, P. M. Fauchet, and N. M. Johnson, J. Appl. Phys. 63, 2316 (1988); Mat. Res. Soc. Symp. Proc. 106, 323 (1988).
15. O. S. Heavens, *Optical Properties of Thin Solid Films*, Dover Press, New York (1985).
16. N. M. Johnson, D. K. Biegelsen, and M. D. Moyer, Appl. Phys. Lett. 40, 882 (1982).
17. N. B. Goodman, Philos. Mag. B45, 407 (1982).
18. T. Tiedje, in *Semiconductors and Semimetals*, Vol. 21C, p. 207, J. I. Pankove, ed., Academic Press, Orlando, Fla. (1984).
19. P. M. Fauchet, D. Hulin, A. Migus, A. Antonetti, J. Kolodzey, and S. Wagner, Phys. Rev. Lett. 57, 2438 (1986).
20. P. M. Fauchet, D. Hulin, A. Migus, A. Antonetti, J. P. Conde, and S. Wagner, J. Non-Cryst. Solids 97&98, 145 (1987).
21. C. Tanguy, D. Hulin, A. Mourchid, P. M. Fauchet, and S. Wagner, Appl. Phys. Lett. 53, 880 (1988).
22. P. M. Fauchet and D. Hulin, J. Opt. Soc. Am. B 6, 1024 (1989).
23. A. Migus, A. Antonetti, J. Etchepare, D. Hulin, and A. Orszag, J. Opt. Soc. Am. B2, 584 (1985).
24. J. Perrin and I. Solomon, J. Non-Cryst. Solids 37, 407 (1980).
25. P. M. Fauchet, Phys. Lett. 93A, 155 (1983).
26. N. Bloembergen, in *Laser-Solid Interaction and Laser Processing*, p. 1, S. D. Ferris et al., eds., Am. Inst. Phys., New York (1979).
27. R. J. Nemanich, D. K. Biegelsen, and W. G. Hawkins, Phys. Rev. B27, 7818 (1983).
28. C. V. Shank, R. Yen, and C. Hirlimann, Phys. Rev. Lett. 50, 454 (1983).
29. K. M. Shvarev, B. A. Baum, and P. V. Gel'd, Sov. Phys. Solid State 16, 2111 (1975).
30. G. E. Jellison, Jr., and D. H. Lowndes, Appl. Phys. Lett. 47, 718 (1985); Appl. Phys. Lett. 51, 352 (1987).
31. K. D. Li and P. M. Fauchet, Appl. Phys. Lett. 51, 1747 (1987).
32. P. M. Fauchet and K. D. Li, J. Non-Cryst. Solids 97&98, 1267 (1987); Mat. Res. Soc. Symp. Proc. 100, 477 (1988).
33. G. M. Gusakov, A. A. Komarnitskii, and S. S. Sarkisyan, Sov. Tech. Phys. Lett. 12, 74 (1986).
34. K. Ujihara, J. Appl. Phys. 43, 2376 (1972).
35. B. Danielzik, P. Harten, K. Sokolowski-Tinten, and D. von der Linde, Mat. Res. Soc. Symp. Proc. 100, 471 (1988).
36. J.-K. Wang, P. Saeta, M. Buijs, M. Malvezzi, and E. Mazur, in *Ultrafast Phenomena VI*, p. 236, T. Yajima et al., eds., Springer-Verlag, Berlin (1988).

Philippe M. Fauchet was born in Reims, France, in 1955. He received the engineer's degree at Faculté Polytechnique de Mons, Belgium, an MS degree in engineering at Brown University, and a Ph.D. in applied physics at Stanford University, where he stayed one year on an IBM postdoctoral fellowship in the Edward L. Ginzton Laboratory. He has been on the faculty of the Department of Electrical Engineering at Princeton University since September 1984. He was also a visiting professor at the Université de Paris VI during the summer of 1985. His research interests are concentrated in ultrafast laser spectroscopy of semiconductors, laser/solid interactions, and physics and technology of noncrystalline semiconductors. At Stanford, his thesis work was on picosecond laser annealing and laser-induced surface ripples. At Princeton, he has worked on picosecond laser-induced nonequilibrium melting, laser-induced damage in semiconductors and optical components, various applications of the Raman microprobe in semiconductor technology, Raman spectroscopy of nanocrystalline objects, and very recently, new optical measurement techniques and soliton-like pulseshaping in femtosecond lasers. Presently, a large fraction of his research group is involved with the study of femtosecond and picosecond carrier dynamics in amorphous semiconductors and with the development of ultrafast electro-optic and opto-optic semiconductor devices. Dr. Fauchet received an IBM Faculty Development Award in 1985, an NSF Presidential Young Investigator Award in 1987, and a Sloan Research Fellowship in 1988. He has authored or coauthored 80 technical publications, served as cochair of the SPIE conference Laser Optics for Intracavity and Extracavity Applications held in January 1988, and is cochair for the Fall 1989 MRS Symposium on Materials Issues in Microcrystalline Semiconductors and for the 1990 SPIE conference on Applications of Ultrashort Laser Pulses in Science and Technology (part of the Int. Congress on Optical Science and Engineering, The Hague, The Netherlands). He also teaches a course on Optical Microscopic Techniques for Characterization of Semiconductor Thin Films.

Ultrafast relaxation dynamics of photoexcited carriers in GaAs

T. Gong, W. L. Nighan, Jr., and P. M. Fauchet

Princeton Laboratory of Ultrafast Spectroscopy
Department of Electrical Engineering
Princeton University, Princeton, NJ 08544

ABSTRACT

We report time-resolved pump-probe measurements of both absorption and refractive index for GaAs thin films with 80 fs time resolution. The probe photon energies are near the band-edge and near the initial excited states, and photoexcited carrier densities are varied from 10^{17} to 10^{19} cm^{-3}. Our results reveal the instantaneous band gap renormalization and the importance of carrier-carrier scattering and intervalley scattering. Mechanisms which cause an ultrafast change in refractive index are also discussed.

INTRODUCTION

The understanding of ultrafast carrier relaxation processes in GaAs is very important for the development of high speed optical and electronic devices. The recent advent of femtosecond lasers has provided a unique tool for exploring such dynamics directly. Different research groups have made many contributions to this field by using femtosecond optical pulses. Pump and continuum-probe transmission measurements were first made by Shank et al [1,2] with subpicosecond time resolution and provided the first observation of ultrafast band-gap renormalization and the investigation of carrier thermalization. Equal-pulse-correlation [3,4] and single wavelength pump-probe [5,6] transmission measurements were made to study the scattering rates from the initial excited states. Recently, the pump and continuum-probe method was also used to investigate hole burning [7,8] and transient absorption saturation [9,10]. Femtosecond lasers were also used to perform time-resolved luminescence experiments [11,12], which provide another way to study hot carrier processes.

In this paper we report femtosecond pump and continuum-probe measurements on GaAs thin films. Carrier-induced changes in both absorption coefficients and refractive indices are presented at probe energies both near the band-edge and near the initial excited states. The importance of different hot carrier processes, such as band gap renormalization, carrier-carrier scattering, intervalley scattering, state and band filling, and their dependence on carrier densities are discussed.

EXPERIMENTAL CONSIDERATIONS

The samples used for our experiments are GaAs thin films grown by MBE at Princeton University, and are prepared using the technique developed by Yablonovitch et al [13]. A 0.3 μm layer of undoped GaAs was grown on top of a thin (0.1 μm) layer of $Al_{0.8}Ga_{0.2}As$ grown on a GaAs substrate. The sample was covered by black wax uniformly and was left in a dilute HF solution at $\sim 0^\circ$C overnight. The thin $Al_{0.8}Ga_{0.2}As$ layer was etched off and the GaAs layer with wax was then released from the substrate and floated on the surface of the acid. It then was carefully placed on a sapphire window where it remained attached due to Van der Waals bonding. The wax was then removed. The film was thinned several times by etching in a solution of $H_3PO_4 : H_2O_2 : H_2O$ (3 : 1 : 50) for a very short time. Therefore we could perform experiments on samples with different thicknesses.

The output of a colliding pulse modelocked dye laser is amplified by a copper vapor laser. Our system [14] generates pulses of 70 fs duration, 10 μJ energy and at a repetition rate of 8 KHz. A small fraction of the pulse at 620 nm ($h\nu$=1.99 eV) is split off as a pump beam. The remainder is focused onto a 1.25 mm thick jet of ethylene glycol, generating a white-light continuum. Interference filters are used to select the desired probe photon energies from the continuum. The polarization of the pump beam is rotated by 90° to reduce the coherent artifact. The pump beam is chopped at 200 Hz and lock-in amplification as well as real-time differential technlques are used for noise suppression. The intensity of the pump pulse is varied over nearly two order of magnitude, and the carrier density is estimated from the energy of the pump pulse absorbed by the film.

The time-resolved transmission (T) and reflection (R) are simultaneously measured at room temperature in the pump-probe configuration near normal incidence. Probe photon energies are near the band-edge (1.38-1.48 eV) and near the initial excited state (1.99-2.18 eV). The carrier densitiy varies from 10^{17} to 10^{19} cm^{-3}. Typical T and R traces are shown in Fig.1 and Fig.2.

In order to explain precisely the transient changes of optical properties of a thin absorbing film on a thick transparent substrate, we developed a computer algorithm which calculates the absorption coefficient (α) and refractive index (n) from the measured T and R. On the other hand, by using the well known optical constants for GaAs [15] and the measured thickness of the film, we also calculated the transmission from our algorithm. A good fit is obtained between calculated and measured transmission as shown in Fig.3.

RESULTS

A. Introduction

Fig.4 illustrates the schematic band structure of GaAs. For pump photon energy near 2 eV, electrons can be excited to the conduction Γ valley from heavy hole, light hole, and spin orbit split-off valence bands. The relative strengths of SO-HH-LH transitions

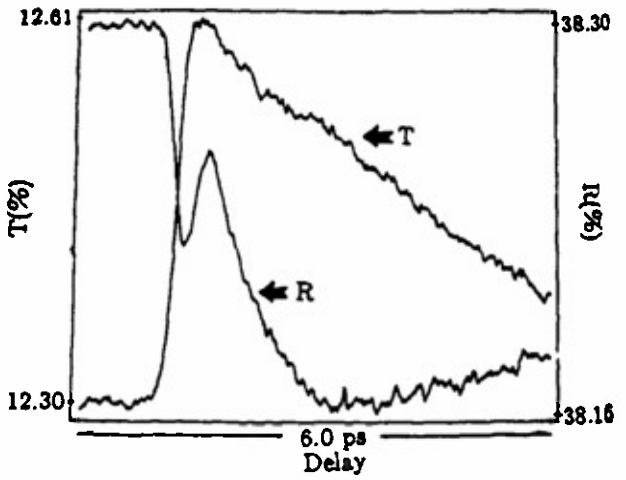

Fig.1: Measured time-resolved transmission and reflection traces at 2.18 eV and for carrier density $4x10^{18}$ cm^{-3} injected at 1.99 eV.

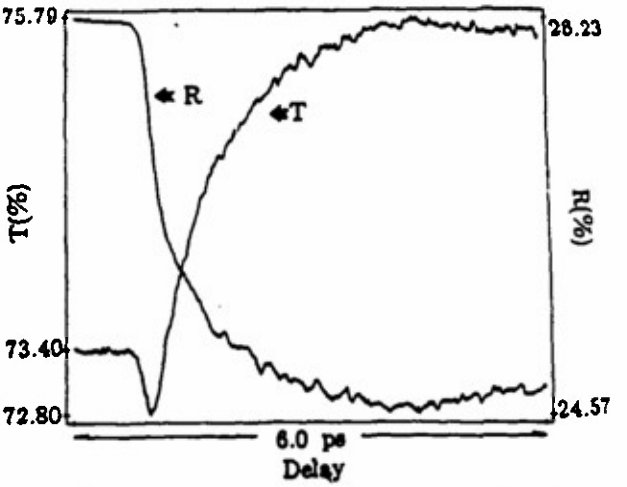

Fig.2: Measured time-resolved transmission and reflection traces at 1.38 eV and for carrier density $3x10^{18}$ cm^{-3} injected at 1.99 eV.

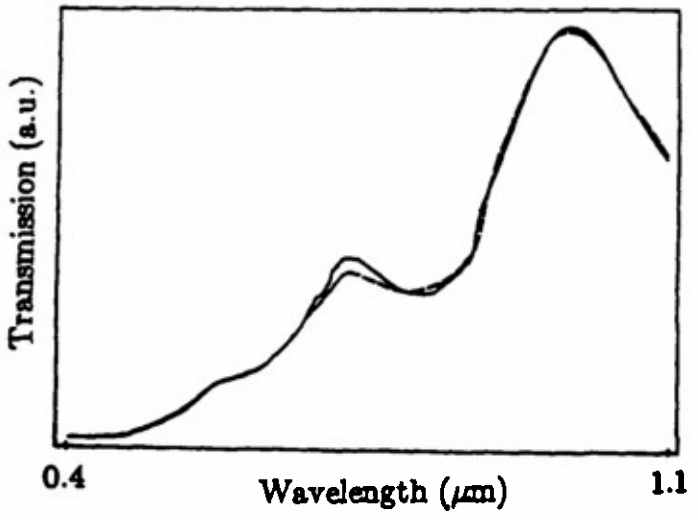

Fig.3: Measured transmission (dashed line) and calculated transmission (solid line) at various wavelengths. The values of n and σ are taken from ref. [15] and thickness of the film is 0.28 μm.

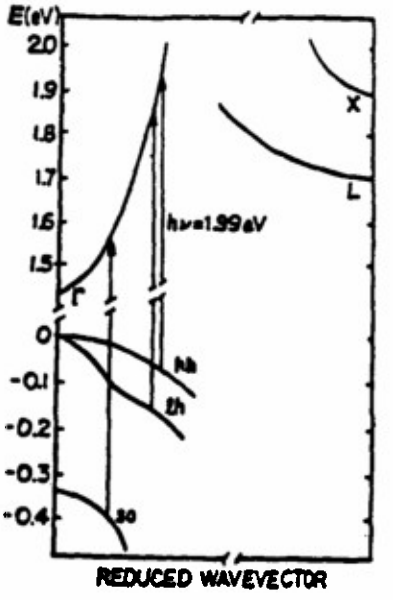

Fig.4: Schematic diagram of GaAs band structure illustrating the allowed transitions for 1.99 eV pump photon energy.

are about 0.15-0.42-0.42 [16]. In our experiments we assume that the momentum relaxation time is much shorter than our pulse width. Thus there is no anisotropy in k-space within our time resolution. This is a reasonable assumption for carrier densities under investigation here [17,18]. After excitation, carriers can scatter away from the initial excited states via carrier-carrier interactions, carrier-LO phonon interactions, and via large wavevector phonons into the X and L satellite valleys. Carriers in the Γ valley change the absorption and refractive index of GaAs due to band gap renormalization, state filling, and band filling. Free carrier absorption is comparitively weak and should be negligible in our case [19]. Carriers in satellite valleys (X and L) only contribute to changes of absorption and refractive index when they again return to the Γ valley.

B. Probe near the band-edge

Fig.5 shows the time-resolved change of absorption for different carrier densities at a probe photon energy 1.38 eV, which is below the band-edge. There is an initial increase in absorption followed by a decrease in absorption and even gain for very large carrier density. We attribute the increase of absorption to band gap renormalization. A similar observation was made by Shank et al [1,2] at low temperature and with 0.5 ps time resolution. Our measurements show that the band gap renormalization can occur in a time shorter than our temporal resolution, certainly before most of the carriers fall to the band-edge. We have estimated the band gap shift from the peak of the induced absorption. For $N \sim 10^{19}$ and 10^{18} cm^{-3}, the shift is about 25 and 15 meV respectively, which is about a factor of 2 smaller than that predicted by theory for a cold plasma [19,20]. The subsequent decrease of absorption indicates that the states near the perturbed band-edge became filled. These states are filled up very rapidly for large N, and relatively slowly for lower N. At very high carrier density, when most of states are filled and a population inversion is created, stimulated emission or gain is obtained.

To investigate the state filling near the band-edge in more detail, the measurement is repeated at a probe photon energy of 1.46 eV, which is 40 meV above the band gap. Fig.6 shows $\Delta\alpha$ for different carrier densities. The decrease of absorption results from the increase of the occupancy of the states near the band-edge. For $N \geq 10^{18}$ cm^{-3}, the rapid decrease of absorption (100-500 fs) indicates that enhanced carrier-carrier collisions scatter carriers directly to the bottom of the Γ valley in hundreds of femtoseconds. This appears to agree with recent measurements by Lin et al [9,10] and our data at higher probe photon energies that will be discussed later. For $N < 10^{18}$ cm^{-3}, the gradual decrease of the absorption on a picosecond scale shows that most carriers scatter to the X and L valleys and return slowly ($\sim$ 2 ps) to the Γ valley. Recent time-resolved photoluminescence measurements and Monte Carlo calculations show the validility of this model [11].

Fig.7 illustrates the changes of refractive index for different carrier densities at 1.38 eV. Unlike the dramatic change in absorption, n decreases monotonically. Below the band gap, the small positive Δn caused by band gap renormalization is offset by the large negative Δn caused by band filling at carrier densities in our experiments. This

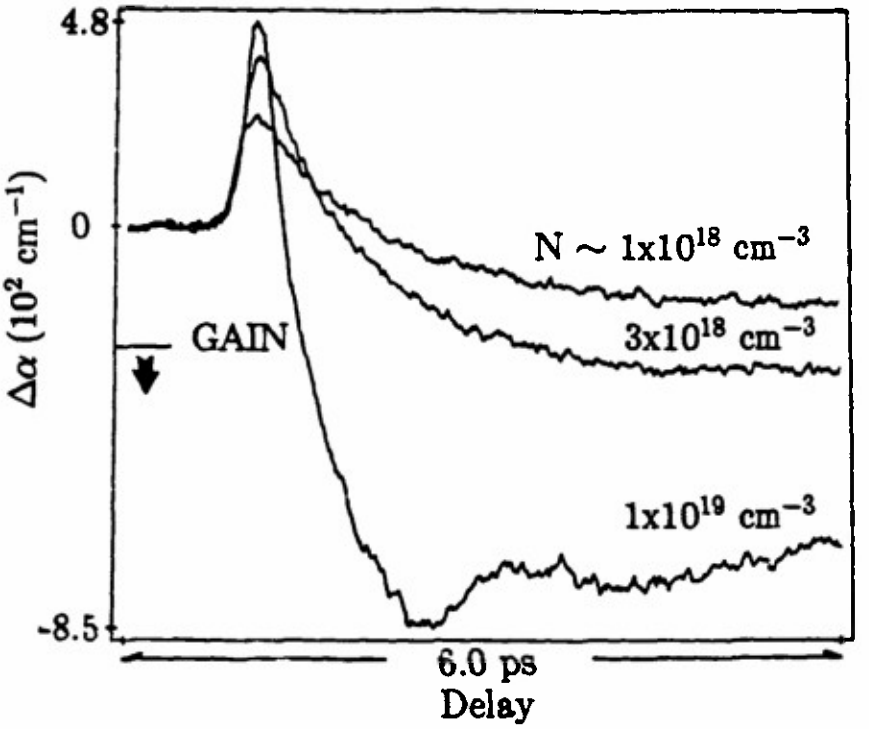

Fig.5: Time-resolved changes of absorption coefficient at 1.38 eV and for different carrier densities. The three curves were adjusted so that the induced absorption peaks coincide in time.

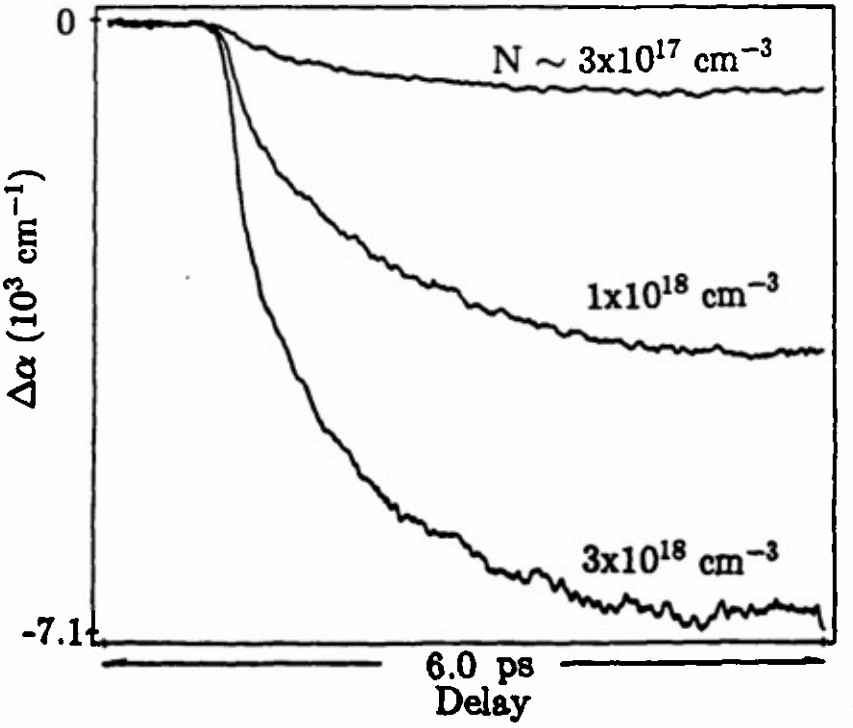

Fig.6: Time-resolved changes of absorption coefficient at 1.46 eV and for different carrier densities.

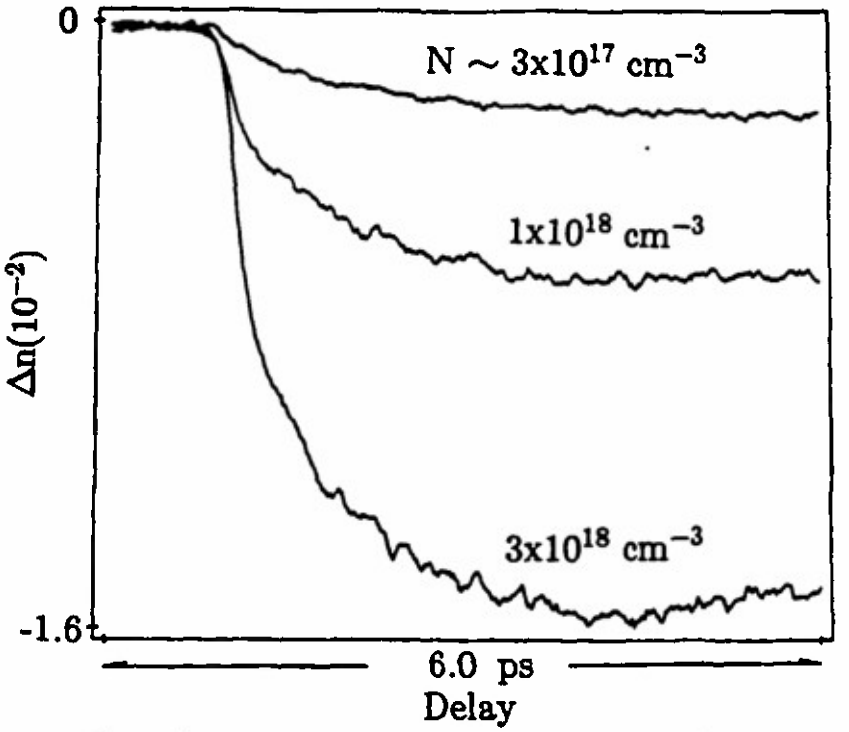

Fig.7: Time-resolved changes of refractive index at 1.38 eV and for different carrier densities.

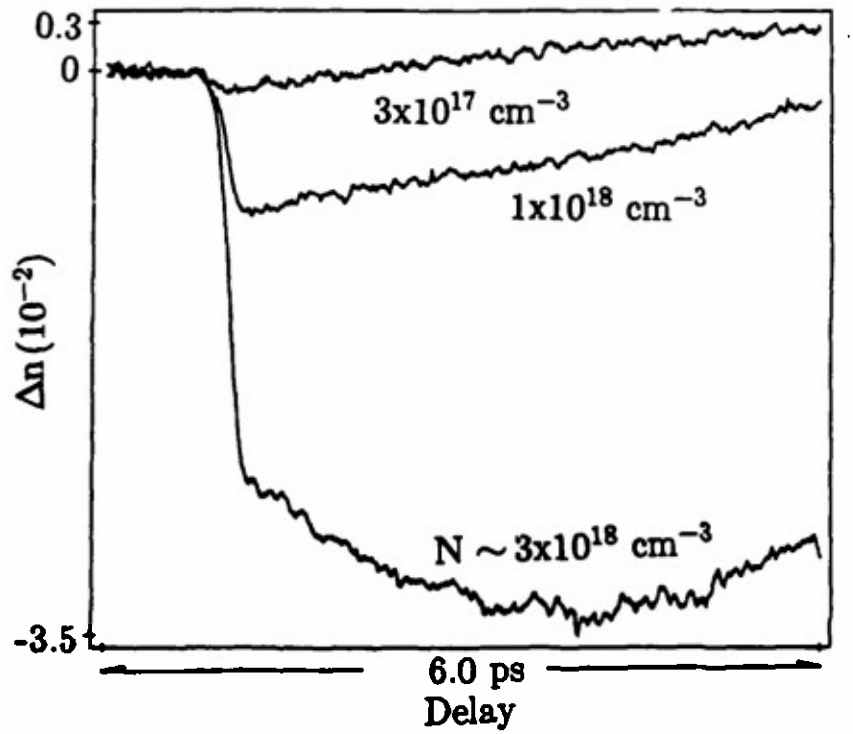

Fig.8: Time-resolved changes of refractive index au 1.46 eV and for different carrier densities.

interpretation agrees well with recent theoretical results [19,21]. It is clear that for large N, n decreases rapidly due to a rapid band filling, and for lower N, n decreases slowly due to a slow band filling.

Fig.8 shows Δn for different carrier densities at 1.46 eV. Band filling can produce a large negative Δn around the band gap. This negative Δn can extend much above the band-edge at high carrier densities [19,21], in agreement with our results for $N > 10^{18}$ cm^{-3}. At lower carrier density, the negative Δn due to band filling does not extend very much above the gap [19,21], and Δn may even be positive. For $N \sim 3x10^{17}$ cm^{-3}, n first decreases because of ultrafast band gap renormalization and lack of band filling at early time, and then recovers as the band is filled slowly. The detail of changes of refractive index is of great interest and will be discussed in a future publication [22].

C. Probe near the initial excited states

To understand the initial carrier relaxation processes we have also performed measurements at probe photon energies from 1.99 to 2.18 eV. Fig.9 and Fig.10 show $\Delta\alpha$ at 1.99 eV and 2.18 eV for different carrier densities. Our results at 1.99 eV are very close to similar experiments by Lin et al [5,6]. There is a transient bleaching spike which gets shorter for larger N. At 2.18 eV, it takes a shorter time for α to reach its minimum at high carrier density than at low carrier density. These observations and our results near the band-edge suggest that at high carrier density enhanced carrier-carrier interaction scatters carriers from their initial excited states in tens of femtoseconds. At similar carrier densities, the ecovery of the bleaching on a picosecond time scale is faster at $h\nu$=2.18 eV than at $h\nu$=1.99 eV, simply because the probe photons at 2.18 eV sample the states higher in the conduction band. At long time (3-12 ps) we found that $\Delta\alpha$ becomes positive, due to band gap renormalization caused by the cold plasma. The behavior of Δn, which is related to state filling, band filling and band gap renormalization, will be discussed in a future publication [22].

DISCUSSION

The short-lived bleaching around the initial excited states involves both intervalley scattering and carrier-carrier scattering. Becker et al [23] used 6 fs pulses to perform similar pump-probe experiments and deduced the intervalley scattering rate. Since the intervalley scattering rate should not be carrier density dependent, the density dependence of this transient implies that carrier-carrier scattering competes efficiently with intervalley scattering.

It is well known that both electrons and holes contribute to the absorption saturation (state filling and band filling), although it is not very clear which contribution is dominant in all pump-probe measurements. The valence bands are flatter in k-space due to the bigger effective masses of holes. The initial scattering of the holes may therefore be faster than that of electrons, since less energy relaxation processes are required to reach the band extrema. It is possible that the rapid absorption saturation behavior, especially near the band-edge, is the result of hole scattering [10].

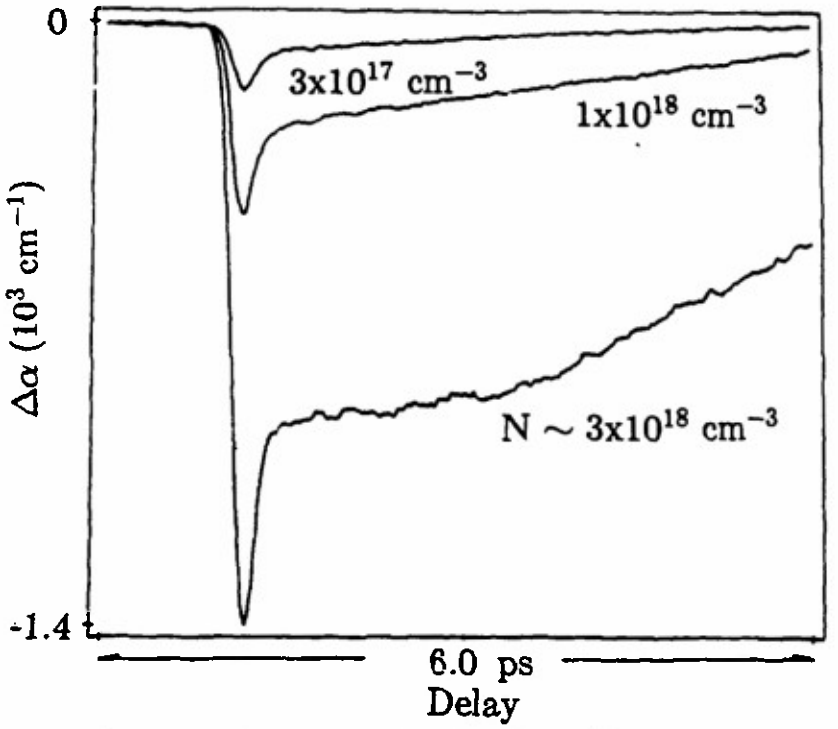

Fig.9: Time-resolved changes of absorption coefficient at 1.99 eV and for different carrier densities.

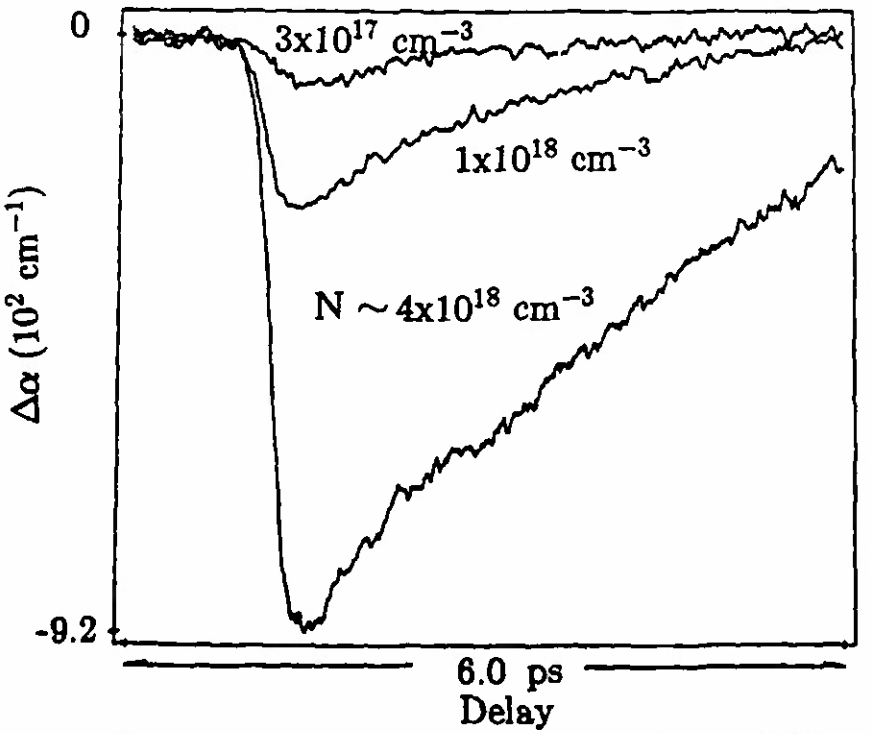

Fig.10: Time-resolved changes of absorption coefficient at 2.18 eV and for different carrier densities.

Near the band-edge, plasma screening, which reduces the exciton binding energy, the Coulomb enhancement of the continuum states (Sommerfeld factor), and the band gap, is an important effect. Recent work by Lee et al [21] shows that plasma screening is also one of the dominant contributions to the change of refractive index, and has similar contribution to the change of absorption due to band gap renormalization. In this sample, we observe no short-lived increase of absorption at 1.46 eV [24], but there is a noticable delay between $\Delta\alpha$ and Δn. This implies that band gap renormalization does compete with state filling right after excitation and that eventually state filling dominates.

CONCLUSIONS

Band gap renormalization happens instantaneously within our 80 fs time resolution after excitation of carriers. The estimated shift caused by hot carriers is a factor of 2 smaller than that predicted by theory for a cold plasma. At carrier densities higher than 10^{18} cm^{-3}, carriers are scattered from their initial excited states in tens of femtoseconds by carrier-carrier interactions, and form a broad energy distribution through the Γ valley in tens to hundreds of femtoseconds. At carrier densities lower than 10^{18} cm^{-3}, most carriers scatter to X and L satellite valleys and return to the Γ valley in 2-3 ps. The band filling is the dominant contribution to the change of refractive index at high carrier density, and can be offset by band gap renormalization at lower carrier density.

ACKNOWLEDGEMENTS

The authors thank M. Shayegan and his group for providing the GaAs samples. We also thank D. A. Young, K. Gzara, K. W. Sun for technical support. We acknowledge support from the National Science Foundation (ECS-8606531 and ECS-8657263) and the U. S. Army Research Office (DAAL03-87-K-0145). T. Gong is supported by a fellowship from the Photonics and Opto-Electronic Materials Advanced Technology Center at Princeton University and P. M. Fauchet is an Alfred P. Sloan Research Fellow.

REFERENCES

1. C. V. Shank, R. L. Fork, R. F. Leheny, and J. Shah, Phys. Rev. Lett., **42**, 112 (1979).

2. R. F. Leheny, J. Shah, R. L. Fork, and C. V. Shank, Solid State Commun., **31**, 809 (1979).

3. A. J. Taylor, D. J. Erskine, and C. L. Tang, J. Opt. Soc. Am., **B2**, 663 (1985).

4. M. J. Rosker, F. W. Wise, and C. L. Tang, Appl. Phys. Lett., **49**, 1726 (1986).

5. W. Z. Lin, J. G. Fujimoto, E. P. Ippen, and R. A. Logan, Appl. Phys. Lett., **50**, 124 (1987).

6. R. W. Schoenlein, W. Z. Lin, E. P. Ippen, and J. G. Fujimoto, Appl. Phys. Lett., **51**, 1442 (1987).

7. J. L. Oudar, D. Hulin, A. Migus, A. Antonetti, and F. Alexandre, Phys. Rev. Lett., **55**, 2074 (1985).

8. W. H. Knox, C. Hirlimann, D. A. Miller, J. Shah, D. S. Chemla, and C. V. Shank, Phys. Rev. Lett., **56**, 1191 (1986).

9. W. Z. Lin, R. W. Schoenlein, J. G. Fujimoto, and E. P. Ippen, IEEE, J. Quantum Electron., **24**, 267 (1988).

10. W. Z. Lin, M. J. LaGasse, R. W. Schoenlein, B. Zysset, and J. G. Fujimoto, SPIE Proceedings, **942**, 83 (1988).

11. J. Shah, B. Deveaud, T. C. Damen, and W. T. Tsang, A. C. Gossard, and P. Lugli, Phys. Rev. Lett., **59**, 2222 (1987).

12. D. Block, J. Shah, and A. C. Gossard, Solid State Commun., **59**, 527 (1986).

13. E. Yablonovitch, T. Gmitter, J. P. Harbison, and R. Bhat, Appl. Phys. Lett., **51**, 2222 (1987).

14. W. L. Nighan Jr. and P. M. Fauchet, CLEO '90 Technical Digest, Anaheim, CA.

15. Handbook of Optical Constants of Solids, E. D. Palik editor, Academic Press Inc, London, 1985, pp 429.

16. J. S. Blakemore, J. Appl. Phys., **53**, 123 (1982).

17. J. L. Oudar, A. Migus, D. Hulin, G. Grillon, J. Etchepare, and A. Antonetti, Phys. Rev. Lett., **53**, 384 (1984).

18. A. L. Smirl, T. F. Boggess, B. S. Wherrett, G. P. Perryman, and A. Miller, IEEE, J. Quantum Electron., **19**, 690 (1983).

19. B. R. Bennett, R. A. Soref, and J. A. Del Alamo, IEEE, J. Quantum Electron., **26**, 113 (1990).

20. H. Haug and S. W. Koch, Phys. Rev., **A39**, 1887 (1989).

21. Y. H. Lee, A. Chavez-Pirson, S. W. Koch, H. M. Gibbs, S. H. Park, J. Morhange, A. Jeffery, N. Peyghambarian, L. Banyai, A. C. Gossard, and W. Wiegmann, Phys. Rev. Lett., **57**, 2446 (1986).

22. T. Gong, W. L. Nighan Jr., and P. M. Fauchet, to be published.

23. P. C. Becker, H. L. Fragnito, C. H. Cruz, J. Shah, R. L. Fork, J. E. Cunninghan, J. E. Henry, and C. V. Shank, Appl. Phys. Lett., **53**, 2089 (1988).

24. In another sample, we did observe a very small induced absorption at 1.46 eV. See T. Gong, W. L. Nighan Jr., and P. M. Fauchet, IQEC '90, Technical Digests, Anahein, CA.

Hot-carrier Coulomb effects in GaAs investigated by femtosecond spectroscopy around the band edge

T. Gong,[a] W. L. Nighan, Jr.,[a] and P. M. Fauchet[b]
Laboratory for Laser Energetics, University of Rochester, Rochester, New York 14623

(Received 15 August 1990; accepted for publication 10 October 1990)

We report the first femtosecond measurements of carrier-induced changes in the absorption and refractive index of GaAs thin films. Absorption measurements in the vicinity of the band edge indicate instantaneous band-gap renormalization as well as instantaneous plasma screening of electron-hole interactions. Band filling and plasma screening appear to be the dominant contributions to the changes of refractive index.

The ultrafast carrier relaxation dynamics in GaAs has been a topic of interest for many years because of its importance in the development of optical and electronic devices. During the past few years several groups have made time-resolved pump-probe measurements on GaAs using ultrashort laser pulses.[1–5] A variety of carrier relaxation mechanisms, such as carrier-carrier interaction, carrier-LO phonon interaction, intervalley scattering, etc., has been widely studied and interpreted with the help of Monte Carlo simulations.[6,7] Most pump-probe experiments typically measured the change of transmission on antireflection-coated GaAs thin films and were limited to measuring the absorption at probe photon energies above the GaAs band gap.

Using a novel technique, we have measured simultaneously the changes of absorption and, for the first time, refractive index, with femtosecond time resolution. Probing around and especially below the band gap of GaAs reveals the dynamics of hot-carrier Coulomb interactions, including band-gap renormalization and plasma screening of electron-hole interactions. These interactions have been studied previously under equilibrium conditions.[8,9] The importance of carrier-carrier scattering and carrier-intervalley scattering is also discussed.

The samples used in our experiments are GaAs thin films grown by molecular beam epitaxy, and prepared using the technique developed by Yablonovitch *et al.*[10] A 0.3 μm layer of undoped GaAs was grown on top of a thin (0.1 μm) layer of $Al_{0.8}Ga_{0.2}As$ grown on a GaAs substrate. The $Al_{0.8}Ga_{0.2}As$ layer was etched away by keeping the black wax covered sample in a dilute HF solution at 0 °C overnight. The 0.3 μm GaAs cap layer was then carefully placed on a sapphire window where it remained attached due to Van der Waals bonding. The wax was then removed. The film was thinned several times by etching in a solution of H_3PO_4:H_2O_2:H_2O (3:1:50) for a very short time. This allowed experiments on samples with different thicknesses.

A copper vapor laser amplified CPM system generates pulses of 75 fs duration and 10 μJ energy.[11] A small fraction of the pulse at 620 nm ($h\nu \sim 2.0$ eV) is split off and attenuated as a pump beam. The remainder is focused onto an ethylene glycol jet and generates a white-light continuum. Interference filters (bandwidth of 10 nm) are used to select the desired probe wavelengths from the continuum. The polarization of the pump beam is rotated by 90° to reduce the coherent artifact. The time-resolved transmission (T) and reflection (R) are simultaneously measured at room temperature in the pump-probe configuration near normal incidence. Lock-in as well as real-time subtraction techniques are used to improve the signal-to-noise ratio. The absorption coefficient (α) and refractive index (n) are then calculated from the measured T and R by inversion of the Fabry–Perot formulae. The carrier density is estimated from the number of photons absorbed by the film and from the measured beam spot size.

Excitation at 2 eV produces three distributions of carriers, which originate from the heavy and light hole valence bands and the spin split-off valence band, with relative strengths of about 42%, 42%, and 15%.[4] Due to the Pauli exclusion principle electrons in the conduction band and holes in the valence band reduce interband transitions through state and band filling. The correlation and exchange interactions among the excited charged carriers reduce the single-particle potential energy and cause a rigid band shift called band-gap renormalization. In addition a large concentration of charged carriers also screens Coulombic interactions between electrons and holes. This plasma screening broadens the bound states (excitons) below the band edge and moves the continuum (Sommerfeld enhancement) band edge downward. The net result of these many-body effects is to reshape the band edge. Furthermore, free-carrier absorption can also be significant at wavelengths where interband transitions are negligible.

Figures 1 (A) and 1 (B) show the time-resolved changes of absorption ($\Delta\alpha$) and refractive index (Δn) for the same carrier density ($N \sim 2\times10^{18}$ cm^{-3}) at probe wavelengths of 880, 890, 900, and 920 nm, which are below the band edge and of 860 nm, which is slightly above the band edge. From 880 to 900 nm there is a short-lived induced absorption spike right after the excitation of carriers, whereas the behavior at 860 and 920 nm is strikingly different. On the other hand, Δn shows a sharp initial decrease, followed by a much slower variation, at all wavelengths.

Let us first consider $\Delta\alpha$. Measurements performed at different carrier densities show that the induced absorption

[a] Also with Dept. of Electrical Engineering, Princeton University
[b] Also with Dept. of Electrical Engineering, University of Rochester.

 0003-6951/90/512713-03$02.00

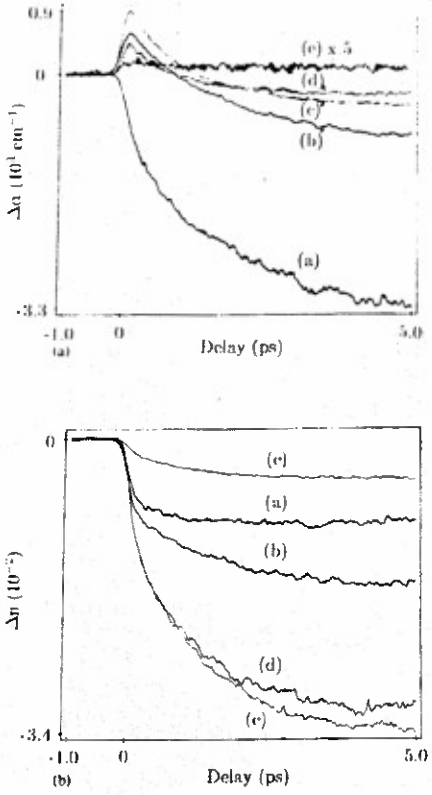

FIG. 1. Measured time-resolved changes of absorption (A), and changes of refractive index (B) for a carrier density 2×10^{18} cm^{-3} injected at 2 eV. The probe wavelengths are (a) $\lambda_p = 860$ nm, (b) $\lambda_p = 880$ nm, (c) $\lambda_p = 890$ nm, (d) $\lambda_p = 900$ nm, (e) $\lambda_p = 920$ nm. The vertical scale of curve (e) in (A) is five times that of (a)–(d).

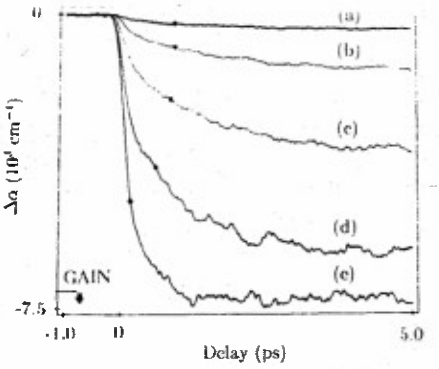

FIG. 2. Measured time-resolved changes of absorption at $\lambda_p = 860$ nm for different carrier densities: (a) $N\sim1.0\times10^{17}$ cm^{-3}, (b) $N\sim3.3\times10^{17}$ cm^{-3}, (c) $N\sim1.0\times10^{18}$ cm^{-3}, (d) $N\sim3.3\times10^{18}$ cm^{-3}, (e) $N\sim1.0\times10^{19}$ cm^{-3}. The dots (●) indicates the time taken for $\Delta\alpha$ to reach 63% of its maximum value. At $N\sim10^{19}$ cm^{-3}, gain is observed.

peak is a sublinear function of carrier density.[12] We attribute this initial increase of absorption to band-gap renormalization, complicated by plasma screening of electron-hole interactions. A similar observation was made by Shank *et al.*[1] at low temperature and with 0.5 ps time resolution. The present results show that band-gap renormalization along with plasma screening can occur in a time shorter than our temporal resolution, before the carriers can be described by a Fermi–Dirac distribution and certainly before most of carriers fall to the band edge and cool to the lattice temperature. The subsequent decrease of absorption indicates that the states near the perturbed band edge become filled. A more pronounced band filling is observed at the shorter probe wavelengths which sample states higher in the perturbed band where the number of states available increases due to the band-gap shift. The observation of stimulated emission (gain) on a picosecond time scale for very high carrier density[12] confirms that the band gap does shift down.

At 920 nm ($\sim$75 meV below the original band edge) we find a small induced absorption ($\sim$25 cm^{-1}) that decays on a long time scale. We attribute this effect to intraband (free carrier) absorption and estimate the total cross section $\sigma = \sigma_e + \sigma_h$ to be 1.2×10^{-17} cm^2. We believe this to be the first measurement of σ at this wavelength. At 860 nm ($\sim$20 meV above the original band edge) we find no short-lived induced absorption. At this wavelength, the large negative $\Delta\alpha$ produced by plasma screening offsets the small positive $\Delta\alpha$ due to band-gap renormalization.

The monotonic decrease of absorption at 860 nm mainly results from the increase of the occupancy of the states near the band edge. Figure 2 shows $\Delta\alpha$ for different carrier densities at 860 nm. The dots (●) indicate the time taken for the change of absorption to reach 63% ($= 1 - 1/e$) of its maximum value. It is clear that this time stays unchanged for $N < 10^{18}$ cm^{-3} and is reduced rapidly for larger carrier densities. This is a strong evidence that for large N, enhanced carrier-carrier collisions scatter many carriers directly to the bottom of the conduction band or the top of the valence band in hundreds of femtoseconds. The very recent Monte Carlo simulations by Stanton *et al.*[7] who used the data taken by Lin *et al.*[4] at 1.55 eV ($\lambda\sim800$ nm) and $N\sim10^{18}$ cm^{-3} suggest that relaxation of holes that are created very close to the top of valence band is in large part responsible for the rapid change of absorption. However, for $N < 10^{18}$ cm^{-3}, we do not observe this ultrafast change. Instead, we find a gradual decrease of absorption on a picosecond time scale, which indicates that most carriers (electrons) first scatter to the satellite (L,X) valleys and then return back slowly ($\sim$2 ps) to the bottom of the Γ valley. Recent time-resolved photoluminescence measurements and Monte Carlo simulations show the validity of this model.[6,13]

Let us now discuss the time-resolved changes of refractive index for different probe wavelengths. It appears that n drops very rapidly right after carrier excitation, then decreases slowly or even stays unchanged. It is also interesting to note that Δn at 920 nm is comparable to that at other wavelengths even though $\Delta\alpha$ is very small at this wavelength. A simple theory predicts that band-gap renormalization produces a positive Δn around the new band edge.[14] However, if plasma screening of the continuum-state Sommerfeld enhancement is included,[9] a large negative Δn offsets the positive Δn due to band-gap renormalization. An important result of our work is that the theory of Ref. 9, which was derived under equilibrium conditions,

seems to also hold qualitatively for very hot carriers. The subsequent slower decrease of n is mainly attributed to band filling which also produces a negative Δn around the band edge.

Measurements were also made at probe wavelengths near the initial excited states. A clear induced absorption on a picosecond time scale is observed, which we attribute to band-gap renormalization caused by a cold plasma.[15]

In conclusion, we have been able to measure simultaneously femtosecond carrier-induced changes in the absorption and refractive index of GaAs thin films around and especially below the band gap. We find that instantaneous band-gap renormalization and plasma screening of electron-hole interactions are the dominant contributions for the change of optical properties around the band edge right after carrier excitation. Band filling, which is also a very fast process at large carrier density because of enhanced carrier-carrier interactions, is dominant after hundreds of femtoseconds. We expect that a quantitative fitting of our data using many-body theory will lead to a more complete understanding of hot-carrier Coulomb interactions.

The authors thank M. Shayegan and his group for providing the GaAs samples. We are also grateful to D. A. Young, K. Gzara, and K. W. Sun for technical support. This work is supported by National Science Foundation (ECS-8657263) and U.S. Army Research Office (DAAL03-87-K-0145). T. Gong acknowledges receipt of a fellowship from the Photonics and Opto-Electronic Materials Advanced Technology Center at Princeton University. P. M. Fauchet is an Alfred P. Sloan Research fellow.

[1] C. V. Shank, R. L. Fork, R. F. Leheny, and J. Shah, Phys. Rev. Lett. **42**, 112 (1979).
[2] J. L. Oudar, D. Hulin, A. Migus, A. Antonetti, and F. Alexandre, Phys. Rev. Lett. **55**, 2074 (1985).
[3] A. J. Taylor, D. J. Erskine, and C. L. Tang, J. Opt. Soc. Am. B **2**, 663 (1985).
[4] W. Z. Lin, R. W. Schoenlein, J. G. Fujimoto, and E. P. Ippen, IEEE, J. Quantum Electron. **24**, 267 (1988).
[5] P. C. Becker, H. L. Fragnito, C. H. Brito-Cruz, J. Shah, R. L. Fork, J. E. Cunningham, J. E. Henry, and C. V. Shank, Appl. Phys. Lett. **53**, 2089 (1988).
[6] M. J. Kann, A. M. Kriman, and D. K. Ferry, Phys. Rev. B **41**, 12659 (1990).
[7] C. J. Stanton, D. W. Bailey, and K. Hess, Phys. Rev. Lett. **65**, 231 (1990).
[8] H. Haug and S. Schmitt-Rink, J. Opt. Soc. Am. B **2**, 1135 (1985).
[9] Y. H. Lee, A. Chavez-Pirson, S. W. Koch, H. M. Gibbs, S. H. Park, J. Morhange, A. Jeffery, N. Peyghambarian, L. Banyai, A. C. Gossard, and W. Wiegmann, Phys. Rev. Lett. **57**, 2446 (1986).
[10] E. Yablonovitch, T. Gmitter, J. P. Harbison, and R. Bhat, Appl. Phys. Lett. **51**, 2222 (1987).
[11] W. L. Nighan, Jr. and P. M. Fauchet, SPIE Proc. 1268 (1990)
[12] T. Gong, W. L. Nighan, Jr., and P. M. Fauchet, SPIE Proc. 1268 (1990).
[13] J. Shah, B. Deveaud, T. C. Damen, W. T. Tsang, A. C. Gossard, and P. Lugli, Phys. Rev. Lett. **59**, 2222 (1987).
[14] B. R. Bennett, R. A. Soref, and J. A. Del Alamo, IEEE, J. Quantum Electron. **26**, 113 (1990).
[15] T. Gong, W. L. Nighan, Jr., and P. M. Fauchet (unpublished).

Generation of solitons, periodic pulsing and nonlinearities in the CPM dye laser.

P. M. Fauchet, W. L. Nighan Jr. and T. Gong

Department of Electrical Engineering
Princeton University
Princeton, NJ 08544

ABSTRACT

We report the generation of a variety of periodically modulated pulse trains in the CPM dye laser. These pulses are reminiscent of high-order solitons. We have identified the nonlinearity which prevents the formation of pulses which are solutions of the nonlinear Schrodinger's equation. A modification of the laser cavity removes this nonlinearity and true N = 2 solitons have been generated.

INTRODUCTION

The pulse train modulations that can be generated in the colliding pulse modelocked (CPM) dye laser and other dye lasers capable of producing femtosecond or picosecond pulses at typically ~ 100 MHz repetition rate have recently been the topic of several experimental and theoretical investigations. Salin et al were the first to report nearly periodic pulse evolution in a CPM laser [1,2] which they described in terms of higher-order solitons. We [3-5] and others [6-8] have performed further experiments and modelling that have led to a much better understanding of these pulses, although several schools of thought still exist. This body of work should be related to earlier studies of the CPM laser [9-11] in its "normal" mode of operation and to recent work on periodic instabilities in synchronously pumped modelocked dye lasers [12,13]. Eventually, it is hoped that a comprehensive model of all cw modelocked dye lasers may emerge [14].

In this paper, we establish in detail the properties of the periodic pulsing reminiscent of solitons encountered in the unmodified Rh6G/DODCI CPM dye laser, we identify the nonlinearity that makes these pulses different from the solutions of the nonlinear Schrodinger's equation, and we produce true solitons by removal of this additional nonlinearity. We also examine some recent results in the light of our model and suggest interesting new areas of investigation.

THE Rh6G/DODCI CPM DYE LASER

Details about our CPM dye laser can be found in [9] and those about our instrumentation in [5]. We start from the "normal" mode of operation of the CPM laser, which produces pulses as short as 35 fsec. Periodic variations of the output pulses can be obtained by increasing the amount of self-phase modulation (SPM) when the saturable absorber jet is translated closer to its corresponding intracavity focus or by increasing the amount of negative group velocity dispersion (GVD) when a prism is translated to reduce the beam path in the glass. Figure 1 shows several intensity autocorrelation traces taken 1) in the "normal" mode, 2) by translating the jet closer to the focus over a 250μm distance (N = 1 to 4 soliton-like pulses), and 3) for an N = 3 soliton-like pulse obtained by reducing the amount of glass by 150μm starting from the N = 2 condition. The oscillations between two or more extreme pulse shapes are visible only because we used a high bandwidth detection system.

As explained in [5], the period of these oscillations is usually in the 100 kHz regime and we have been able to time-resolve the spectrum, the intensity and interferometric autocorrelations during the period. In Figure 2, we plot interferometric autocorrelation traces of an N = 2 soliton-like pulse taken at 250 nsec intervals during its 2.5 μsec period. The pulse is made of two *coherent* pulses, which start with equal energy. As one of the pulses is delayed, its energy decreases but it remains coherent with the main pulse. Figure 3 is a plot of the evolution of the peaks during the period. Further results can be found in [3-5].

We have also observed a wide variety of exotic periodic pulsing in the CPM laser. Some have already been reported in [5]. Here, we mention a regime of operation which seems to correspond to beating between two soliton-like pulse trains of slightly different periods. This situation can be maintained long enough to allow some characterization. In Figure 4 a, we show an intensity autocorrelation trace and in Figure 4 b, we show a Fourier spectrum corresponding to this regime. The $\sim$ 10 kHz modulation results from beating between two soliton-like pulse trains having slightly different periods in the 5μsec regime. The deep modulation in the intensity autocorrelation is thus *not* due to generation of extremely short pulse within the $\sim$ 100 fsec envelope. This erroneous interpretation given in [15] is also inconsistent with the width of the spectrum observed in this regime. It is not obvious to us why two soliton-like pulses that appear to be related in phase should coexist in the CPM laser. It is clearly an area worthy of further investigation.

Despite striking similarities with solitons, none of these periodic pulses are solutions of the nonlinear Schrodinger's equation (self-phase modulation and group velocity dispersion are provided by the saturable absorber jet and the four prisms, respectively). Additional nonlinearities modify this equation and the solutions, although reminiscent of solitons, are *not* solitons. Examples of nonlinearities that have been discussed previously include saturable absorption, saturable gain, and interaction between the clockwise and counterclockwise beams in the saturable absorber. In the next section, we identify an additional nonlinearity which also prevents generation of solitons. This nonlinearity can be removed and the pulses generated by the CPM laser then become solutions of the nonlinear Schrodinger's equation.

GENERATION OF SOLITONS BY A MODIFIED CPM LASER

Nearly ten years ago, a resonant Raman line having a shift of 620 cm^{-1} was reported in DODCI in ethylene glycol illuminated by a HeNe laser [16]. In the CPM laser, the wavelength of the beam is nearly identical to that of the HeNe laser and the beam intensity in the saturable absorber jet exceeds 10^{10} W/cm^2. Thus, each time the pulse passes through the saturable absorber, there is relatively efficient generation of Stokes shifted radiation. The Stokes component generated during the n^{th} pass may be amplified during the $(n + 1)^{th}$ pass by stimulated emission and the Stokes intensity may thus increase dramatically. The gain of the Stokes line in the Rh6G jet is much smaller than that of the main spectral line and a steady-state situation results. We find evidence for this effect in the "normal" mode of operation of the CPM laser. For pulses shorter than $\sim$ 60 fsec, the red tail that appears in the spectrum is shifted by approximately 600 cm^{-1} with respect to the short wavelength part of the main spectral peak. Filtering out the red tail does not lengthen the pulse [17], indicating that it is an independent Fourier component.

Starting from the shortest "normal" pulse operation, we have inserted an edge filter between prisms 2 and 3 to remove the red tail, added more glass by translating a prism and obtained pulses which can be quantitatively described as asymmetric N = 2 solitons. Figure 5 compares the measured and calculated evolutions of the spectrum during the 5 μsec period of the soliton (additional results can be found in [5]). From these results, it is clear that true solitons can be generated by the CPM laser and that we have identified the nonlinearity that prevents their formation. By preventing the growth of the Stokes line, we effectively remove the additional nonlinearity and the usual terms in the nonlinear Schrodinger's equation describe the pulse evolution adequately.

CONCLUSIONS

We have controlled the generation of stable solitons and soliton-like pulses in the CPM dye laser. True solitons have been obtained for the first time and the nonlinearity that may prevent their formation has been identified as Raman scattering in the DODCI/ethylene glycol saturable absorber jet. CPM dye lasers operating at other wavelengths use different dye/solvent combinations [18]. If the Stokes shift is much larger than 620 cm^{-1}, then true solitons may be produced without spectral filtering.

We acknowledge support from the Army Research Office, the National Science Foundation, Newport Corporation and Coherent Inc. P. M. Fauchet is an Alfred P. Sloan Research Fellow.

REFERENCES

1. F. Salin, P. Grangier, G. Roger, and A. Brun, Phys. Rev. Lett. **56**, 1132 1986.
2. F. Salin, P. Grangier, G. Roger, and A. Brun, Phys. Rev. Lett. **60**, 569 1988.
3. W. L. Nighan, T. Gong, and P. M. Fauchet, in *Ultrafast Phenomena VI*, Springer-Verlag Series in Chemical Physics, T. Yajima, K. Yoshihara, C. B. Harris, and S. Shionoya, Eds., vol. 48. Berlin: Springer-Verlag, 1988, pp. 109-111.
4. W. L. Nighan, T. Gong, and P. M. Fauchet, Optics Lett. **14**, 447, 1989.
5. W. L. Nighan Jr., T. Gong and P. M. Fauchet, IEEE. J. Quantum Electron. **QE-25**, 2476, 1989.
6. F. W. Wise, I. A. Walmsley, and C. L. Tang, Optics Lett. **13**, 129, 1988.
7. H. Avramopoulos, P. M. W. French, J. A. R. Williams, G. H. C. New, and J. R. Taylor, IEEE J. Quantum Electron. **QE-24**, 1884, 1988.
8. D. Kuhlke, T. Bonkhofer, U. Herpers and D. von der Linde, in *Ultrafast Phenomena VI*, Springer-Verlag Series in Chemical Physics, T. Yajima, K. Yoshihara, C. B. Harris, and S. Shionoya, Eds., vol. 48. Berlin: Springer-Verlag, 1988, pp 106-108.
9. J. A. Valdmanis and R. L. Fork, IEEE J. Quantum Electron. **QE-22**, 112, 1986.
10. O. E. Martinez, R. L. Fork, and J. P. Gordon, Optics Lett. **9**, 156, 1984.
11. J. C. Diels, W. Dietel, J. J. Fontaine, W. W. Rudolph, and B. Wilhemi, J. Opt. Soc. Amer. **B2**, 680, 1985.
12. D. L. MacFarlane, L. W. Casperson and A. A. Tovar, J. Opt. Soc. Am. **B5**, 1144, 1988.
13. D. L. MacFarlane and L. W. Casperson, J. Opt. Soc. Am. **B7**, 285, 1990.
14. a first attempt towards that goal can be found in: V. Petrov, W. Rudolph, U. Stamm and B. Wilhelmi, Phys. Rev. **A40**, 1474, 1989.
15. C.-Y. Wang, P. L. Baldeck, Y. Budansky and R. R. Alfano, Optics Lett. **14**, 497, 1989.
16. Y. G. Fuh, R. F. Code, and R. P. Wolf, J. Luminescence, **26**, 329, 1982.
17. K. L. Schehrer, E. S. Fry, and G. T. Bennet, Appl. Opt. **27**, 1908, 1988.
18. P. Georges, F. Salin and A. Brun, Optics Lett. **14**, 940, 1989.

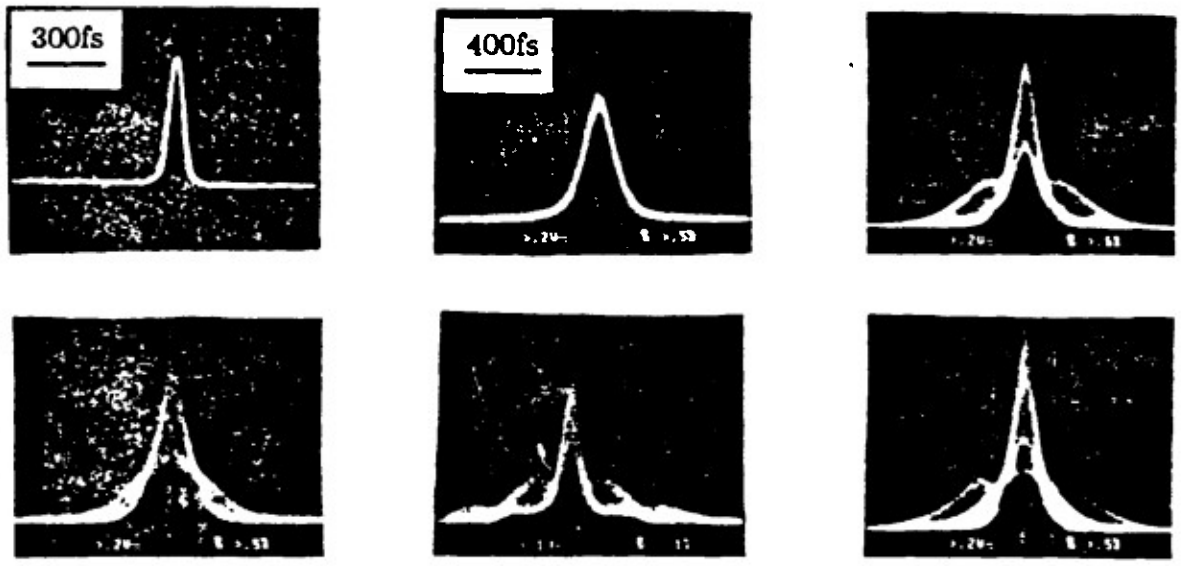

Figure 1 Single-sweep intensity autocorrelations for six cavity configurations. Clockwise, from top left: normal, ~ 50 fsec pulse; N=1 to N=3 soliton-like pulses obtained with saturable absorber jet 250 μm from the focus, 50 μm from the focus and at the focus; N=4 soliton-like pulse; N=3 soliton-like pulse obtained as described in the text. The 1st and 5th traces have different time scales.

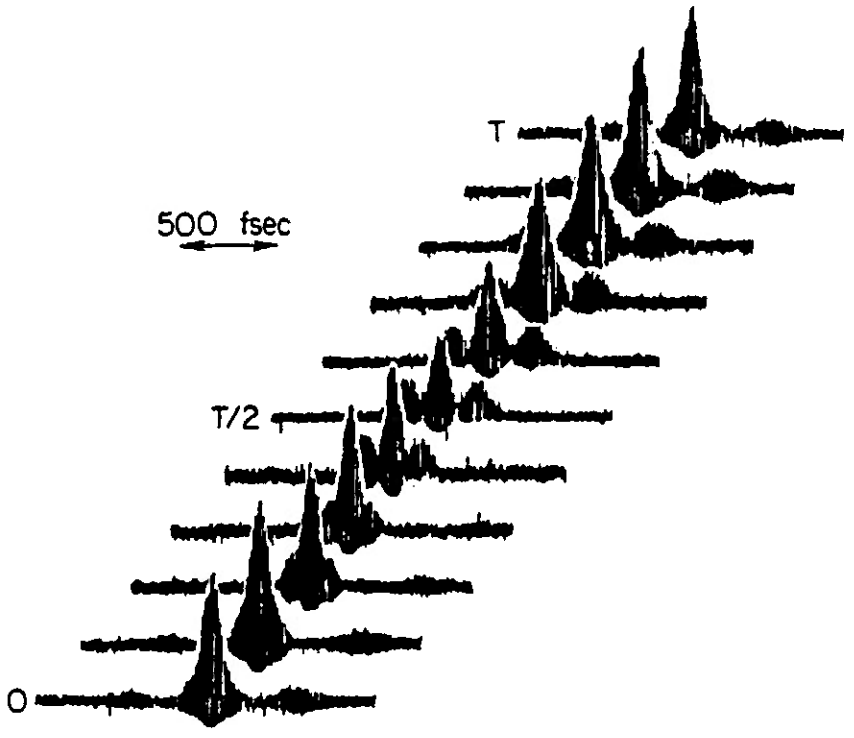

Figure 2 Interferometric autocorrelations of an N=2 soliton-like pulse sampled ten times during its 2.5 μsec period. Two coherent pulses coexist.

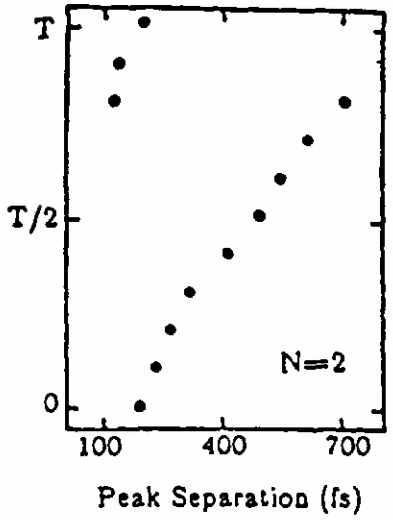

Figure 3 Evolution of the separation between the two peaks of Fig. 2 during the period.

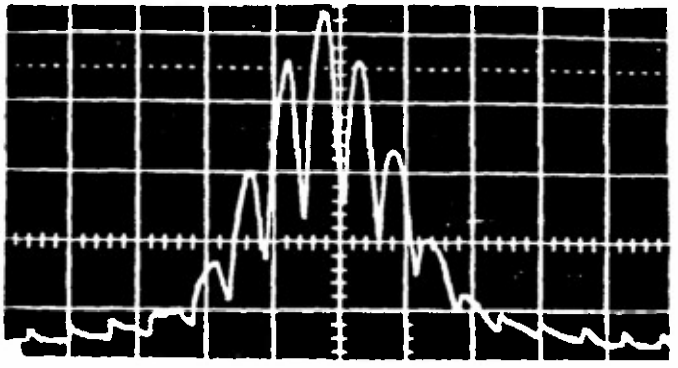

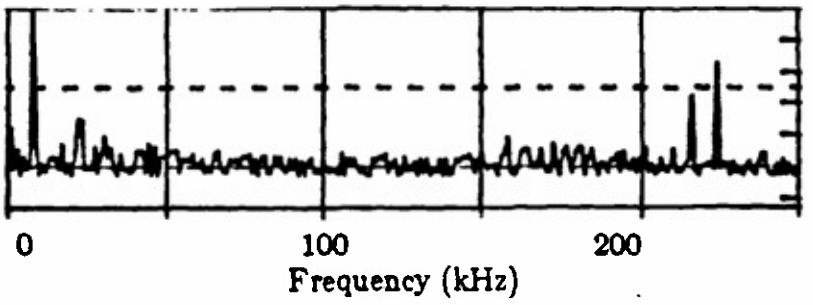

Figure 4 a) Single-sweep intensity autocorrelation trace showing what appears to be sub-100 fsec modulation (27 fsec delay per division or 0.1 msec per division) b) Frequency content of the output train showing beating between two solitons with ~ 5 μsec periods for a situation similar to Fig. 4 a). The ~ 10 kHz beat frequency produces the deep modulation seen in Fig. 4 a) because one arm of the autocorrelator is driven at a low audio frequency.

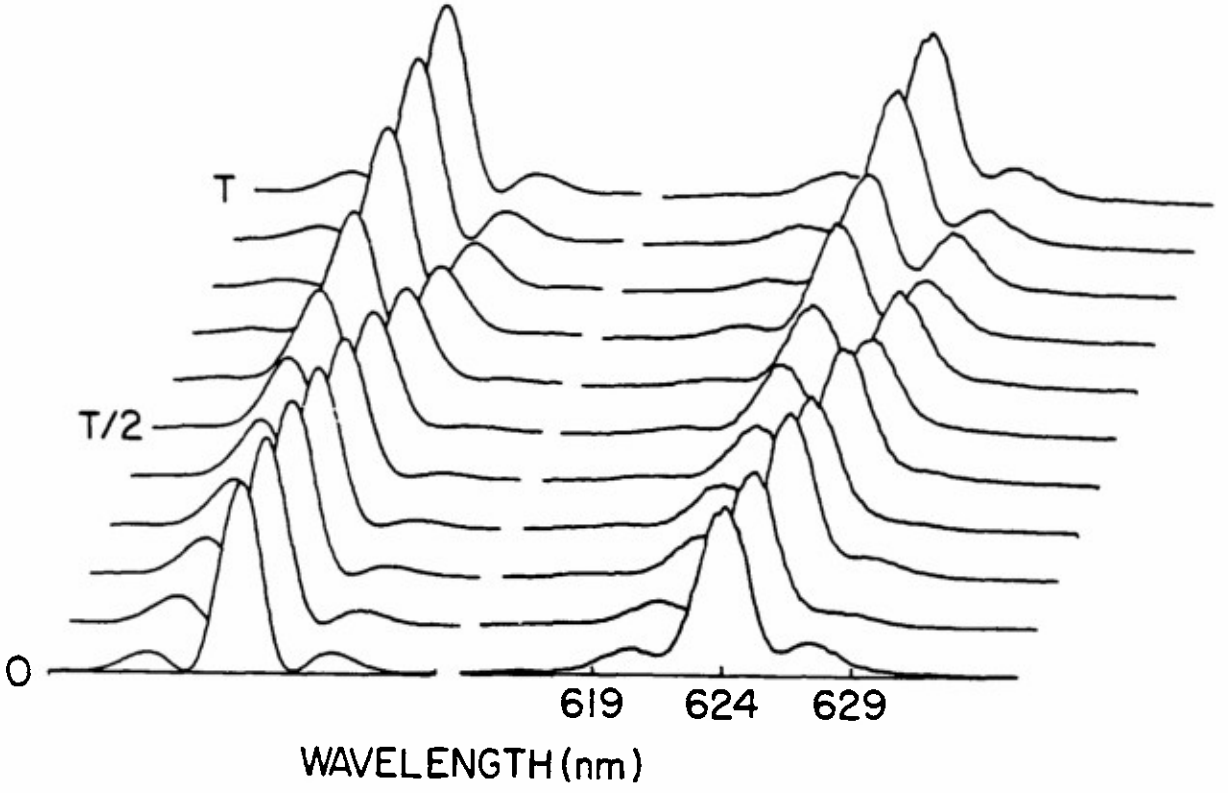

Figure 5 Measured (right) and calculated (left) spectra of an N=2 asymmetric soliton sampled ten times during its 5 μsec period. The agreement is excellent and quantitative. Note that the measured spectral intensity does not go to zero in the first trace because of the limited resolution of the experiment.

High efficiency, high energy optical amplifier for femtosecond pulses

W.L. Nighan Jr., and P.M. Fauchet

Princeton Laboratory for Ultrafast Spectroscopy
Department of Electrical Engineering
Princeton University, Princeton, NJ 08544

1. ABSTRACT

We report on the design and performance of an improved copper vapor laser pumped amplifier for femtosecond optical pulses. Consideration of the large duration mismatch between pump and seed pulses, the short energy storage time of the gain dye, spatial mode matching, and polarization effects led to an amplifier design of 1.5% efficiency, which is greater than previous designs. Pulses of >10 μJ energy and $\sim$65 fsec duration are generated that are focussable to less than twice the diffraction limit. The multiple pass amplifier incorporates optimized mode matching, an antireflection coated flowing dye cell, and a polarized, spatially smoothed pump beam.

2. INTRODUCTION

Femtosecond laser pulses have found use in investigations of ultrafast phenomena in a wide range of fields [1]. From the first production of pulses shorter than 0.1 psec, or 100 fsec, with a ring dye laser named the "colliding pulse modelocked" (CPM) laser [2] in 1981, rapid progress has been made in the development of reliable sources [3-5]. Advancements in sychronously pumped dye laser technology have brought pulse durations down to below $\sim$200 fsec [6]. The most recently updated version of the CPM laser includes intracavity dispersion compensation and can produce pulses $\sim$30 fsec in duration, which stand as the shortest from a laser oscillator [5].

The passively modelocked CPM laser and the actively modelocked synchronously pumped dye lasers produce pulses of energies $\sim$100 pJ and $\sim$1 nJ, respectively, at repetition rates between 75 and 125 MHz. These relatively low pulse energies correspond to peak powers of 1-10 kW, which are not sufficient for many experiments. To raise the peak powers from these oscillators to the megawatt or gigawatt range, an optical amplifier with a gain of 10^3 to 10^7 is required. A typical optical amplifier for femtosecond pulses consists of one or several gain stages, one or several saturable absorbers, and ideally imparts no irreversible temporal or spatial distortion on the femtosecond seed pulse. The repetition rate of the output of such an amplified optical system is dictated by the repetition rate of the pump source to the amplifier, which is typically an additional pulsed laser that must be be synchronized with the femtosecond seed laser. An immediate and very useful

application of the high power ultrashort pulses from these systems is the generation of a white light continuum (WLC), typically acheived by focussing the pulses to a high intensity in transparent materials such as water or ethylene glycol [7]. The intensity threshold for this process is typically 10^{12} to 10^{13} W/cm^2, which is 0.1 to 1 μJ in 100 fsec focussed down to a 10 μm spot [7,8]. The femtosecond continuum described in Reference [7] can extend from 190 nm to 1500 nm, and can be comparable in duration to the original generating pulse [7]. For the ultrafast spectroscopist performing a classic pump and probe experiment, the ability to choose a femtosecond probe pulse over such a wide spectral range is a very important degree of freedom. This in itself has been a driving force in the development of reliable optical amplifiers for femtosecond pulses.

3. REVIEW OF OPTICAL AMPLIFIERS FOR FEMTOSECOND PULSES

A number of optical amplification schemes have been devised that yield pulses of sufficient quality for white light continuum generation. A general survey of the state of fsec optical amplification as of February 1988 was presented by Knox in Reference [8]. For the shortest pulses, dyes are still the most suitable medium for amplification [8]. A brief review of dye-based systems is presented here.

The multiple stage, Q-switched Nd:YAG or excimer laser pumped system can typically amplify fsec pulses to ~1 mJ at a ~10 Hz repetition rate [9-11]. Such systems have been rugged "work horses" in a number of laboratories. The peak powers from such systems can be ~10 GW (1 mJ in 100 fsec). While this peak power is very high, the pulses from the first generation of these amplifiers suffered from a poor spatial profile that did not allow tight focussing. This problem is alleviated somewhat by the use of Bethune cells [12] for the gain dye, which prevent some of the gain inhomogeneity problems associated with the non-Gaussian spatial mode of the Q-switched Nd:YAG or excimer pump laser. The low ~10 Hz repetition rate can limit the signal-to-noise ratio in certain experiments. A higher repetition rate configuration, still based on Nd:YAG technology, is the sychronously pumped dye laser and regenerative amplifier system [13]. Energies of 1-5 μJ are obtained at up to ~1kHz, for pulses of duration ~100 fsec. This system seems to be limited to the amplification of pulses from synchronously pumped dye lasers, since the picosecond pump pulse from the CW modelocked Nd:YAG laser acts as the "clock" and seeds the regenerative Nd:YAG amplifier, the picosecond output of which pumps the dye amplifier. The repetition rate is limited to ~1 kHz by thermal effects in the Pockels cell(s) of the regenerative amplifier [8]. Very high repetition rates of ~ 3 MHz have been demonstrated using a cavity-dumped argon ion laser as a pump source [14-16], but pulse energies were not sufficient for continuum generation.

A copper vapor laser (CVL) pumped amplifier for femtosecond pulses from a CPM laser was demonstrated by Knox *et al* in 1984 [17], combining the desirable features of relatively high repetition rate (5-10 kHz) and energy (1-3 μJ), and recompressed pulse durations below 100 fsec. The higher repetition rate allows the use of phase sensitive detection, and higher signal-to-noise ratios in most applications [8]. In this amplifier, the

2-3 mJ output of the CVL, split between 511 nm and 578 nm in a ~15 nsec pulse, was focussed to a ~1 mm spot in a 1 mm thick flowing jet of SR640 dye in ethylene glycol, produced by a sapphire nozzle. The absorption spectrum of the SR640 dye is a good match to CVL wavelengths, and its gain spectrum is broad enough to support pulses shorter than ~30 fsec at the ~620 nm center wavelength of the CPM pulses [8]. The <100 fsec pulses from the CPM laser were directed through the gain jet six times, with one pass through a thinner (<300 μm) saturable absorber jet of malachite green placed between the fourth and fifth passes. The saturable absorber reduces the build-up of parasitic amplified spontaneous emission (ASE). This multiple pass amplifier has been called the "bowtie" amplifier, which describes the appearance of the beam patb from above [18]. Dispersion in the lenses and gain dye temporally broadened the pulses, but tbe pulses were almost completely recompressible to their original durations upon passage through a prism sequence that provided a compensating negative dispersion [19]. Near diffraction limited focussing was obtained, which facilitated the generation of white light continuum at ~8 kHz. The threshold for continuum generation was found to be $<10^{13}$ W/cm^2, which was achieved by focussing a 1 μJ, 100 fsec pulse down to a 10 μm spot in a 1 mm thick flowing jet of ethylene glycol [17].

While this system seems to combine a number of highly desirable features, the efficiency is typically only ~0.1%. We define the efficiency of the amplifier as the ratio of the amplified pulse energy to the pump pulse energy that impinges upon the gain medium. An output of 1 μJ for a pump pulse of 1 mJ represents an efficiency of 0.1%. In this paper, we report our recent efforts towards the development of a highly efficient CVL pumped amplifier for fsec pulses from a CPM laser. Higher efficiency can result in higher amplified pulses energy, enhanced stability in some cases, and allows the use of some of the CVL light to pump an additional amplifier [20]. To date, we have achieved ~1.5% efficiency in a new single stage multi-pass design, with >10 μJ energy in a pulse of ~65 fsec duration.

4. DESIGN AND PERFORMANCE OF A HIGH EFFICIENCY AMPLIFIER

The efficiency of nanosecond pumped dye amplifiers for femtosecond pulses is limited by gain saturation [8], the short energy storage time of the gain medium, and the large duration mismatch between the pump and seed pulses. Additionally, the ring structure of the CVL transverse mode can frustrate attempts at good mode matching between the pump and seed pulses. Our goals are to achieve high efficiency, high energy, and high stability, as well as low irreversible temporal and spatial distortion. The seed pulses in our work are the 35-100 fsec pulses at ~620 nm from a CPM laser constructed in the manner reported by Valdmanis and Fork [5], and Beisser [21]. We have performed a rather detailed study of the higher order soliton-like behavior of this laser [22]. In the amplifier, the gain/absorber dye pair is SR640/malachite green, after Knox [8].

The concerns of the typically short energy storage time of dyes and the large duration mismatch between the nanosecond CVL pump pulse and the femtosecond CPM seed pulse are best addressed in an amplifier design that incorporates multiple passes through a minimal number of gain stages. The original bowtie design of Knox *et al* [8,17] meets this criterion, as do some alternative designs more recently presented by Fork *et al* in Reference [23] and Khoroshilov *et al* in Reference [24]. The reasoning behind the multi-pass principle follows. Since the fluorescence lifetime of the dye (~2 nsec [23]) is 5-10 times shorter than the CVL pump pulse duration, the temporal evolution of the gain available for the femtosecond seed pulse will closely match the temporal structure of the CVL pulse. In this case, multiple passes through a single gain stage provide a means for much more efficient energy extraction than is possible with a single pass. For maximum energy extraction, as many passes as possible would be made during the nanosecond illumination of the gain dye, until the gain was fully saturated. However, this degree of saturation would likely lead to severe temporal distortion of the femtosecond seed pulse [8]. The physical mechanisms behind the gain saturation problems encountered in amplification of femtosecond pulses are still not well understood [8]. This effect can be forestalled in a multipass configuration by enlarging the spot size appropriately upon successive passes [23,24]. While strong gain saturation can lead to irreversible temporal broadening of the femtosecond pulse [8] and is usually to be avoided, we observe that some degree of gain saturation is actually beneficial in stabilizing the output of the amplified system. In general, we find that more efficient amplifier designs are also more stable, with the stability of the femtosecond output approaching that of the CVL pump laser for the most efficient configurations. In spite of this signature of the onset of gain saturation, we have achieved nearly complete recompression (typically to ~65 fsec) with all of the amplifiers we have investigated.

We built a version of the bowtie amplifier, following that of Knox [8,17], and Beisser [21], and achieved a typical efficiency of 0.1% and energy of 1-3 μJ. We found that the bowtie amplifier efficiency could be doubled by polarizing the typically unpolarized CVL pump beam. A polarizing beamsplitter was used to split out the component that was perpendicular to the field of the fsec seed pulse, while the parallel component pumped the gain jet (the unused component is now free to pump another amplifier [20]). Depending upon the exact parameters of the amplifier, most notably the dye solvent and degree of gain saturation, we found that the parallel component of the CVL leads to a six pass gain that is 4 to 15 times greater than does the perpendicular component. This rather surprisingly large difference arises from the reorientation time of the dipoles excited by the CVL photons. To test this hypothesis, we measured the small signal single pass gain in a standing 2 mm cell, using SR640 in solvents of various viscosity. The single pass gain for parallel pump and seed polarizations was compared to that for perpendicular polarizations. The ratio of these two gains varied from ~1.2 for the least viscous solvent (ethylene glycol) to ~1.5 for the most viscous solvent (glycerol), in agreement with the ratios observed for the ratio of six pass gains. For dyes in viscous solvents, the dipole reorientation time can be many hundreds of psec [25]. Therefore, dipoles produced within ~1 nsec prior to any given amplification pass will result in amplification only if they are produced by the component of the pump pulse with its field parallel to the seed pulse. In

addition, the fluorescence lifetime is of the order of the reorientation time, and some of the dipoles perpendicular to the seed field will relax before they can contribute to amplification. This suggests that in low repetition rate systems, where even slow dye flow rates are sufficient to remove heat from the gain volume between shots, a solvent of higher viscosity may actually lead to more efficient amplification when pumped by a properly polarized pump laser. In our high repetition rate amplifier, it is not possible to use a solvent significantly more viscous than the typical ethylene glycol. However, we find splitting out the perpendicular polarization of the CVL light leaves the amplified pulse energy virtually unchanged, even though the pump energy reaching the gain medium has been cut in half. This doubles the efficiency to 0.2%, reduces the ASE background by 50%, and reduces the potential for spatial distortion of the seed pulse due to heating in the gain jet. The perpendicularly polarized component can be used to pump another amplifier [20].

It has been recently reported that a higher amplified pulse energy was possible by replacing the gain jet with a flowing dye cell [26]. Indeed, the sapphire nozzle that is typically used to create the 1 to 1.25 mm gain jet of dye in ethlyene glycol is expensive, and produces only a small (1-2 mm^2) interferometrically flat region. We have designed and implemented a novel celi of minimal cost. A 10 mm diameter quartz tube is fused to one end of a fused silica cuvette of 2 mm path length, while the other end of the cuvette is open and directed into a catch tube. This reduces the load on the pump and allows a higher flow rate than closed systems using stock flowing cells. The use of a flowing cell allows the choice of a longer gain path length than possible with nozzle [26]. The cells may also be antireflection coated. Without other modification to the bowtie amplifier [8,17], insertion of the cell did not result in significantly more efficient amplification. However, its larger flat area removes the beam distortion problems sometimes experienced with the thick, sapphire nozzle driven jets. This larger useful area also provides flexibility in the overall amplifier design, which was our next step in improving the amplifier performance.

Consider Figure 1, which depicts the first two passes of the bowtie amplifier of References [8,17]. The spatial offset between the two passes in the gain medium helps to frustrate ASE and is achieved with a minimal amount of optics, but at the expense of preventing one or both of the beams from passing through the center of the roughly cylindrical gain volume (~1 mm diameter by 1-2 mm length) created by the absorbed CVL light. Depending upon the angles and spot sizes, this spatial offset technique may not allow the maximum gain extraction. A poor transverse profile may also result, since the waist of the CVL beam exhibits a ring structure. Figure 2 depicts the first two passes of our new amplifier, which is based upon an arrangement of telescopes. The lenses L_1 and L_2 need not be of equal focal length, but they are separated by $\sim f_1+f_2$, with the gain volume G approximately at the focal plane. Both passes can be independently aligned through the center of the pumped volume G, which allows extraction of the maximum gain. Passes three and four are based upon a similar telescope, followed by a short telescope with a saturable absorber at its focus (malachite green in a ~200 μm jet of ethylene glycol, produced by a conventional steel nozzle). The last two passes (five and six) are

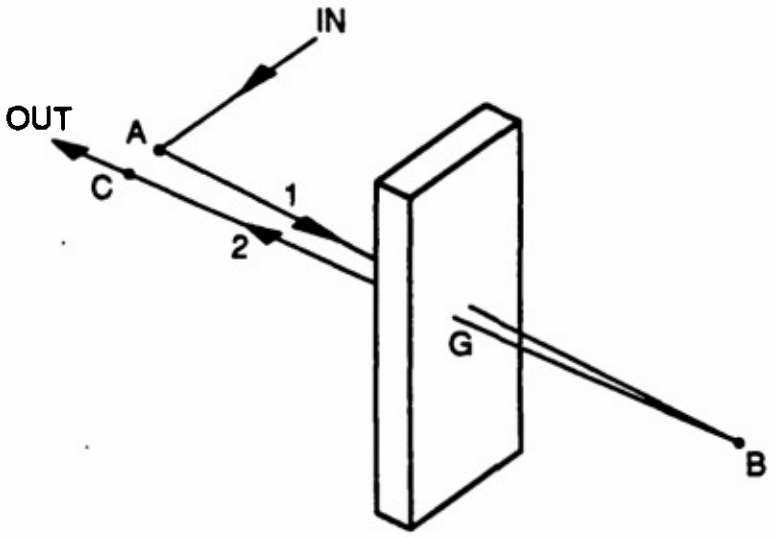

Figure 1. The first two passes through the gain jet or cell G in the bowtie amplifier of Refs. [8,17]. The first pass is ray AB, which passes through G and strikes a mirror at point B. The second pass is ray BC, originating from a mirror at B. Ray BC must be directed to avoid a mirror at A. Thus a spatial offset exists between the two passes in G; at least one ray cannot pass through the center of the pumped region of G.

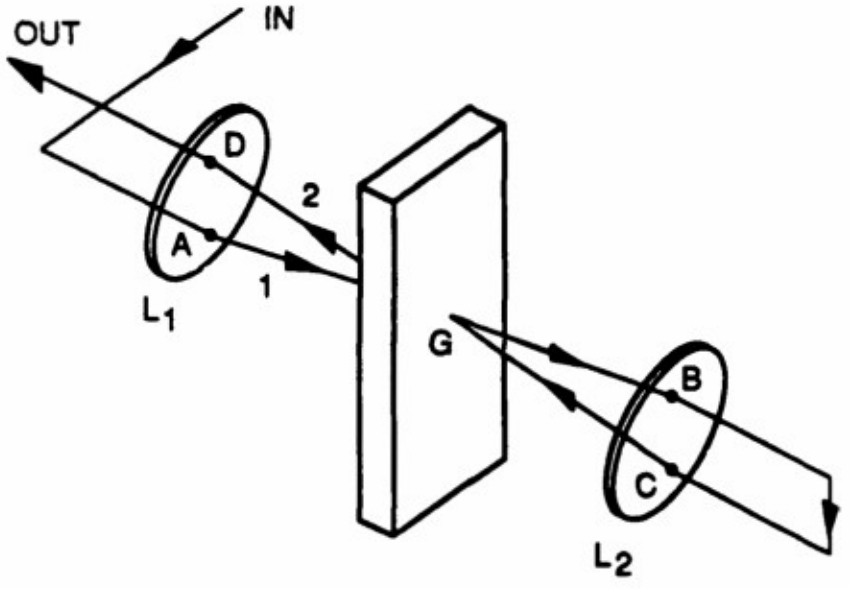

Figure 2. The first two passes through the gain jet or cell G in the BAT amplifier (see text). Lenses L_1 and L_2 form a telescope of ~unity magnification. G is ~$f_1(f_2)$ from $L_1(L_2)$. The first pass is ray AB, and the second pass is ray CD. Two mirrors act to downwardly displace and retroreflect the beam after L_2. Both beams can pass through the center of the pumped region of G.

nearly collinear with the CVL pump beam (all passes are within 10° of collinearity with the pump beam). The optics are arranged to enlarge the seed pulse spot size upon successive passes [23,24] in order to forestall gain saturation until the later passes: the spot size of the first pass is ~30 μm, while the last approximately matches the CVL spot size of ~1 mm. It should be noted that while the beam paths of the bowtie amplifier of References [8,17] lie in a single plane, here the telescopes provide a three-dimensional beam path that pieces this plane. We refer to this combination of *b*owtie-*a*nd-*t*elescopes as the BAT amplifier. It should also be noted that in spite of the intersection of beam paths in the center of the gain volume, we do not observe any spatial gain depletion. This consistent with the short energy storage time and absence of significant long-lived hole burning in the nanosecond pumped gain dye [27].

In this design, the efficiency is improved to 0.5% and the energy raised to >5 μJ. Addition of antireflection coatings to the cell limits losses due to parasitic laser action normal to the cell, and results in 1.0% efficiency and energy >10 μJ. The ASE background is typically 1-5%. In spite of the introduction of ~6 cm of glass (lenses plus cell) in the beam path, we were able to recompress the amplified pulses to ~65 fsec, using an SF14 prism sequence [19]. Since little irreversible temporal distortion is imparted, the use of transmissive optics is not a disadvantage. The amplification of shorter pulses may require additional consideration of the effect of dispersion within the amplifier [23,28].

Additional performance enhancement is possible upon the spatial smoothing of the CVL pump beam, which typically exhibits a concentric ring structure when focussed down to ~1 mm in the gain cell. This makes clean mode matching difficult, and can transfer spatial structure to the amplified pulse. We use ~2 meters of large diameter (1 mm) optical fiber to transport the pump beam to the amplifier, following Ulman *et al* in Reference [20]. This results in a spatially smooth, flat-topped intensity distribution at its output. The 30 mm diameter CVL beam is focussed into the fiber with an f=300 mm lens, which is the longest focal length possible for good coupling efficiency. At the fiber output, a unity magnification imaging system (two f=100 mm lenses) is used to relay the pump beam to the gain cell. The removal of spatial inhomogeneities in the gain medium allows more precise mode matching between the pump and seed beams, and more consistent spatial quality in the amplified beam from day to day. The amplified pulses can typically be focussed to less than twice the diffraction limit, and a white light continuum generation is routinely generated in a 1.25 mm ethylene glycol jet. The spatial quality of the continuum is high enough to allow focussing of certain spectral components to within twice the diffraction limit as well (<3 μm at 800 nm, using 20x microscope objectives). The efficiency of the BAT amplifier rises to 1.5% with fiber-smoothing of the pump beam, partly due to the improved mode matching, but also due to the fact that the relatively unfocussable super-radiant fraction of the CVL pulse does not couple into the fiber and therefore does not reach the gain cell. The super-radiant output of the CVL constitutes a significant fraction of the laser's total pulse energy (20-30%) but it cannot contribute to amplification in most schemes, owing to its poor focussability.

5. CONCLUSIONS AND FUTURE DIRECTIONS

A high efficiency, high energy amplifier CVL pumped amplifier for femtosecond optical pulses has been demonstrated. The design incorporates multiple passes through a single antireflection coated dye cell, near collinear mode matching between pump and seed beams, and a polarized, spatially smoothed pump beam. To date we have achieved 1.5% efficiency with >10 μJ of energy in a $\sim$65 fsec pulse that is focussable to within twice the diffraction limit. An improvement in stability accompanies the increased efficiency, presumably due to the onset of gain saturation. Additional enhancement in efficiency seems possible based upon our preliminary work with additional (seventh and eighth passes) through the gain. Shorter CVL pulses also result in higher efficiency. Both of these observations are consistent with the fact that the large time duration mismatch between pump and seed pulses and short energy storage time of the gain dye require special consideration when designing an nanosecond pumped femtosecond amplifier. It should also be noted that thicker cells, and hence longer gain paths, may help to limit losses to ASE [29], which can deplete the gain. We believe that with careful design, nanosecond pumped optical amplifiers for femtosecond pulses can be built that rival picosecond pumped amplifiers in efficiency and energy.

6. ACKNOWLEDGEMENTS

This work was supported by the National Science Foundation under Grants ECS-8606531 and ECS-8657263, Coherent, Inc., and the Newport Corporation through the Presidential Young Investigator Program, and the Army Research Office under Contract DAAL03-87-K-0145. The work of P. M. Fauchet was also supported by an Alfred P. Sloan Research Grant.

References

1. See for example *Ultrafast Phenomena VI*, T. Yajima, K. Yoshihara, C. B. Harris, and S. Shionoya, eds., (Berlin, Springer-Verlag, 1988).
2. R. L. Fork, B. I. Greene, and C. V. Shank, Appl. Phys. Lett. **38**, 671 (1981).
3. See for example Special Issue on Ultrafast Phenomena, IEEE J. Quantum Electron. **QE-24**, 183-481 (1988).
4. See for example Special Issue on Ultrafast Phenomena, IEEE J. Quantum Electron. **QE-25**, 2415-2682 (1989).
5. J. A. Valdmanis, R. L. Fork, IEEE J. Quantum Electron. **QE-22**, 112 (1986).
6. D. L. Macfarlane, L. W. Casperson, S. M. Janes, IEEE J. Quantum Electron. **QE-25**, 2485 (1989).
7. R. L. Fork, C. V. Shank, C. Hirlimann, and R. Yen, Opt. Lett. **8**, 1 (1983).
8. W. H. Knox, IEEE J. Quantum Electron. **QE-24**, 388 (1988).
9. R. L. Fork, C. V. Shank, and R. Yen, Appl. Phys. Lett. **41**, 223 (1982).
10. A. Migus, A. Antonetti, J. Etchepare, D. Hulin, and A. Orszag, J. Opt. Soc. Am. **B2**, 584 (1985).

11. C. Rolland, and P. Corkum, Opt. Commun. **59**, 64 (1985).
12. D. S. Bethune, Appl. Opt. **20**, 1897 (1981).
13. I. N. Duling, III, T. Norris, T. Sizer, II, P. Bado, and G. Mourou, J. Opt. Soc. Am. **B2**, 613, 1985.
14. M. C. Downer, R. L. Fork, and M. Islam, in *Ultrafast Phenomena IV*, D. H. Auston and K. B. Eisenthal, eds., (New York: Springer- Verlag,1984) p. 27.
15. T. L. Gustafson and D. M. Roberts, Opt. Commun., **43**, 141 (1982).
16. K. J. Choi and T. L. Gustafson, IEEE J. Quantum Electron. **25**, 2441 (1989).
17. W. H. Knox, M. C. Downer, R. L. Fork, and C. V. Shank, Opt. Lett. **9**, 552 (1984).
18. A commercial version of this amplifier, also called the "bowtie", is available from Clark Instrumentation, Inc.
19. R. L. Fork, O. E. Martinez, and J. P. Gordon, Opt. Lett. **9**, 150 (1984).
20. M. Ultnan, R. W. Schoenlein, J. G. Fujimoto, in *Technical Digest of OSA Annual Meeting* (Optical Society of America, Washington, DC, 1989).
21. F. Beisser, private communication.
22. W. L. Nighan, Jr., T. Gong, and P. M. Fauchet, IEEE J. Quantum Electron. **QE-25**, 2476 (1989).
23. R. L. Fork, F. A. Beisser, and D. K. Fork, Revue Phys. Appl. **22**, 1665 (1987).
24. E. V. Khoroshilov, I. V. Kryukov, P. G. Kryukov, and A. V. Sharkov, in *Ultrafast Phenomena VI*, T. Yajima, K. Yoshihara, C. B. Harris, and S. Shionoya, eds., (Berlin, Springer-Verlag, 1988), p. 22.
25. J. M. Heritier, and A. E. Siegman, IEEE J. Quantum Electron. **QE-19**, 1551 (1983).
26. D. Nickel, D. Kuhlke, and D. von der Linde, Opt. Lett. **14**, 36 (1989).
27. C. H. Brito-Cruz, R. L. Fork, W. H. Knox, and C. V. Shank, Chem. Phys. Lett. **132**, 341 (1986).
28. R. L. Fork, H. Avramopoulos, H. L. Fragnito, P. C. Becker, K. L. Schehrer, C. Hirlimann, Opt. Lett. **14**, 1069 (1989).
29. A. A. Hnilo and O. E. Martinez, IEEE J. Quantum Electron. **QE-23**, 593 (1987).